SYNTHESIS, CHARACTERISATION AND CATALYTIC PROPERTIES OF INTRA-ZEOLITE TRANSITION METAL COMPLEXES

A THESIS SUBMITTED TO THE

UNIVERSITY OF PUNE

FOR THE DEGREE OF

DOCTOR OF PHILOSOPHY

(IN CHEMISTRY)

BY

TRISSA JOSEPH

INORGANIC AND CATALYSIS DIVISION

NATIONAL CHEMICAL LABORATORY

PUNE 411 008

INDIA

JANUARY, 2003

CERTIFICATE

Certified that the work incorporated in the thesis **"Synthesis, Characterisation and Catalytic properties of intra-zeolite transition metal complexes"** submitted by **Ms. Trissa Joseph,** for the degree of Doctor of Philosophy, was carried out by the candidate under our supervision in the Inorganic and Catalysis Division, National Chemical Laboratory, Pune, India. Materials obtained from other sources have been duly acknowledged in the thesis.

Dr. S. Gopinathan **Dr. S. B. Halligudi**

Research Guide **Research Co-Guide**

ACKNOWLEDGEMENTS

I express my profound gratitude to my research guide, Dr. Sarada Gopinathan for her invaluable guidance, numerous discussions and constructive suggestions through out the course of this investigation. I take this opportunity to express my deepest sense of gratitude and reverence towards my co-guide Dr. S. B. Halligudi, for his constant inspiration and for guiding me in the right direction throughout the course of this work. My deep personal regards are due for him forever.

I would like to express my profound gratitude to Dr. A. V. Ramaswamy, Head, Catalysis Division, NCL, for providing me all facilities required for my work.

It gives me a great pleasure to express my deep sense of gratitude and indebtedness to Dr. C. V. V. Satyanarayana, Dr. S. Sivasanker, Dr. D. Srinivas, Dr. C. S Gopinath, Dr. M. Hartmann, Dr. S. Ernst, Dr. F. Lefebvre, Dr. B. Moroz, Dr. C. Gopinathan, Dr. R. Kumar, Dr. S. S. Deshpande, Dr. Pardhy, Dr. Deogaonkar, Dr. Muralisastry, Ms. Violet, Dr. Mohan Badbade, Dr. Renu, Dr. R. Gonnade, Dr. Saguna, Dr. Vijaymohan, Dr. V. Ramaswamy, Ms N. Jacob, Dr. P. Manikandan, Mr. Kashinathan and all the other scientific and non-scientific staff of NCL for their help and inspiring guidance and suggestions in carrying out the research work.

I take the opportunity to thank my friends, Biju, Dhanashri, Shanbag, Kalaraj, Smita, Surekha, Patra, Laha, Mandal, Thomas, Shiju, Sabastian, Pai, Vinu, Elangovan, Sajani, Rajani, Nirupa, Kusum, Gosh, Mahesh, Raina, Vandana, Sindhu, Bennur, and many others and my family members from whom I have received unfailing support, tremendous patience and encouragement during many years of studies that they have shown to me in their own special way.

Finally, my thanks are due to the former director of NCL, Dr. P. Ratnasamy, and the present director Dr. S. Shivram, for allowing me to carry out research at NCL and extending all possible infrastructural facilities at NCL and to the Council of Scientific and Industrial Research (CSIR), New Delhi, India, for providing me a research fellowship.

Trissa Joseph

ABBREVIATIONS

APTES	3-aminopropyl triethoxysilane
CPTES	3-chloropropyl triethoxysilane
CTAB	Cetyltrimethylammonium bromide
DTA	Differential thermal analysis
EPR	Electron paramagnetic resonance
FAU	Faujasite
FID	Flame ionization detector
FT-IR	Fourier- Transform Infrared Spectroscopy
ICP-AES	Inductively coupled plasma atomic emission spectrometer
LCT	Liquid - crystal templating
LTA	Linde type A
MAS NMR	Magic angle spinning nuclear magnetic resonance
MCM-41	Mobil's Crystalline Materials-41
MFI	Mobil's FIVE
ml	milliliter
MR	Membered ring opening
Pluronic P123	poly(ethylene oxide)-poly(propylene oxide) poly(ethylene oxide)
Salen	N, N'-ethylenebis(salicylideneamine)
Saloph	N, N'-phenylenebis(salicylideneamine)

Salten	3-[N,N'-Bis-(salicylidenamine)ethyltriamine]
SBA-15	Santa Barbara Amorphous
TACN	Triazocyclonane
TBHP	*tert*-butylhydroperoxide
TEM	Transmission Electron Microscopy
Temp.	Temperature
TEOS	Tetraethylorthosilicate
TG	Thermogravimetry
TMAOH	Tetramethylammonium hydroxide
TPP	Triphenylphosphine
UHP	Urea hydrogen peroxide
UTD-1	University of Texas at Dallas number 1
UV-Vis	Ultra Violet Visible Spectroscopy
XPS	X-Ray Photoelectron Spectroscopy
XRD	X-ray diffraction
XRF	X-Ray Fluorescence
ZEMC	Zeolite encapsulated metal complex

CONTENTS

CHAPTER 1

INTRODUCTION

1.1 GENERAL BACKGROUND AND INTRODUCTION

Awareness of environmental issues has proven a potent driving force in the development of environment friendly processes and technologies in the chemical industry [1,2]. This has manifested itself in determined effort, on behalf of the industry, to develop catalytic processes which obviate waste production, i.e. solving the problem at the beginning and not dealing with waste disposal later [3]. Even though the oxidation and hydroxylation of organic compounds at ambient conditions using non-corrosive environment friendly oxidizing agents is of widespread occurrence in nature, such processes are not in common practice either in the laboratory or in the industry. Some of the extensively studied systems for the oxidation and hydroxylation of aromatic compounds are the Fenton's reagent, peracids, the Hamilton-Friedman and the Udenfriend reagents and the Cu^{2+}-O_2^- morpholine system. All these oxidation/hydroxylation systems are homogeneous in nature. Hence there is a need to find an efficient and "clean" oxidation process, which is likely to be in greater demand in the future, especially in fine chemicals industry. As a consequence of the inherent advantages of heterogeneous catalysts, much effort has been directed towards the development of heterogeneous processes and the heterogenization of known active homogeneous catalysts [4]. For similar reasons, selective catalytic oxidation of organic compounds utilizing heterogeneous catalysts is proving more important in organic synthesis [5]. Even though lot of knowledge has been acquired regarding heterogeneous catalysis, the fine and specialty chemical industry is still based on stoichiometry rather than on catalysis.

Transition metal complexes have a metal center, which acts as an active site, and possess the tendency to catalyze diverse chemical reactions. Transition metal complex

promoted oxidation reactions are of considerable interest because of their relevance to organic chemistry. The known active homogeneous metal complexes can be heterogenized by immobilization, grafting, anchoring or encapsulating them in an inert polymer or inorganic support

Various attempts for the development of new catalyst system led to the emergence of a new class of catalyst called "Zeolite Encapsulated Metal Complexes" (ZEMC). The ability of transition metal complexes to catalyze diverse chemical reactions is coupled with the shape selectivity and engineering advantages of zeolites by incorporating catalytically active transition metal complexes in the cavities and voids of the zeolite. As the metal complex is not bounded to the host, it is anticipated that it retains solution like activity, and the zeolite support imparts size and shape selectivity to the catalysts. Additionally, the zeolite provides a stabilizing effect and the catalyst can be separated easily from the product by simple filtration and does not lose its catalytic activity in first cycle itself due to irreversible dimerization and irreversible oxidation of ligands. In addition, they behave functionally similar to many enzyme catalysts in some selective oxidation reactions and, due to this biomimetic character; they are often referred to as "zeozymes" (zeolite-based enzyme mimics) [6-10]. The zeolite replaces the protein mantle of the enzyme and the entrapped metal complex mimics the active site of the enzyme (e.g. an iron-porphyrin).

Romanovsky et al [11-14] was the first to report such catalysts, consisting of metal phthalocyanines encapsulated inside the supercages of zeolite Na-Y in 1977. Since then a number of groups have synthesized such encapsulated metal complexes and characterized their physicochemical and catalytic properties [15-16]. Jacobsen's Mn(Salen) complex encapsulated in Na-Y has emerged as an important catalyst for the oxidation of olefins [17-

18]. Such zeolite encapsulated metal complexes are also known as 'Ship- in- a bottle' complexes.

However, the major drawback for the use of conventional zeolites is the small pore sizes (4-13 Å), which makes it difficult for substrates to diffuse and access the active sites and for products to diffuse out of the pores. Hence, there has been an ever-growing interest in expanding the pore sizes of the zeolite materials from micropore to mesopore region. In Table 1.1 different porous materials, along with typical examples, are classified.

Table 1.1

Pore-size regimes and representative porous silica based materials

Type and pore size (nm)	Examples	Actual size range[a] (nm)
Microporous (<2)	Zeolites	0.45 × 0.45 (LTA, 8 MR)
		0.56 × 0.56 (MFI, 10 MR)
		0.74 × 0.74 (FAU, 12 MR)
		0.75 × 1.0 (UTD-1, 14 MR)
Mesoporous (2-50)	Aerogels	>10
	Pillard layer clays	1, 10[b]
	M41S	2-10
	SBA-15	5-20
Macroporous (>50)	Glasses	>50

[a]MR = membered ring opening.

[b] Bimodal pore-size distribution.

The recently discovered mesoporous materials (MCM-41, SBA-15) synthesized by silicate condensation around surfactant micelles and by using a triblock co polymer-poly(ethylene oxide)-poly(propylene oxide) poly(ethylene oxide) [EO_n-PO_m-EO_n] as structure directing agent respectively, due to their regular arrays of uniformly sized channels with pore diameter in the range of 2-20 nm, afford new opportunities for the catalytic conversion of substrates with larger molecular size. These materials also are promising for the immobilization of larger metal complexes and clusters of potential catalytic significance [19-23]. Another major interest of these materials concerns with their excellent properties as support for impregnation of 12-tungstophosphoric acid for different catalytic functions [24].

In constrained environments these encapsulated complexes lose some of their degrees of freedom they had in the neat state, adopt particular geometries, hooks on to groups on the support, alter their stoichiometries, changes their coordination sphere and geometry, relaxes or restricts their sphere of influence depending on whether they are accommodated inside the sodalite cages of microporous materials or in the regular channels of mesoporous materials and thus exhibit altered reactivity so as to promote reaction in geometry restricted (shape selective) or redox potential controlled pathways.

1.2 MICROPOROUS MATERIALS: ZEOLITES

Zeolites are crystalline microporous silica based solids, which are used extensively in adsorption and catalytic process. The practical importance of these materials has led the studies focused on the characterization and applications of different types of zeolites and

related materials such that they form an important part of material science, inorganic chemistry and catalysis [25-32].

Zeolites are classified as crystalline materials in which the Si and Al are tetrahedrally coordinated by oxygen atoms in a three dimensional network. The crystallographic unit cell of the zeolites may be represented as:

$$M_{x/n}[(AlO_2)_x (SiO_2)_y] zH_2O$$

Where M is a charge compensating cation with valency 'n'. The ratio 'x/y' may have any value ranging from zero to one. The number of water molecules, which can be reversibly adsorbed and desorbed in the zeolite pores, is represented by 'z'. The presence of trivalent Al atoms in the lattice develops a unit negative charge per Al atom in the framework, which is compensated by a cation such as proton (H^+) producing acidity in zeolites. The cation is quite mobile and may be exchanged to varying degrees by other cations like B^{3+}, Ga^{3+}, Fe^{3+}, Cr^{3+}, Ti^{4+}, Zr^{4+} and $V^{4+/5+}$ [33-38].

Moreover, zeolites and related materials have earned the reputation of 'green catalysts' in oil refining, petrochemistry and organic synthesis in the production of fine and specialty chemicals due to several important environmental factors e.g. waste minimization, simple operation, easy work up, regeneration and reuse of the catalyst for several times.

1.2.1 Synthesis of Microporous Materials: Zeolites

In the late 1940's Milton developed a method that involved hydrothermal crystallization of reactive alkali metal aluminosilicate gels at low temperatures and pressures. During the synthesis of low silica zeolites with alkali metal aluminosilicates it was proposed that the hydrated alkali cation *templates* or *stabilizes* the formation of zeolite

structural subunits. Alkali hydroxide reactive forms of alumina, silica and water were combined to form a gel and crystallization was carried out at around 373K.

In the 1960's, addition of quarternary ammonium cations to alkali aluminosilicate gels was started, initially to produce intermediate silica zeolites. Subsequently, it led to the discovery of high silica zeolites and silica molecular sieves. The synthetic chemistry of both high silica and early low silica molecular sieves is similar except for the addition of quaternary ammonium ions and the crystallization temperatures. The pH of the gel in both types of zeolites is high and is around 10 to 14. The framework composition of the zeolite is generally determined by the silica to alumina ratio and the crystalline framework structure. Organic (template), inorganic cations, and OH ion concentration also influence zeolite structure. During crystallization both the aluminum and silicon dissolve to form aluminate and silicate ions. These ions are brought together (by template / or metal ion) to form a gel by condensation or polymerisation.

1.2.2 Encapsulation of Metal Complexes in Microporous materials

Heterogenization of homogeneous catalysts has been an interesting area of research and from the industrial point of view; this could provide an ideal method for combining the advantages of homogeneous catalysts (high activity and selectivity etc.) with the engineering advantages of heterogeneous catalysts (easy catalyst separation, long catalytic life, continuous operation, easy catalyst regenerability and recycle etc.) [39-41]. Zeolites such as faujasite (Na-Y and Na-X), which are microporous materials having the cage size (1.2 nm) and a 3D chamber with SiO_2:Al_2O_3 = 3 to 5, have been used extensively in the preparation of zeolite encapsulated transition metal complex catalysts [6-8, 42-46].

There are different methods of encapsulating transition metal complexes.

1.2.2.1 Adsorption method

Metal carbonyl complexes are usually encapsulated in zeolites by adsorbing them from the gas phase and on dry zeolites [47]. Multinuclear clusters like $Rh_6(CO)_{16}$, $Rh_4(CO)_{12}$ and $Ir_4(CO)_{12}$ as well as bimetallic derivatives like $Rh_{6-x}Ir(CO)_{16}$, x=(0-6) have been encapsulated in Y type zeolite by the reaction of CO/H_2 or CO/H_2O with rhodium or iridium ion exchanged Y zeolites [48-54].

1.2.2.2 Ion exchange method

Cationic transition metal complexes can be encapsulated by direct ion exchange with the counter ion balancing the negative charge of AlO_4 tetrahedra of the zeolite framework. The complex must be stable and sufficiently small to pass through the pore openings of the zeolite. Peigneur et al [55] encapsulated $[Cu(\text{ethylene diamine})_2]^{2+}$ complexes in faujasites by this method.

1.2.2.3 Zeolite synthesis method

This method is applicable to complexes that are stable under zeolite synthesis conditions. This method leads to encapsulation of well-defined intrazeolite complexes without contamination from free ligands as well as uncomplexed and partially complexed metal ions. The important condition that has to be satisfied for encapsulation using this method is there should be no requirement of subsequent template molecule removal, which may necessitate calcinations of the zeolite at higher temperature leading to thermal damage to the complex. Phthalocyanines have been encapsulated in faujasites and aluminophosphate molecular sieves by this method [56-57].

1.2.2.4 Flexible ligand method

The principle involved in this method is the diffusion of ligands into an already metal exchanged zeolite pores. Diffusion of the ligands can be carried out either by dissolving the ligand in an appropriate solvent or by diffusing it inside the metal exchanged zeolite in molten form (for details refer chapter 2). The ligand employed in the later method should not decompose during adsorption on the metal exchanged zeolites. This method is exemplified by the encapsulation of metal salen complexes in synthetic faujasite- type zeolites. The salen ligand is diffused into the cavities of zeolite wherein it complexes with the transition metal cation in ion exchange positions forming metal salen complexes in the cavities of the zeolite. This complex is too large to exit the cavities through the channels whose dimensions are smaller than the cavities.

1.3 MESOPOROUS MATERIALS

The synthesis of mesoporous molecular sieves called M41S is one of the most exciting discoveries in the field of materials synthesis in the last decade [58-60]. The M41S family is classified into three members: MCM-41 (hexagonal), MCM-48 (cubic) and MCM-50 (lamellar). These mesoporous silicate and aluminosilicate materials, with well-defined pore sizes of 0.2-10 nm, break past the pore size constraint of microporous zeolites. With high surface area and control of pore sizes are among the many desirable properties that have made such materials the focus of great interest. The synthesis of these materials opens definitive new possibilities for preparing catalysts with uniform pores in the mesoporous region, which will allow the ingress and egress of relatively large molecules in their mesopores for catalytic transformations. Obviously, lot of research

activity has occurred within a few years, which includes new investigations on different aspects such as synthesis procedures and synthesis mechanisms, heteroatom insertion, stability, physico-chemical characterization, adsorption, metal complex immobilization and catalytic properties [61-64].

In 1998, Stucky et al [65] synthesized a new ordered hexagonal mesoporous silica with much thicker walls named SBA-15 using triblock co polymer- poly(ethylene oxide)-poly(propylene oxide) poly(ethylene oxide) [EO_n-PO_m-EO_n] as structure directing agent. These mesoporous materials because of their high surface area, tunable pore size and well modified surface properties [66-67] are finding use as adsorbents for the removal of toxic heavy metal ions from waste water [68], enzyme carriers [69], catalysts [70], and materials to sequester and release proteins [71].

1.3.1 Synthesis of Mesoporous Materials: MCM-41 and SBA-15

The synthesis of mesoporous materials (MCM-41) was carried out originally under aqueous alkaline condition [72]. Similar to zeolite synthesis, organic molecules (surfactants) function as templates forming an ordered organic-inorganic composite material [73]. Via calcination the surfactant is removed, leaving the porous silicate network. However, in contrast to zeolites, the templates are not single organic molecules but liquid-crystalline self-assembled surfactant molecules. The formation of organic-inorganic composites is based on electrostatic interactions between the positively charged surfactants and the negatively charged silicate species. Amongst the various building mechanisms of MCM-41 investigated earlier, the "liquid-crystal templating" (LCT) mechanism suggested by Beck et al. [59] seems to include all the mechanisms proposed earlier, (Scheme-1.1). They proposed two main pathways, in which either the liquid-crystal

phase is intact before the silicate species are added (pathway 1) or the addition of the silicate results in the ordering of the subsequent silicate- encased surfactant micelles (pathway-2). The reason for the apparently different reaction pathway results from changes in surfactant properties, depending on the surfactant concentration in water and the presence of other ions [74-75]. MCM-41 can be synthesized with surfactant concentrations as low as the critical micelle concentration (CMC) up to concentrations where liquid crystals are formed [76]. In very dilute aqueous solutions (~ 10^{-3} to 10^{-2} mol $^{-1}$ surfactant concentration) the existing species are spherical micelles.

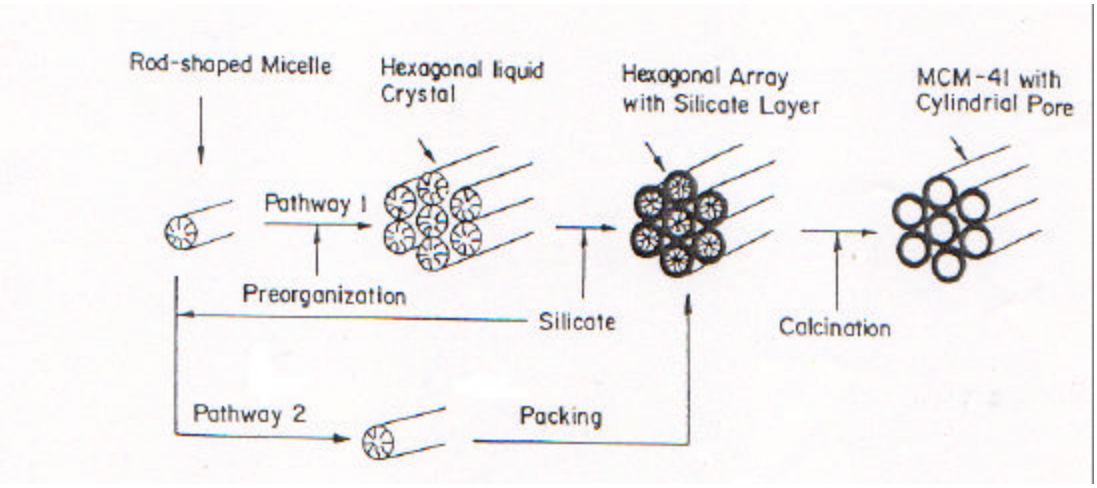

Scheme-1.1 Mechanistic pathways for the formation of MCM-41

On the contrary the synthesis of mesoporous SBA-15 is achieved by use of a triblock copolymer surfactant in acid media [65]. Less attention has been focused on the synthesis and applications of SBA-15 mesoporous silica since it was discovered in 1998. It has been proposed that the assembly of the mesoporous silica organized by triblock

copolymer species in acid media occurs through a $(S^{\circ}H^{+})(X^{-}I^{+})$ pathway [77]. Furthermore, the relative times required for silica mesophase precipitation to occur depend on the presence of Cl^{-} anion when used in the form of hydrochloric acid. However, this unique mesoporous material can provide more possibilities for the design and synthesis of open pore structures because of its high surface area and easily controllable uniform pore size that may be extended to ca. 30nm.

1.3.2 Metal Substituted Mesoporous Materials

In order to generate potential catalytic activity, the incorporation of heteroatoms into the inert framework or walls of the pure siliceous mesoporous materials is an important method to modify the nature of the framework and make them catalytically active. The incorporation of trivalent metal ions such as Al [78], B [79], Ga [80] etc in the walls of silica network mesostructure produces framework negative charges that can be compensated by protons providing acid sites and therefore, such materials are important from the point of view of acid catalysis. For reactions involving high molecular mass hydrocarbons, low diffusion resistance is observed due to the large pore diameters. The incorporation of transition metals such as Ti [81], V [82], Co [83] and Mn [84] etc is also important to prepare mesoporous catalysts with redox catalytic properties.

1.3.3 Immobilization of Metal Complexes in Mesoporous Materials

The immobilization of metal complexes on the surface of mesoporous silicates allows the preparation of multifunctional molecular sieves with desired catalytic properties. Mesoporosity and very high surface area of mesoporous materials (particularly MCM-41 and SBA-15) have been largely used for the immobilization of different metals as well as bulky metal complexes. The process of metal immobilization includes wet

impregnation [85], vapor deposition [86], treatment with $(NH_4)2MF_6$ ($M=Si^{4+}$, Ti^{4+} etc.[87] and metal alkoxides [88] ion exchange with metal salts etc.[89-90]. Immobilization on mesoporous materials can be done using different techniques.

1.3.3.1 Impregnation Method

In this method the metal complexes are incorporated in the mesoporous hexagonal channels of MCM-41 by simply embedding or impregnating the transition metal complex into the mesopores [91]. Leaching of transition metal complex is a major potential problem when the complexes are incorporated using this method and used for oxidation reactions performed in liquid phase.

1.3.3.2 Ion exchange method

Immobilization of metal complex using this method is mostly done by ion exchange of the calcined Al-MCM-41 with known amounts of the complex dissolved in appropriate solvent at room temperature. The solid is then filtered, washed with solvent and then vacuum dried [22].

1.3.3.3 Covalent Anchoring of Metal Complexes

Since there are chances of leaching of the metal complexes by the previous methods, immobilization is mostly achieved by modifying the mesoporous materials with various modifying agents and the covalently anchoring the metal complex on to the functionalized mesoporous materials. Functionalization of mesoporous materials is achieved by silanation of the mesoporous surface by 3-amino or 3-halogeno-propyl alkoxysilane in an apolar solvent (Scheme-1.2).

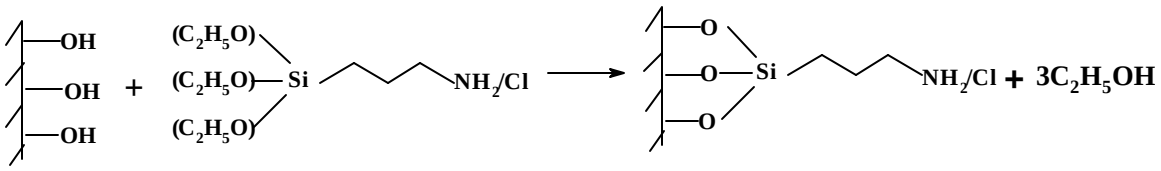

Scheme-1.2 Functionalization of mesoporous materials

The presence of large amount of silanol groups [(-O-)SiOH] in MCM-41 and HMS materials attracted the researchers primarily for anchoring the organic functional groups using the concept of organic functionalization in silica and then those organic functional groups or ligands were used for anchoring different types of metals, metal complexes and proteins with or without modification of the parent functional groups. The chemical reactivity of these mesoporous materials facilitates the covalent anchoring of various functional groups to the walls. The preparation of such inorganic-organic hybrid materials is of growing interest [92-93] especially for the attachment of various metal complexes. The advantages of inorganic-organic hybrid materials arise from the fact that inorganic materials can provide mechanical, thermal or structural stability, while the organic features are more readily modified for specific applications in catalysis, separation or sensing. These functionalized mesoporous materials are synthesized using two methods.

1.3.3.3.1 In situ Synthesis Method

Organo-functionalized mesoporous silicas were prepared conveniently at room temperature [94] or at higher temperature [95] by the condensation of tetraalkoxysilane ($Si(OR)_4$) and organosiloxanes ($R`-Si(OR)_3$) in the presence of surfactant (template) and auxiliary chemicals. Thus, a variety of inorganic-organic hybrid materials, where the organic functional groups are attached covalently with the silica surface of MCM-41 through O-Si-C bonds, are very important for their various potential applications. An

acidic solvent extraction technique is generally used to remove the surfactant from the product to yield an organo-functionalized ordered porous silica material [94-95].

1.3.3.3.2 Post Synthesis Method

Organo functional groups can also be introduced to the pore surface of mesoporous silica as the terminal groups for organic monolayers by post synthesis modification. The treatment of mesoporous silica with organosiloxane precursors produces hybrid inorganic-organic materials by hydrolysis and finally condensation of organosiloxane groups [96]. Although, organo functional groups have been introduced into mesoporous silica in both ways, *in situ* and post synthetic methods, metal complexes attached covalently to the pore surface are introduced only by post synthesis modifications [97-98].

1.3.3.4 Grafting of metal complexes.

Surface attachment of transition metal oxides and metals or bimetal complex without the use of intermediate silane coupling agents is achieved by direct reaction of surface hydroxyl groups with reactive species. Titanocene dichloride was anchored to MCM-41 using this method [99]. The complex was converted to titanium-oxo species through calcinations in air (Scheme-1.3).

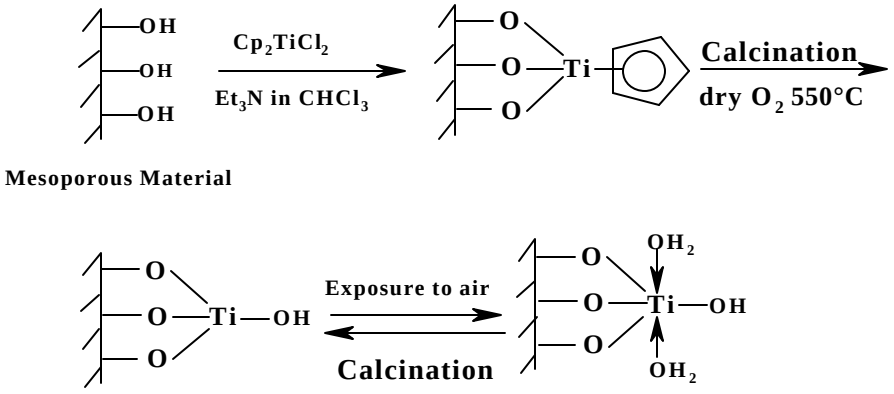

Scheme 1.3 Grafting of titanocene dichloride on mesoporous materials.

Same authors have also reported the inclusion of a cobalt complex and studied it for the oxidation of cyclohexane [100]. The reactivity of chloride ligands towards hydroxyl groups of the MCM-41host has also been exploited for the grafting of ethylenebis(indenyl) zirconium dichloride [101].

1.4 PHYSICO- CHEMICAL CHARACTERIZATION

A number of techniques have been used to characterize different types of complex encapsulated/immobilized on microporous and mesoporous materials. Each technique is unique by itself and provides important information for understanding distribution of complex over the host, degree of complexation, type of coordination, influence of host-guest interaction on the structure and the stability of the complex. Among the various techniques used, the most commonly used methods for characterization of complex encapsulated in micro- and meso-porous materials are spectroscopic methods, such as, powder X-ray diffraction (XRD), energy dispersive X-ray analysis (EDX), UV-Vis, FTIR, solid state magic angle spinning (MAS) NMR, and electron paramagnetic resonance (EPR), etc. They give information about the structure and location of the complex inside the cages and channels of the support. In addition to the spectroscopic techniques, microscopic techniques like, transmission electron microscopy (TEM), X-Ray photoemmision spectroscopy (XPS), volumetric (adsorption and surface area analysis by BET method), and thermogravimetric (thermogravimetric-differential thermal analysis (TG-DTA)) are also essential for thorough characterization of the materials.

1.4.1 X-ray Diffraction

Powder X-ray diffraction is the most important and commonly used tool to identify and measure the uniqueness of structure, phase purity, degree of crystallinity and unit cell parameters of crystallite materials. As the powder pattern is the fingerprint of the molecular sieve structure, phase purity and percent crystallinity of the synthesized molecular sieve can be ascertained by comparing with the standard pattern for the molecular sieve under investigation. It is used to study the cation distribution inside the zeolite matrix [40, 42]. Microscopic solids show characteristic peaks in the 2θ range of 5-50° whereas the mesoporous materials exhibit characteristic peaks in the low angle region between 0.8-10°. The unit cell dimension determined by XRD is used to calculate the framework wall thickness (FWT) of hexagonal channels in mesoporous materials before and after immobilization.

1.4.2 Sorption Studies

The ability to absorb selective molecules of comparable sizes through the pores into the channels of molecular sieves made them interesting and useful in the field of heterogeneous catalysis. The sorption properties of molecular sieves provide information about the hydrophobic/hydrophilic character, pore size distribution and pore volume as well as surface area before and after encapsulation/immobilization. The absorption of nitrogen measured by Brunauer- Emmett-Teller (BET) equation at low pressure (10^{-4} Torr) and liquification temperature of N_2 (77 K) is the standard method for the determination of surface area and pore volume and pore size distribution in molecular sieves [102].

1.4.3 UV-Vis Spectroscopy

The UV-Vis Spectroscopy is known to be very sensitive and useful technique for the identification of the electronic state of the metal atom as well as ligand geometry in intrazeolite complexes. It gives information about the d-orbital splitting through the d-d transitions and the ligand-metal interaction through the ligand to metal charge-transfer transitions. The mechanism of reaction over "neat" complexes can be investigated by *in situ* UV-Vis spectroscopy.

1.4.4 Fourier- Transform Infrared (FTIR) Spectroscopy

The FTIR spectroscopy provides information on whether ligand molecules have coordinated to transition metal cations if different patterns appear in the free or in the chelated state, or if characteristic bands exhibit defined shift upon chelation. FTIR spectroscopy in the framework region (400-4000 cm^{-1}) provides additional information about the structural details of the support. In addition to the above, ligand features can be seen when the metal complex is encapsulated/immobilized in the cavities or channels of microporous and mesoporous materials.

1.4.5 Nuclear Magnetic Resonance (NMR) Spectroscopy

High-resolution magic angle spinning Nuclear Magnetic Resonance (NMR) Spectroscopy both in the liquid and the solid state, is an important tool for understanding the catalytically active transient species at the molecular level and the local environment of the metal ion. It is also used to study the interaction of the complex with the host. The ^{13}C CP MAS NMR spectra gives information about the incorporation of intact organic structure directing agents inside the channels of the micro- and mesoporous materials.

1.4.6 Electron Paramagnetic Resonance (EPR) Spectroscopy

Electron Paramagnetic Resonance (EPR) Spectroscopy is the resonance absorption of the electromagnetic (microwave) radiation by magnetically split states of unpaired electrons. It is a very important tool for determining the oxidation states of the metal and for elucidating the reaction mechanism by *in situ* EPR Spectroscopy for neat as well as encapsulated metal complexes. This technique provides information about the redox sites and paramagnetic charge-transfer in the complex.

1.4.7 Transmission Electron Microscopy (TEM)

The topographic information obtained by TEM at near atomic resolution has been a key method for the structural characterization and identification of the various phases of molecular sieves i.e. hexagonal (MCM-41), cubic (MCM-48), lamellar (MCM-50) phases. The hexagonal pore structures with similar XRD patterns as that of MCM-41 materials have been observed by high-resolution TEM [103]. These structures were also observed in the mesoporous materials after immobilization with the complex. The hexagonal shape is the most energetically favorable, since this is the only way to maintain a constant wall thickness, which in turn maximizes surfactant-silicate surface interaction [104]. In addition to structural characterization, it can also be used to detect the location of metal clusters and heavy cations in the framework.

1.4.8 X-Ray Photoelectron Spectroscopy

XPS is among the most frequently used techniques in catalysis. It gives information on the elemental composition and the oxidation state of the elements. X-ray photoelectron spectroscopy gives information about the homogeneity of the distribution of the encaged complexes, i.e. either uniform throughout the zeolite crystal or enriched in a shell close to

the crystal surface, the degree of complexing, the structure of the complex and its interaction with the framework.

1.4.9 Thermal Analysis (TG-DTA)

The thermoanalytical technique has been widely used to get information on the thermal stability of microporous and mesoporous molecular sieves. It can provide information about amount of intrazeolite complex, the presence of free and uncomplexed ligand, and the thermal stability of the encapsulated complex. Further, it provides information about the desorption of physisorbed water, oxidative decomposition of organic materials and dehydroxylation of Si-OH groups in the molecular sieves. From diferential thermal analysis (DTA), phase transformations can also be known of the materials.

1.5 CATALYTIC APPLICATIONS AND PROSPECT OF TRANSITON METAL COMPLEXES IN MICROPOROUS AND MESOPOROUS MATERIALS

The catalytic properties of immobilized complexes have been explored in various selective oxidation and hydrogenation reactions. General benefits of the heterogenization of homogeneous catalyst are easy catalyst separation from the reaction medium and the possibility of using a large variety of different solvents and reaction conditions. Examples of the advantages introduced by immobilizing in an inorganic matrix are the possibility of shape-selective catalysis due to constrained environment, a higher catalytic activity, and stability of the encapsulated complexes. The latter arises from the spatial isolation, which prevents dimerization of the monomeric complexes and also strongly suppresses an oxidative self-destruction. It was reported that encapsulation enhances the catalytic activity of the metal complexes [105]. In some cases, improved selectivities were also observed

[106]. Zeolite encapsulated iron-phthalocyanine complexes are able to catalyze the selective oxidation of alkenes to alcohols and ketones under ambient conditions with iodosobenzene [7] or t-butylhydroperoxide [107] as oxygen atom donors. In addition to the difference in activity, Herron also observed interesting selectivity changes upon immobilization of the complex in microporous matrix [7]. Stereoselectivity was also reported in the epoxidation of stilbene wherein the trans form is preferentially epoxidized over Mn(Salen)-Y [43]. Other oxidation reactions over ZEMC include the oxidation of CO [108], the direct conversion of methane with oxygen to methanol over ruthenium-, cobalt-, or manganese-phthalocyanine or tetraphenylporphyrins [109] and oxidation of toluene with H_2O_2 using VO(Salen)-Y complex [110]. More recently, and from an industrial point of view, the direct synthesis of adipic acid from cyclohexane or cyclohexene using ZEMC was reported [111]. Besides many examples of oxidation reactions over ZEMC a few examples of hydrogenation reactions have also been reported [112-113].

The unique physical properties such as high surface area, large pore size, etc. of MCM-41 and SBA-15 have made these materials highly desirable hosts for the fixation of large active metal complexes [114]. Since direct immobilization of such complexes onto the mesoporous support is not advantageous due to the possibilities of leaching, the anchoring of these metal complexes through an organic spacer to the support is preferred. These inorganic-organic hybrid materials offer great scope for the development of new catalysts [70, 97, 115-117]. Based on the spectroscopic evidences it was envisaged that the complex retains its structure inside the channels and it hangs like a pendant inside mesoporous materials. Brunel has reported immobilization of large number of complexes inside the channels of these materials [96]. The amine functions of triazocyclonane

(TACN) was reacted with the epoxy groups of MCM-41 grafted (3-glycidyloxypropyl)-trimethoxy silane and was used to anchor 2-hydroxyalkyl-substituted TACN ligands to MCM-41 and its manganese complex was used for the epoxidation of styrene with H_2O_2 [118]. Similarly, Ruthenium (II)mesotetrakis(4-chloropheny porphyrin) was anchored on to the walls of MCM-41 modified with 3-aminopropyl triethoxysilane and was used for the alkene oxidation by TBHP [119].

Due to large void space, the diffusional restrictions of reactants/products are absent and therefore, these materials are most suitable for catalytic applications involving larger reactant and product molecules [20, 114]. Many oxygen sources like iodosyl benzene, amine n-oxides, peracids, perchlorates, periodate, organic peroxides, H_2O_2 and O_2 can be used in oxidation reactions catalyzed by such immobilized complexes.

Initially, the catalytic studies with mesoporous molecular sieves focused mainly on acid catalysis [85, 120] and redox reactions [61, 121]. Since then, a wide variety of applications including deposition of heteroatom onto the surface of mesoporous walls have been established and the field is still expanding rapidly.

1.6 SCOPE AND OBJECTIVE OF THE THESIS

It is evident from the literature survey on microporous and mesoporous materials, that these materials have opened new opportunities in the field of catalysis. The present work deals with the detailed and systematic study of the synthesis, characterization and catalytic properties of transition metal complexes encapsulated/immobilized on microporous and mesoporous materials using different techniques like encapsulation, grafting and covalently anchoring of the metal complex through a functional group.

Considerable amount of literature is available on the study of Phthalocyanine and Salen metal complexes encapsulated in zeolites (Na-Y). However, the chemistry of such complexes immobilized/anchored onto mesoporous supports MCM-41 and SBA-15 and their applications as catalysts for organic substrates is less known. This motivated us to take up the investigations and find out whether such metal complexes can be immobilized/anchored onto the channels of mesoporous materials (Si-MCM-41 and Si-SBA-15) and yet possess rotational and vibrational freedom and without being leached out of its channels during the catalytic reactions. For the purpose of comparison, Salen and Saloph metal complexes were also encapsulated inside the cages of Na-Y, characterized and used for the oxidation of various substrates, with special emphasis on synthesis of compounds used for preparation of natural products.

Bi-functional organo-functionalized mesoporous materials can be potentially used to prepare a class of mixed-metal complexes in a single inert matrix with desired catalytic properties. Further a novel use of these organo-functionalized mesoporous materials were recently demonstrated for size selective entrapment and stabilization of Au nanoprticles from a mixture of Au-Pt colloidal nanoparticles in solution. [122-123]. The above advantages of mesoporous supports attracted our attention for the functionalization and anchoring of metal complexes onto the walls of Si-MCM-41 and Si-SBA-15 with the aim to exploit the heterogeneity of these materials as a substitute of homogeneous systems. In view of the above, the synthesis, characterization and catalytic properties of transition metal complexes of Co, Ru and V containing schiff base ligands such as Salen, Saloph, and Salten encapsulated/anchored on microporous (zeolite Na-Y) and mesoporous materials (MCM-41, SBA-15) are discussed in detail. To understand the chemistry and

catalysis of immobilized catalyst systems on different supports, schiff base Salen and Saloph complexes of Co, Ru and V were synthesized, encapsulated in the cages of zeolite Y and characterized by a wide variety of physico-chemical techniques. These were then tested for their catalytic activities in the oxidation of p-cresol [124], β-isophorone [125], α-pinene [126], styrene and t-stilbene [127]. Details such as, optimization of reaction conditions to obtain higher yields of the desired oxidation products, comparison of the catalytic activities (TOF) with their homogeneous analogues, kinetic and mechanistic studies were essential parts of the present investigation. To study the role and effect of mesoporous support, VO(IV)Saloph complex was immobilized onto Al-MCM-41 and its catalytic activity with respect to conversion of styrene and t-stilbene and selectivities for the desired products were investigated and compared with that of VO(IV)Saloph complex encapsulated in zeolite-Y [127]. A hydrido chloro-triphenyl phosphine complex of ruthenium was immobilized onto amine functionalized Si-MCM-41 and Si-SBA-15 through displacement of a phosphine ligand and its catalytic performance in the hydrogenation of olefins were also investigated [128]. To confirm with our objectives, Salten complex of vanadium was covalently anchored onto the walls of mesoporous materials like MCM-41 and SBA-15 and their performance as catalysts in the oxidation of adamantaine [129] and limonene have been studied in detail. Mechanistic studies under *in situ* conditions have been made to support the stability of the metal complexes in zeolite cages or channels of the mesoporous materials for recycling of catalyst in reactions.

1.7 OUTLINE OF THE THESIS

The thesis has been divided into five chapters.

CHAPTER I: INTRODUCTION

Chapter 1 presents a general introduction to the importance of homogeneous transition metal complexes and the purpose and aim of encapsulation/immobilizing these on different mineral supports like zeolites (Na-Y) and mesoporous materials like MCM-41 and SBA-15. The different methods used for immobilization of these metal complexes are also discussed briefly in this chapter. The necessity of characterizing these heterogenized materials for better understanding of their stability and catalytic activity inside the support is also discussed. The use of these heterogenized complexes for various chemical transformations with special emphasis on oxidation reactions is also described. Finally the scope of the thesis is outlined.

CHAPTER II: SYNTHESIS

This chapter describes the procedure of synthesis of various ligands, (Salen, Saloph and Salten) metal complexes, (Cobalt, Ruthenium and Vanadium) and supports like MCM-41 and SBA-15. The synthesis procedures of materials that have been used as such (i.e.not prepared in the laboratory) have not been mentioned specifically. Various methods of modification of the supports and further the immobilization of these complexes on them are also described.

CHAPTER III: CHARACTERIZATION

This chapter describes the details of the characterization of the above materials by XRD, BET surface area measurement, elemental analysis, TGA/DTA, XPS, FTIR

spectroscopy, UV- Vis spectroscopy, NMR, ESR, XRF, ICP-AES and AAS. A small description of the characterization tools is also mentioned.

CHAPTER IV: CATALYTIC ACTIVITY

Chapter IV is divided into 6 parts (A-F) each part describes the catalytic activity of the catalysts for different substrates.

Part A describes the oxidation of *p*-cresol to *p*- hydroxy benzaldehyde. Co(II)Salen and substituted Salen encapsulated in zeolite –Y were used as catalyst and air was used as an oxidant. The conversion and selectivity for various products using different catalyst have been discussed. The optimization of reaction condition was carried out by varying different reaction parameters.

Part B describes the catalytic activity of Co(II)Saloph and substituted Saloph encapsulated in zeolite-Y for the oxidation of β-isophorone (BIP) to keto isophorone (KIP) using air as oxidant. The reaction conditions have been optimized by varying different parameters.

Part C describes the study on allylic oxidation of α-pinene to corresponding oxygenates. The major product formed is D-Verbenone, which is industrially important for the synthesis of taxol. Apart from the various reaction parameters studies, effect of two different encapsulated metal complexes (Co(II)Saloph and Ru(III)Saloph) encapsulated in zeolite - Y on the rate of oxidation of α-pinene were also studied.

Part D describes the catalytic activity of styrene and *trans*-stilbene using VO(IV)Saloph encapsulated/immobilized on zeolite-Y and Al-MCM-41 using TBHP as oxidant. The mechanistic aspects of the epoxidation reaction have been investigated by *in situ* studies with EPR and UV-Vis spectroscopy. The effect of the support on the structure and its catalytic activity of the complex are also discussed.

Part E describes the oxidation of adamantane to 1-adamantanol and 2-adamantanone using Vanadium Salten complex covalently anchored onto Cl-functionalized MCM-41 using Urea hydroperoxide (UHP) as the oxidizing agent. The use of UHP as an oxidizing agent facilitates slow release of hydroperoxide into the reaction medium and also the use of an anhydrous oxidizing agent for oxidation reaction.

Part F describes the immobilization of a Ruthenium hydrido-chloro triphenyl phosphine complex onto amine functionalized MCM-41 and SBA-15. The effect of immobilization on the structure of the complex has been studied using FTIR and NMR techniques. This catalyst has been used for the hydrogenation of various olefins.

CHAPTER V: SUMMARY AND CONCLUSIONS

Chapter V, presents the overall summary of the work and mentions the major findings of the study followed by conclusions derived from it.

1.8 REFERENCES

1. Pei-Shing Eugene Dai, Catal Today 26 (1995) 3.
2. R. A. Sheldon, J. Mol. Catal. A: General 107 (1996) 75.
3. J. H. Clark and D. J. Macquarrie, Chem. Soc. Rev. 25 (1996) 303.
4. E. R. Hartley, Catalysis by Metal Complexes, Supported Metal Reagents, Reidel, Dordrecht, 1984.
5. P. A. Chaloner, Handbook of Coordination Catalysis in Organic Chemistry, Butterworths, London, 1986 (Chapter 6).
6. R. F. Parton, I. F. J. Vankelecom, M. J. A. Casselman, C. P. Bezoukhanoua, J. B. Uytterhoeven, P. A. Jacob, Nature. 370 (1994) 541.
7. N. Herron. J. Coord. Chem. 19 (1988) 25.
8. N. Herron. Inorg. Chem. 25 (1988) 4714.
9. D. E. De Vos, F. T. Starzyk, P. A. Jacob. Angew Chem. Int. Engl. 33 (1994) 431.
10. N. Herron. Che. Tech. 9 (1989) 542.
11. V. Yu. Zakharov and B. V. Ramanovsky, Vestn. Mosk. Univ., Ser. Khim., 18 (1977) 142. [Eng. Trans in Sov. Mosc. Univ. Bull., 32 (1077) 16].
12. B. V. Ramanovsky, R. E. Mardaleishvili, V. Yu. Zakharov and O. M. Zakharova, Vestn. Mosk. Univ., Ser. 2: khim., 18 (1977) 232.
13. V. Yu. Zakharov and B. V. Ramanovsky, Vestn. Mosk. Univ., Ser. 2: Khim., 18 (1977) 349.
14. V. Yu. Zakharov, O. M. Zakharova, B. V. Ramanovsky and R. E.

Mardaleishvili, React. Kinet. Catal. Lett., 6 (1977) 133.

15. F. Bedioui, E. De Boysson, J. Devynck, K.J. Balkus Jr., J.Chem. Soc. Farady Trans. 87 (1991) 3831.

16. L. Gallion, N. Sajot, F. Bedioui, J. Devynck and K.J.Balkus Jr., J. Electroanalytical Chem. 345 (1993) 157.

17. T. Katsuki. Coord. Chem. Rev. 140 (1995) 189 and the references therein.

18. W. Zhang, J. L. Loebach, S. R. Wilson, E. N. Jacobson, J. Am. Chem. Soc. 112 (1990) 2801.

19. S. Ernst and M. Selle, Microporous Mesoporous Mater. 27 (1999) 355.

20. C. Liv, Y. Shan, X. Xang, X. Ye, Y. Wu, J. Catal. 168 (1997) 35.

21. B. M. Choudhary, M. Laxmikantam, B. Bharathi, P. Sreekanth, F. Figueras, J. Mol. Catal. A: Chemical 159 (2000) 417.

22. S.-S.Kim, W. Zhang and T. J. Pinnavaia, Catal. Lett. 43 (1997) 149.

23. M. Eswaramoorthy, Neeraj and C. N. R. Rao, Chem. Commun. (1998) 615.

24. I. V. Kozhevnikov, A. Sinnema, R. J. J. Jansen, K. Pamin and H. van Bekkum, Catal. Lett. 30 (1995) 241.

25. R. M. Barrer, "Hydrothermal Chemistry of Zeolites" Academic Press**,** New York, (1982).

26. D.W. Breck, *"Zeolite Molecular Sieves"*, Wiley, New York (1974).

27. R. Szostak, "Molecular Sieves: Principles of Synthesis and Identifications", Van Nostrand Reinhold, New York (1989).

28. M. E. Davis, Acc. Chem. Res. 26 (1993) 111.

29. P. G. Schultz, Angew. Chem. Int. Ed. Engl. 28 (1989) 1283.

30. A. Corma, Chem. Rev. 95 (1995) 559.

31. I. W. C. E. Arends, R. A. Sheldon, M. Wallau, and U. Schuchardt, Angew. Chem. Int. Ed. Engl. 36 (1997) 1144.

32. J. M. Thomas, Angew. Chem. Int. Ed. 38 (1999) 3588.

33. M. Taramasso, O. Forlani, G. Manara and B. Notari, U. K. Pat. 2023562 (1979).

34. B. L. Meyers, S. R. Ely, N. A. kutz J. A. Kudak and E. Van den Bossche, J Catal. 91 (1985) 352.

35. B. D. McNicol and G. T. Pott, J. Catal. 25 (1972) 223.

36. R. Kumar and P. Ratnasamy, Catal. Lett. 22 (1993) 227.

37. M. Taramasso, G. Perego and B. Notari, U. S. Pat. 410501 (1983).

38. A. V. Ramaswamy, S. Sivasanker and P. Ratnasamy, Catal. Lett. 22 (1993) 236.

39. Y. Iwasawa: in Tailored Metal Catalysts (D.Reidel Publishing Comp., Holand, 1986).

40. A. Kozlov, K. Asakura and Y. Iwasawa, Microporous and Mesoporous Mater. 21 (1998) 571.

41. M. Ichikawa, Platinum Metals Review. 44 (2000) 3.

42. K. J. Balkus Jr., A. K. Khanmamedova, K. M. Dixonand, F. Bedioui, Applied Catal., A: 143 (1996) 159.

43. C. Bowers and P.K. Dutta. J. Catal. 122 (1990) 271.

44. C. R. Jacob, S. P. Varkey and P. Ratnasamy. App. Catal., A: 168 (1998) 353.

45. S. P. Varkey, C. Ratnasamy and P. Ratnasamy. J. Mol. Catal., A: 135 (1998)

295.

46. C. R. Jacob, S. P.Varkey and P. Ratnasamy. Appl. Catal., A: 182 (1999) 353.

47. V. Yu. Zakharov and B. V. Ramanovsky, Vestn. Mosk. Univ., Ser. 2: Khim., 20 (1979) 78.

48. L. F. Rao, A. Fukuoka and M. Ichikawa, J. Chem. Soc., Chem. Commun., (1988) 458.

49. L. F. Rao, A. Fukuoka, N. Kosugi, H. Kuroda and M. Ichikawa, J. Phys. Chem., 94 (1990) 5317.

50. N. Takahashi, A. Mijin, H. Suematsu, S. Shinoohara and H. Matsuoka, J. Catal., 177 (1989) 348.

51. B. E. Hanson, M. E. Davis, D. Taylor and E. Rode, Inorg. Chem., 23 (1984) 52.

52. P. Gellin, C. Naccache and Y. B. Taarit, Pure Appl. Chem., 60 (1988) 1315.

53. M. Ichikawa, L. F. Rao A. and Fukuoka, Catal. Sci. Tech., 1 (1991) 111.

54. A. Fukuoka, L. F. Rao, N. Kosugi, H. Kuroda and M. Ichikawa, Appl. Catal., A: 50 (1989) 295.

55. P. Peigneur, J. H. Lunsford, W. De. Wilde and R. A. Schoonheydt, J. Phys. Chem. 88 (1977) 1179.

56. S. Kowalak and K. J. Balkus Jr., Collect. Czech. Chem. Commun. 57 (1992) 774.

57. K. J. Balkus Jr., C. D. Hargis and S. Kowalak, ACS Symp. Ser. 499 (1992) 347.

58. C. T. Kresge, M. E. Leonowicz, W. J. Roth, J. C. Vartulli and J. S. Beck, Nature 359 (1992) 710.

59. J. S. Beck, J. C. Vartulli, W. J. Roth, M. E. Leonowicz, C. T. Kresge, K. D. Schmitt, C. T-W. Chu, D. H. Olson, E. W. Sheppard, S. B. McCullen, J. B. Higgins and J. L. Schenker, J. Am. Chem. Soc. 114 (1992) 10834.

60. J. C. Vartulli, C. T. Kresge, M. E. Leonowicz, A. S. Chu, S. B. McCullen, I. D. Johnson and E. W. Sheppard, Chem. Mater, 6 (1994) 2070.

61. A. Sayari, Chem. Mater, 8 (1996) 1840.

62. A. Corma, Chem. Rev. 97 (1997) 2373.

63. J. Y. Ying, C. P. Mehnert and M. S. Wong, Angew. Chem. Int. Ed. 38 (1999) 56.

64. U. Ciesla and F. Schüth, Microporous Mesoporous Mater. 27 (1999) 131.

65. D. Y. Zhao, J. L. Feng, Q. S. Huo, N. Melosh, G. H. Fredrickson, B. F. Chmelka and G. D. Stucky, Science, 279 (1998) 548.

66. X. Feng, G. E. Fryxell, L.-Q. Wang, A. Y. Kim, J. Liu and K. M. Kemner, Science, 276 (1997) 923.

67. L. Mercier and T. J. Pinnavia, Adv. Mater., 9 (1997) 500.

68. A. M. Liu, K. Hidajat, S. Kawi and D. Y. Zhao, Chem. Commun (2000) 1145.

69. H. Takahashi, Bo Li, T. Sasaki, C. Miyazaki, T. Kajino and S. Inagaki, Microporous Mesoporous Mater. 44-45 (2001) 755.

70. C. Huber, K. Moller and T. Bein, Chem. Commun. (1994) 2619.

71. Y-J. Han, G. D. Stucky and A. Butler, J. Am. Chem. Soc. 121 (1999) 9897.

72. X. S. Zhao, G. Q. Lu and G. J. Millar, Ind. Eng. Chem. Res. 35 (1996) 2075.

73. J. S. Beck, J. C. Vartulli G. J. Kennedy, W. J. Roth and S. E. Schramm, Chem.

Mater. 6 (1994) 1816.

74. P. A. Windsor, in: G. W. Gray, P. A. Windsor (Eds.) Liquid Crystals and Plastic Crystals, vol. 1, Ellis Horwood, Chichester (1974).

75. P. Ekwall, in: G. H. Brown (Ed.), Advances in Liquid Crystals, vol. 1, Academic, New York, 1975.

76. C.-F. Cheng, Z. Chan and J. Klinowski, Langmuir 11 (1995) 2815.

77. D. Zhao, Q. Huo, J. Feng, B. F. Chmelka and G. D. Stucky, J. Am. Chem. Soc., 120 (1998) 6024.

78. R. Ryoo, C. H. Ko, and R. F. Howe, Chem. Mater., 9 (1997) 1607.

79. A. Sayari, C. Danumah and I. L. Moudrakovski, Chem. Mater. 7 (1995) 813.

80. C.-F. Cheng, H. He, W. Zhou and J. Klinowski, J. A. S. Goncalves and L. F. Gladden, J. Phys. Chem., 100 (1996) 390.

81. A. Corma, M. T. Navarro and J. P. Pariente, J. Chem. Soc. Chem. Commun., 147 (1994).

82. K. M. Reddy, L. Moudrakovski and A. Sayari, J. Chem. Soc. Chem. Commun., (1994) 1059.

83. A. Jentys, N. H. Pham, H. Vinek, M. Englisch and J. A. Lercher, Microporous Mater. 6 (1996) 13.

84. R. K. Rana and B. Viswanathan, Catal. Lett. 52 (1998) 25.

85. A. Corma, A. Martinez, V. Martinez-Soria, and J. B. Monton, J. Catal. 153 (1995) 25.

86. G. Grubert, J. Rathouky, G. Schulz-Ekloff, M. Wark, and A. Zukal,

Microporous Mesoporous Mater. 22 (1998) 225.

87. A. M. Velarde, P. Bartl, T. E. W. Niessen and W. F.Hoelderich, J. Mol. Catal., A: 157 (2000) 225.

88. W. S. Ahn, D. H. Lee, T. J. Kim, J. H. Kim, G. Seo, and R. Ryoo, Appl. Catal., A: 181 (1999) 39.

89. R. Ryoo, Mi J. Kim, J. M. Kim and S. Jun, Chem. Commun. (1997) 2225.

90. S-C. Shen, and S. Kai, Chem. Lett. (1999) 1293.

91. L. Frunza, H. Kosslick, H. Ladmesser, E. Höft and R. Fricke, J. Mol. Catal. A: 123 (1997) 179.

92. T. Asefa, M. J. Maclachlan, N. Coombs, G. A. Ozin, Nature, 402 (1999) 867.

93. B. F. G. Johnson, S. A. Raynor, D. S. Shephard, T. Mashmeyer, J. M. Thomas, G. Sanker, S. Bromley, R. Oldroyd, L. Gladden and M. D. Mantle, Chem. Commun. (1999) 1167.

94. S. L. Burkett, S. D. Sims, and S. Mann, Chem. Commun. (1996) 1367.

95. M. H. Lim, C. F. Blanford, and A. Stein, J. Am. Chem. Soc. 119 (1997) 4090.

96. D. Brunel, Microporous Mesoporous Mater. 27 (1999) 329.

97. P. Sutra, and D. Brunel, J. Chem. Soc., Chem. Commun. (1996) 2485.

98. W. A Carvalho, M. Wallau, and U. Schuchardt, J. Mol. Catal., A: 144 (1999) 91.

99. T. Maschmeyer, F. Rey, G. Sankar and J. M. Thomas, Nature, 378 (1995) 159.

100. T. Maschmeyer, R. D. Oldroyd, G. Sankar, J. M. Thomas, I. J. Shannon, J. A. Klepetko, A. F. Masters, J. K. Beattie and C. R. A. Catlow, Angew. Chem., Int.

Ed. Engl., 36 (1997) 1639.

101. Y. S. Ko, T. K. Han, J. W. Park and S. I. Woo, Macromol, Rapid Commun., 17 (1996) 749.

102. S. Brunauer, P. H. Emmett, and E. Teller, J. Am. Chem. Soc., 60, 309 (1938).

103. A. Cheenite, Y. L. Page, and A. Sayari, Chem. Mater. 7 (1995) 1015.

104. V. Alfredsson, M. Keung, A. Monnier, G. D. Stucky, K. Unger and F. Schüth, Chem. Commun. 921 (1994).

105. S. Chavan, D. Srinivas and P. Ratnasamy, Topics Catal. 11/12 (2000) 359.

106. S. A. Chavan, D. Srinivas and P. Ratanasamy, J. Catal. 204 (2001) 409.

107. R. F. Parton, L. Uytterhoeven and P. A. Jacobs, Stud. Surf. Sci. Catal. Amsterdam, 59 (1991) 395.

108. B. V. Ramanovsky and A. G. Gabrielov, Mandeleev Commun. (1991) 14.

109. Y. –W. Chan and R. B. Wilson, Preprints, Div of Petroleum Chemistry, J. Am. Chem. Soc., 33(3) (1988) 453.

110. N. Ulagappan, Proceedings of the 31st annual convention of chemists, Varanasi, paper F1 (1994).

111. P. P. Knops-Gerrits, F. T. Starzyk and P. A. Jacobs, Stud. Surf. Sci. Catal. Amsterdam, 84B (1994) 1411.

112. S. Kowalak, R. C. Weiss and K. J. Balkus, Jr., J. Chem. Soc. Chem. Commun. (1991) 57.

113. D. E. De Vos and P. A. Jacobs in Proceedings from ninth international zeolite conference, 2 (1993) 615.

114. C-J. Liu, W. Y. Yu, S-G. Li, C. M. Che, J. Org. Chem, 63 (1998) 7364.

115. J. Diaz, S.G. Li, W. Q. Pang, C. M. Che, Chem. Commun. (1997) 641.

116. J. H. Clerk D. J. Macquarrie, Chem. Commun (1998) 853.

117. J. Chisem, I. C. Chisem, J. S. Rafelt, D. J. Macquarrie, J. H. Clerk Chem. Commun. (1997) 2203.

118. Y. V. S. Rao, D. E. De Vos, T. Bein and P. A. Jacobs, Chem. Commun (1997) 355.

119. C-J. Liu, S-G. Li, W-Q. Pang and C-M. Che, Chem. Commun (1997) 65.

120. E. Armengol, M. L. Cano, A. Corma, H. Garcia and M. T. Navarro, J. Chem. Soc., Chem. Commun. 519 (1995).

121. I. Vankelecom, K. Vercruysse, N. Moens, R. Parton, J. S. Reddy and P. A. Jacobs, Chem. Commun. 137 (1997).

122. P. Mukherjee, C. R. Patra, R. Kumar and M. Sastry, Phys. Chem. Commun., 4 (2001) 24.

123. S. Chilukuri, T. Joseph, S. Malwadkar, C. Damle, S. B. Halligudi, B. S. Rao, M. Sastry and P. Ratnasamy, Stud. Surf. Sci. Catal., " In Press".

124. T. Joseph, C. S. Sajanikumari, S. S. Deshpande and S. Gopinathan, Indian Journal of Chem. 38 (A) (1999) 792.

125. T. Joseph, S. B. Halligudi, C. Satyanarayan, D. P. Sawant and S. Gopinathan, J. Mol. Catal. A: 168 (2001) 87

126. T. Joseph, D. P. Sawant, C. S. Gopinath and S. B. Halligudi, J. Mol. Catal. A: 184 (2002) 289.

127. T. Joseph, D. Srinivas, C. S. Gopinath, and S. B. Halligudi, Catal. Lett., 83, 3-4 (2002) 209.

128. T. Joseph, S. S. Deshpande and S. B. Halligudi, J. Mol. Catal. A: "Communicated".

129. T. Joseph and S. B. Halligudi, J. Mol. Catal. A: "In Press".

CHAPTER 2

SYNTHESIS

2.1 INTRODUCTION

The present chapter deals with the detailed description of the synthesis of ligands (Schiff base), transition metal complexes of Co, Ru and V [1], zeolite-Y encapsulated metal complexes (Co, Ru and V) [2-7], mesoporous materials like pure silicates (Si-MCM-41) alumino-silicate (Al-MCM-41) and a new ordered hexagonal mesoporous silica with thicker walls named Si-SBA-15 [8], functionalized (modified) mesoporous materials (inorganic-organic hybrid materials) (MCM-41/SBA-15/NH_2 and Cl) [9] and metal complexes immobilized and anchored to mesoporous materials [10-11]. The material zeolite Na-Y used as received without any modification is not described specifically.

2.2 EXPERIMENTAL

2.2.1 SYNTHESIS OF LIGANDS

2.2.1.1 Synthesis of Saloph / Salten / Salen and substituted Saloph / Salen ligands

Salicylaldehyde (2.44 g) dissolved in ethanol (25 ml) is added drop by drop to *ortho*-phenylene diamine solution (1.08 g in 25 ml ethanol). The contents were refluxed for 3 h and a bright yellow precipitate of Saloph was obtained. The yellow precipitate was separated by filtration, washed with ethanol and dried in vacuum. It was then recrystalized from ethanol to yield Saloph (3.0 g). The synthesis of Salen / Salten ligands were also carried using a similar procedure, except that an ethanolic solution of ethylene diamine/diethyl triamine were added instead of an ethanolic solution of *ortho*-phenylene diamine. In the case of Salten excess of solvent was removed under vacuum and a dark yellow colored oily product was obtained. Similarly dichloro, dibromo and dinitro Saloph/Salen ligands were synthesized by using the corresponding salicylaldehyde

derivatives. Elemental and melting point analysis confirmed the molecular composition of ligands.

2.2.2 SYNTHESIS OF "NEAT" COMPLEXES

2.2.2.1 Synthesis of "neat" Co(II)Saloph/ Co(II)Salen/ VO(IV)Saloph/ VO(IV)Salten complexes

Cobaltous acetate tetrahydrate (0.83 g) dissolved in ethanol (25 ml) was added to a solution of Saloph (1.05 g in 25ml ethanol) and refluxed for 3 h. On cooling the reaction mixture, dark brown crystals of Co(II)Saloph were obtained (1.5 g). For the synthesis of VO(IV)Saloph/ VO(IV)Salten an ethanolic solution of $VOSO_4.5H_2O$ was used. Dichloro, dibromo and dinitro substitutes of Co(II)Saloph/Salen complexes were prepared using the corresponding ligands. Elemental and spectroscopic analysis confirmed the composition of these metal complexes. The schematic representation of the method of preparation of ligands and complexes is as shown in Scheme - 2.1.

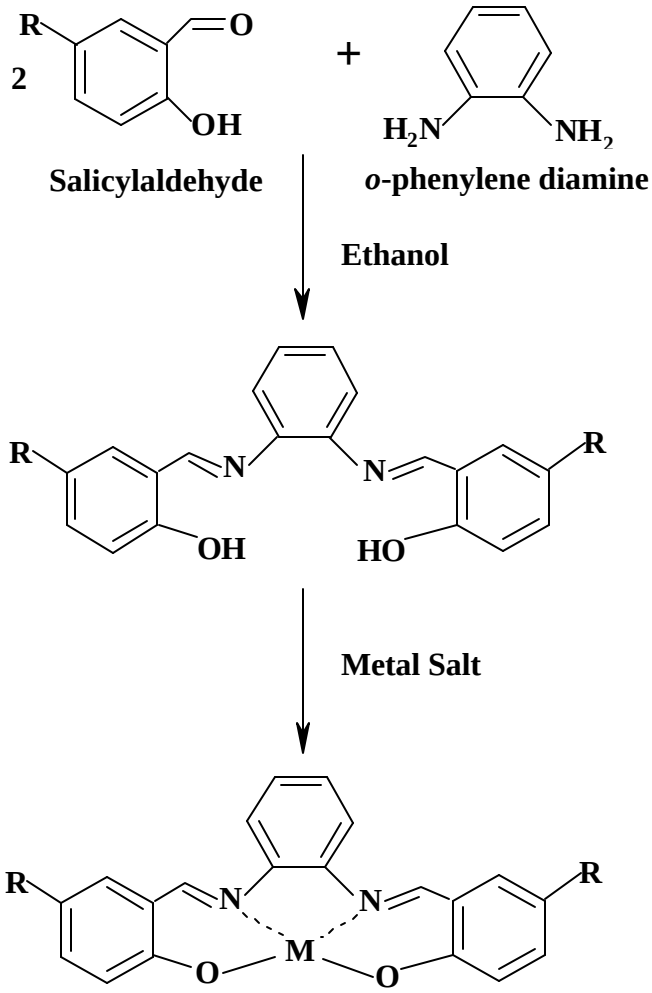

Scheme- 2.1 Synthesis of metal complex

2.2.2.2 Synthesis of $K_2[RuCl_5(H_2O)]$

$K_2[RuCl_5(H_2O)]$ was prepared by following the procedure described elsewhere [12]. A known amount of $RuCl_3.3H_2O$ (0.25 g) was dissolved in 12 M HCl and refluxed for 30 h and to it stoichiometric amount of KCl was added and the solution was stirred with mercury until the solution became green, indicating the formation of Ru(II).

Mercurous chloride formed was removed by filtration. This solution was evaporated to small volume and cooled. The resulting red crystals were separated by filtration, washed with ethanol and recrystallized from 6 M HCl to give $K_2[RuCl_5(H_2O)]$.

2.2.2.3 Synthesis of "neat"[Ru(III)(Saloph)Cl_2] complex

Saloph (0.01 mol) was dissolved in 25 ml ethanol to which $K_2[RuCl_5(H_2O)]$ was added in an equimolar ratio. This mixture was refluxed for 15 h and the reaction mixture was filtered and the filtrate was concentrated to a small volume by evaporating the solvent. To this solution ether was added to precipitate a brown colored complex [Ru(III)(Saloph)]. The purity of the complex was confirmed by FT-IR and melting point.

2.2.2.4 Synthesis of hydrido chlorocarbonyl tris-(triphenylphosphine)ruthenium(II) complex "neat"[RuHCl(CO)(PPh_3)$_3$]

A solution of $RuCl_3.3H_2O$ (2.61 g) in 2-methoxyethanol (200 ml) and aqueous formaldehyde (200 ml, 40% w/v) were added rapidly and successively to a vigorously stirred boiling solution of triphenylphosphine (15.8 g) in the same solvent (300 ml). The mixture was refluxed for 10min, allowed to cool, filtered, washed with ethanol and hexane successively and dried in vacuum to obtain a light cream colored solid in good yield. The purity and structure of the complex was confirmed by melting point *FT-IR* and NMR spectroscopy.

2.2.3 SYNTHESIS OF TRANSITION METAL COMPLEXES IN MICROPOROUS MATERIAL

2.2.3.1 Synthesis of Co(II)-Y/Ru(III)-Y/VO-Y

$Co(OAc)_2.4H_2O$ (3.5 g) was dissolved in warm distilled water (700 ml) to which zeolite Na-Y (Aldrich, 7.5 g) was added and the contents were refluxed for 8 h. The resulting pink colored solid was separated by filtration and washed thoroughly with hot demineralised water till the washings were colorless. The cobalt-exchanged zeolite was dried in air overnight at 383 K. Ru(III)-Y/VO-Y were synthesized by the same procedure using aqueous solution of $RuCl_3.3H_2O$/ $VOSO_4.5H_2O$ for ion exchange.

2.2.3.2 Synthesis of Co(II)Saloph-Y / Ru(III)Saloph-Y/ VO(IV)Saloph-Y by flexible ligand method

Saloph (0.4 g) was dissolved in 80 ml of of *tert*-butanol and to it Co(II)-Y (2.0 g) was added and this mixture was stirred for 16 h at 343 K. The mixture was cooled and the brown solid obtained was separated by filtration, dried and then Soxhlet extracted with *tert*-butanol. It was then treated with 1 M NaCl (50 ml) and refluxed for 3 h to neutralize the charge on the zeolite. After this, the solid product was filtered and washed with warm demineralized water to remove the adsorbed chloride ions. The completion of chloride ion removal was confirmed with $AgNO_3$ solution. The above product was then dried at 383 K for 12 h and the brown solid retained its color. This indicated the retention of complex inside the zeolite super cages. The complex deposited as such by impregnation method on the external surface of the zeolite, was Soxhlet extracted with *tert*-butanol and the zeolite regained its white color, indicating the complete removal of complex from the external surface of zeolite. These experiments indicated the location of complex inside the pores of

the zeolite and not on the external surface. This was verified in preparation of all zeolite-Y exchanged complexes. Similarly, other substituted Saloph of cobalt, Co(II)Cl-Saloph-Y, Co(II)Br-Saloph-Y and Co(II)nitro-Saloph-Y catalysts were also prepared by treating Co(II)-Y with respective ligands by following the above flexible ligand method. Ru(III)Saloph-Y and VO(IV)Saloph-Y was synthesized using the corresponding metal exchanged zeolite.

2.2.3.3 Synthesis of Co(II)Salen– Y/ substituted Salen-Y by flexible ligand method

The Salen ligand (3 g) was melted in a round bottom flask kept in an oil bath at 160°C. To the molten Salen was added Co(II)-Y (1 g) and the contents were kept at the same temperature for 24 h. The molten mass was then cooled to get a brown solid, which was powdered, and Soxhlet extracted with methylene chloride. The product was then refluxed with 0.1 M NaCl solution for 4 h to remove the charge on the zeolite. The solid was then washed with hot water till free from chloride ions. Similarly the substituted Salens were encapsulated using the above procedure.

2.2.4 SYNTHESIS OF MESOPOROUS MATERIALS

2.2.4.1 Synthesis of Al-MCM-41

Al-MCM-41 was synthesized by, taking the molar composition of the synthesis gel - SiO_2 : 0.01 Al_2O_3 : 0.33 TMAOH : 0.55 CTAB : 60H_2O. To 20.8 g of TEOS, a solution of TMAOH (12.08 g in 10 ml distilled water) was added drop-wise, and the mixture was allowed to stir for 1 h. Then, 0.233 g of sodium aluminate in 10 ml water was added. After 1 h of stirring, a solution of CTAB (27.33 g in 88 ml water) was added drop-wise. The mixture was stirred overnight. The gel was transferred to a teflon-lined autoclave and kept

at 373 K for 5 days. The solid Al-MCM-41 obtained was filtered, washed and dried at 373 K and then calcined at 823 K for 8 h. Si/Al ratio was found to be 38 (XRF).

2.2.4.2 Synthesis of Si-MCM-41

TMAOH(12.08 g) in 10 ml distilled water was added under constant stirring to 20.8 g of TEOS and the mixture was allowed to stir for 1h. Then a solution of CTAB(27.33 g) in 98 ml water was added drop wise. The composition of the resultant gel was SiO_2 : 0.33 TMAOH : 0.55 CTAB : 60 H_2O. This mixture was stirred overnight. The gel was transferred to a Teflon-lined autoclave and kept at 373 K for 5 days. The solid SiMCM-41 obtained was filtered, washed and dried at 373 K in air and then calcined at 823 K for 8 h in nitrogen and then kept at this temperature for 6 h in air.

2.2.4.3 Synthesis of Si-SBA-15

SBA-15 has been synthesized from a typical synthesis batch with the composition of 4 g Pluronic P123 [EO_{20}-PO_{70}-EO_{20}], 120g of 2M HCl and 9 g TEOS. Typically 4 g of triblock co-polymer [EO_n-PO_m-EO_n] was dispersed in 30 g distilled water and stirred for 3 h. To the resultant solution 120 g of 2M HCl was added under stirring and finally 9 g of TEOS was added drop wise and the mixture was maintained at 313 K for 24 h under stirring and then for 48 h at a temperature of 383 K under static condition in a polypropylene bottle. The crystallized product was filtered, washed with warm distilled water and dried at 383 K for 24 h and then calcined at 813 K in nitrogen for 12 h and then maintained at 813 K in air for 5 h to completely remove the template. The structure was confirmed by XRD and surface area.

2.2.5 SYNTHESIS OF TRANSITION METAL COMPLEXES IN MESOPOROUS MATERIALS

2.2.5.1 Preparation of VO-Al-MCM-41

VO-Al-MCM-41 was prepared by ion exchanging 2 g of Al-MCM-41 with an aqueous solution (150 ml) of $VOSO_4.5H_2O$ (1 g).

2.2.5.2 Preparation of VO(IV)Saloph-Al-MCM-41

To a solution of 0.4 g of Saloph dissolved in 80 ml *tert*-butanol, 2 g of VO-Al-MCM-41 was added. The suspension was refluxed for 8 h. The solid was filtered out and Soxhlet extracted with *tert*-butanol.

2.2.6 ANCHORING OF TRANSITION METAL COMPLEXES

2.2.6.1 Synthesis of NH_2/Cl modified MCM-41 and SBA-15

In a typical surface modification process activated Si-MCM-41 and Si-SBA-15 (3 g, 423 K) under vacuum was refluxed in toluene (50 ml distilled over freshly cut sodium and dried over zeolite A) with 3-aminopropyl triethoxysilane (APTES) (3g) / 3-chloropropyl triethoxysilane (CPTES) (3 g) for 3 h under argon atmosphere. The separated solid was washed with diethyl ether and Soxhlet extracted with 250 ml dichloromethane yielding covalently anchored 3-amino/chloropropyl triethoxysilane moieties NH_2/Cl-MCM-41/ NH_2/Cl-SBA-15 (Scheme- 2.2).

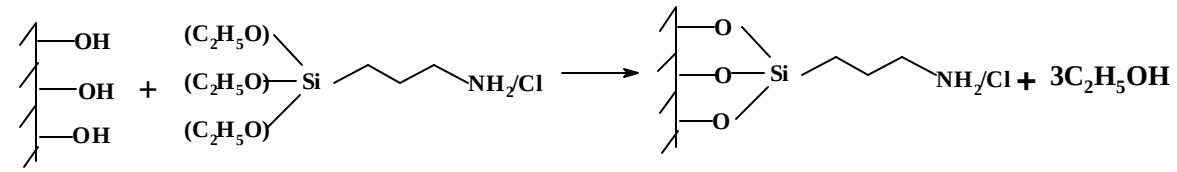

MCM-41/SBA-15 APTES/CPTES

Scheme-2.2 Synthesis of covalently anchored 3-amino/chloropropyl triethoxysilane moieties.

2.2.6.2 Immobilization of [RuHCl(CO)(PPh$_3$)$_3$] over NH$_2$-MCM-41/ NH$_2$-SBA-15

To a suspension of freshly activated NH_2-MCM-41/ NH_2-SBA-15 (1 g) in dry toluene (40 ml) a solution of [RuHCl(CO)(PPh_3)$_3$] (0.1 g) in anhydrous toluene (10 ml) was added and the resulting solution was refluxed for 3 h and the separated solid was Soxhlet extracted with anhydrous toluene and vacuum dried for 24 h to obtain [RuHCl(CO)(PPh_3)$_2$]-NH_2-MCM-41and [RuHCl(CO)(PPh_3)$_2$]-NH_2-SBA-15 (Scheme-2.3).

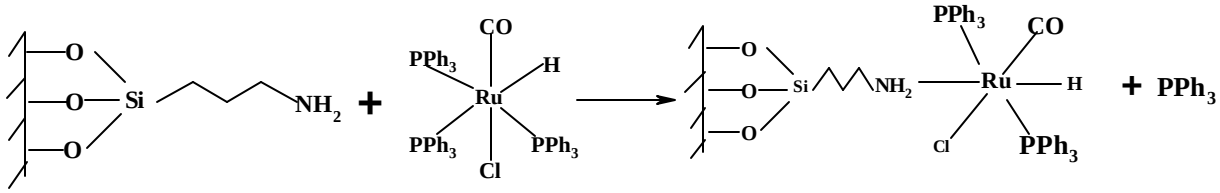

Scheme-2.3 Immobilization of [RuHCl(CO)(PPh_3)$_3$] over NH_2-MCM-41/ NH_2-SBA-15

2.2.6.3 Covalent anchoring of VO(IV)Salten over Cl-MCM-41/Cl-SBA-15

To a suspension of freshly activated Cl-MCM-41/Cl-SBA-15 (1 g) in dry toluene (40 ml) a solution of Salten ligand (0.1 g) in anhydrous toluene (10 ml) was added and the resulting solution was refluxed for 3 h and the separated yellow colored solid was Soxhlet extracted with anhydrous toluene to remove the unreacted Salten ligand adsorbed on the

external surface of Cl-MCM-41/Cl-SBA-15 and vacuum dried for 24 h. Then to a suspension of this solid (1 g) in dry ethanol (40 ml) a solution of $VOSO_4.5H_2O$ (0.1 g) in anhydrous ethanol (25 ml) was added. The solution immediately turned green indicating the formation of a vanadium complex (Scheme-2.4). This was refluxed for 3 h. The green solid was separated by filtration, was dried and Soxhlet extracted with dry ethanol to remove any unreacted vanadium from the surface.

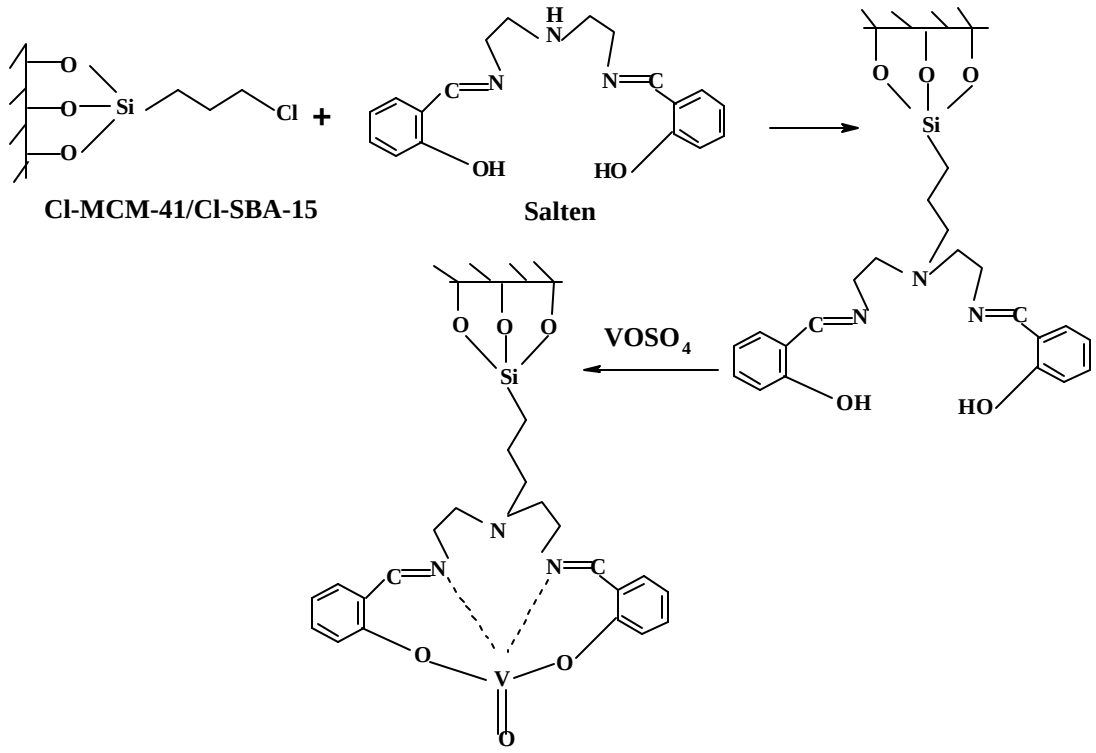

Scheme-2.4 *Covalent anchoring of VO(IV)Salten over Cl-MCM-41/Cl-SBA-15*

2.3 REFERENCES

1. R. H. Bailes and M. Calvin, J. Am. Chem. Soc. 69 (1947) 1886.
2. N. Herron Inorg. Chem. 25 (1986) 4714.
3. K. Putyera, G. Plesch, L. Benco, J. Dobrovodsky, A. V. Tchuvaev, V.I. Nefedov and M. Zikmund, Proc. 12th Conf. Coord. Chem., 295 (1990).
4. F. Bedioui, E. DeBoysson, J. Devynck and K. J. Balkus Jr., J. Chem. Soc., Farad. Trans., 87 (1991) 3831.
5. F. Bedioui, L. Roue, L. Gaillon, J. Devynck, S. L. Bell and K. J. Balkus Jr., Petrol. Preprints, 38 (1993) 529.
6. N. Ulagappan, Proceedings of the 31st annual convention of chemists, Varanasi, paper F1 (1994).
7. K.J. Balkus Jr., A.K. Khanmamedova, K.M. Dixon and F. Bedioui, Appl. Catal. A: 143 (1996) 159.
8. D. Y. Zhao, J. L. Feng, Q. S. Huo, N. Melosh, G. H. Fredrickson, B. F. Chmelka and G. D. Stucky, Science, 279 (1998) 548.
9. P. Sutra, D. Brunel, Chem. Commun. (1996) 2485.
10. D. Brunel, F. Fajula, J. B. Nagy, B. Deroide, M. J. Verhoef, L. Veum, J. A. Peters and H. van Bekkum, Appl. Catal. A: 213 (2001) 73.
11. C-J. Liu, S-G. Li, W-Q. Pang and C-M. Che, Chem. Commun. (1997) 65.
12. T. L. Barr. " Practical surface analysis, Volume 1" (D. Briggs and M. P. Seah, Eds.) p 412, Wiley, New York.

CHAPTER 3

CHARACTERIZATION

3.1 INTRODUCTION

Microporous and mesoporous materials need to be characterized to elucidate their structural features, pore architecture and catalytic behavior. A complete charaterization of such materials require information from a number of physical, chemical and spectroscopic techniques. Characterization of encapsulated metal complex requires the use of various techniques in tandem to characterize the real state of the encapsulated compounds and of the support used for encapsulation. Characterization gives information about any unreacted or uncomplexed remnants of either the metal ion or ligand, the location of the complex and the preservation of the structure and crystallinity of the support.

3.2 EXPERIMENTAL

3.2.1 Chemical analysis

The C, H & N analysis of "neat" and encapsulated/immobilized complex was done on a Carlo Erba (Model EA 1108) elemental analyzer. Si and Al contents were estimated by wavelength dispersive XRF spectrometer (Rigaku 3670E). An atomic absorption spectrometer (AAS, Hitachi Model Z-8000) and an inductively coupled plasma atomic emission spectrometer (ICP-AES) estimated the metal content in the samples. A known amount of the encapsulated complex was digested in a mixture of hydrochloric acid and nitric acid in a volumetric flask till the entire complex leaches out of the support. Then the solution was made upto the mark of the volumetric flask with distilled water and was then analyzed for cobalt and vanadium by atomic absorption spectroscopy. A solution was made in a similar manner for ruthenium and the ruthenium content was analyzed by inductively coupled plasma atomic emission spectrometer (ICP-AES).

3.2.2 X-ray diffraction

The encapsulated/immobilized samples of Na-Y and MCM-41 were analyzed for phase identification on a computer controlled X-ray powder diffractometer (Rigaku Model D/MAX III VC, Japan). Ni filtered CuKα radiation (λ=1.504 Å) was used with a curved graphite crystal monochromater and a NaI scintillator. All measurements were made at room temperature. The powder X-ray diffraction patterns of the SBA-15 materials were collected on a SIEMENS D5005 diffractometer using CuKα (λ = 0.154 nm) radiation. Data were collected in the 2θ range 5-40 degrees at a scan rate of 4°/min in the case of microporous (zeolite –Y) materials and in the 2θ range 1.5-15 degrees at a scan rate of 1°/min in the case of MCM-41 type materials and in the 2θ range 0-10 degrees at a scan rate of 1°/min in the case of SBA-15 type materials. Silicon was used as the internal standard for calibrating the instrument. The d values and the relative intensities I/I_0 of the peaks were calculated. The catalysts were finely powdered before they were loaded in the sample compartment.

3.2.3 Sorption studies

The textural properties of the immobilized complexes were determined from N_2 adsorption isotherms measured on an Omnisorb 100 CX Coulter instrument. Prior to the adsorption measurements, the samples were activated at 373 K for 12 h, in high vacuum (1.33×10^{-6} Pa). After evacuation the samples were cooled at room temperature and the weight was taken. The samples were then cooled to 78 K using liquid nitrogen and then nitrogen was allowed to adsorb on them. The volume of nitrogen adsorbed (cc.g at STP) and the BET surface areas were then measured.

3.2.4 Infrared spectroscopy

The Infrared spectra were recorded using a Shimadzu (Model 8201PC) spectrophotometer in a frequency range 4000-400 cm^{-1}. Nujol and flurolube were used as the mulling agent. Band intensities were expressed as transmittance (T). The spectra of the complex immobilized on mesoporous samples were recorded after drying them over toluene to remove even trace amount of water.

3.2.5 Nuclear Magnetic Resonance (NMR) Spectroscopy

The structure of the "neat" and the complex inside the mesoporous materials was characterized by MAS NMR spectroscopy (Bruker DSX-300 spectrometer). The ^{1}H NMR and ^{31}P NMR spectrum of the "neat" complex was recorded immediately after dissolution of the complex in $CDCl_3$ with the residual protons of the solvent as internal reference (for ^{1}H NMR spectra) and with H_3PO_4 as external reference for ^{31}P NMR spectra.

3.2.6 Electron Spin Resonance (ESR) Spectroscopy

ESR spectra were recorded at 77 and 298 K on a Bruker EMX spectrometer operating at X band frequency ($\nu \approx 9.78$ GHz) and 100 kHz field modulation. ESR spectral simulations and manipulations were done using the Bruker Simfonia and WINEPR software packages.

3.2.7 X-ray photoelectron spectroscopy

XPS spectra are recorded on a VG Microtech Multilab – ESCA 3000 spectrometer equipped with a twin anode of Al and Mg. All measurements are made on as received powder samples using Mg Kα X-ray at room temperature. Base pressure in the analysis chamber was $4x10^{-10}$ Torr. Multi channel detection system with 9 channels is employed to collect the data. The overall energy resolution of the instrument is better than 0.7 eV, determined from the full width at half maximum of the $4f_{7/2}$ core level of gold surface. The

errors in all the BE values were within ±0.1 eV. AlKα (1486.6 Å) was used for excitation and photoelectron kinetic energy was increased with reference to the Fermi energy. The samples were ground to a fine powder and a homogeneous mixture was made with isopropanol. It was deposited in a nickel strip for analysis. The peaks were resolved after background subtraction and a gaussian equation as used to fit the curves.

3.2.8 Transmission electron microscopy

The structure of the mesoporous materials was confirmed using TEM (JEOL Model 1200 EX). It has been used to provide information of mesoporous materials at near atomic resolution. A fine suspension of the sample was made in acetone and was mounted on a copper grid. Images were recorded on conventional sheet films.

3.2.9 Thermal analysis

TG and DTA analysis of the neat and zeolite encapsulated metal complexes were recorded on Rheometric Scientific (STA 1500) Analyzer. The thermograms of the samples were recorded taking 30 mg of the sample and heating at a rate of 5°/min in N_2 atmosphere. A known weight of the encapsulated complex was taken in a platinum crucible with lid and heated at 393 K to get the dry weight of the sample. The sample was weighed after equilibration. The difference in weights gives the loss on heating.

3.3 RESULTS AND DISCUSSION

3.3.1 Chemical analysis

Table 3.1

Metal content of the encapsulated/immobilized complexes

Catalyst	Metal Wt. %
Co(II)-Y	2.47
Ru(III)-Y	2.6
VO-Y	2
Co(II)Saloph-Y	1.5
Co(II)Cl-Saloph-Y	1.1
Co(II)Br-Saloph-Y	1.09
Co(II)Nitro-Saloph-Y	1
Ru(III)Saloph-Y	2.11
VO(IV)Saloph-Y	1.46
VO(IV)Saloph-Al-MCM-41	2.14
VO(IV)Salten -Si-MCM-41	0.8
VO(IV)Salten -Si-SBA-15	1.2
$[RuHCl(CO)(PPh_3)_2]$-NH_2-MCM-41	0.88
$[RuHCl(CO)(PPh_3)_2]$-NH_2-SBA-15	1.3

3.3.2 X-ray diffraction

X-ray diffraction (XRD) is used for the identification of the phase and the purity of the zeolite matrix. It also provides information on the change in the unit cell and

morphological parameters arising as a result of encapsulation of the transition metal complexes. XRD evaluates the integrity and crysallinity of the support matrix around the transition metal complex.

Figure. 3.1 shows the XRD patterns of VO-Y, VO(IV)Saloph-Y, Al-MCM-41 and VO(IV)Saloph-Al-MCM-41. No appreciable loss in crystallinity was observed as a consequence of metal complex encapsulation. However, changes were noticed in the intensities of (331), (311), (220) peaks of zeolite-Y. In NaY (not shown) and VO-Y (Figure 3.1 a), the relative intensities of the peaks varied in the order: (331) > (220) > (311) indicating a random distribution of the exchangeable cations within the zeolite lattice. However, in VO(IV)Saloph-Y (Figure 3.1 b), the peak intensities varied in the order: (331) > (311) > (220) suggesting displacement of cations in the supercages by the Saloph complexes [1]. The XRD patterns of Al-MCM-41 and VO(IV)Saloph-Al-MCM-41 reveal that the mesoporous structure is retained even after the encapsulation (Figure 3.1 c and d.

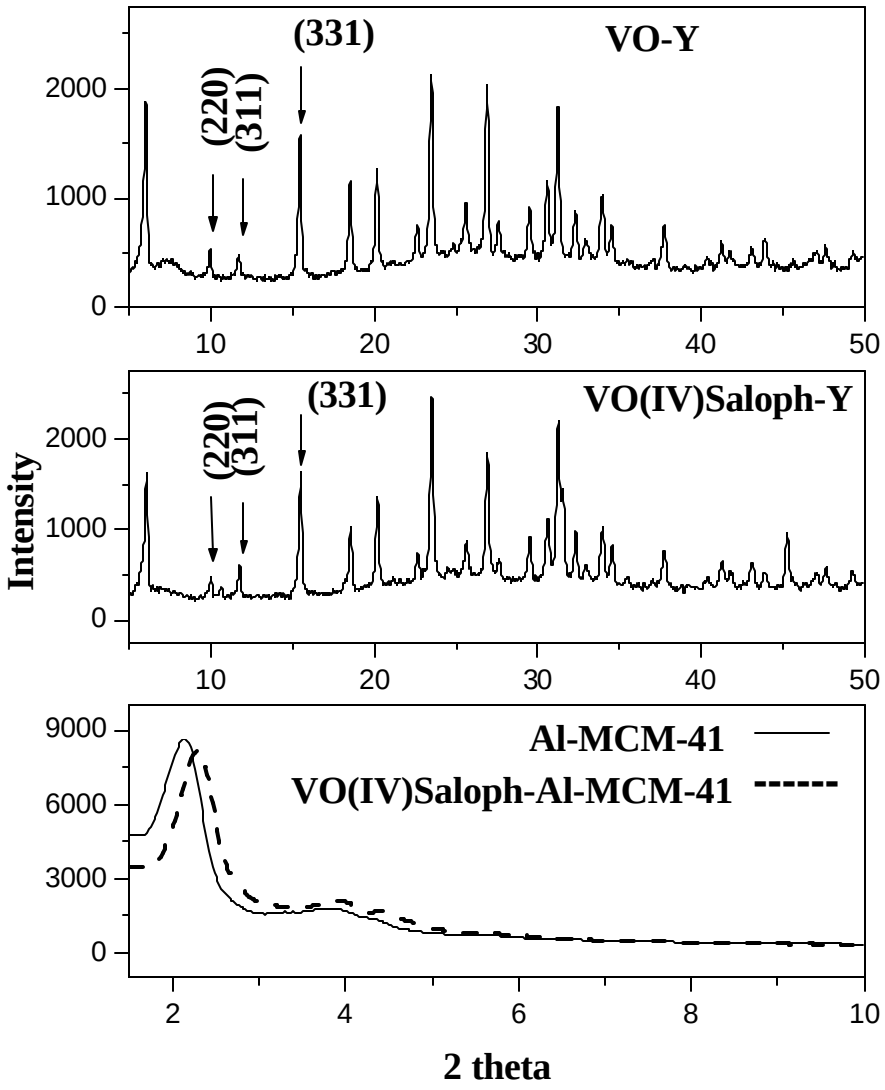

Figure 3.1 XRD patters of (a) VO-Y, (b) VO(IV)Saloph-Y, (c) Al-MCM-41 and (d) VO(IV)Saloph-Al-MCM-41.

Figure 3.2 shows the XRD patterns of Si-MCM-41, Cl-Si-MCM-41 and VO(IV)Salten-Si-MCM-41. XRD pattern of Si-MCM-41 (Figure 3.2 a) shows a very intense peak assigned to reflections at (100) and two additional peaks with low intensities

at (110) and (200) reflections respectively which can be indexed to hexagonal lattice. Some loss in the intensities of the peaks was observed upon modification with 3-CPTES (Figure 3.2 b), which shows that though there is some reduction in the crystallinity of Si-MCM-41, the mesoporosity of Si-MCM-41 is retained. No further loss in the intensity of the peak at

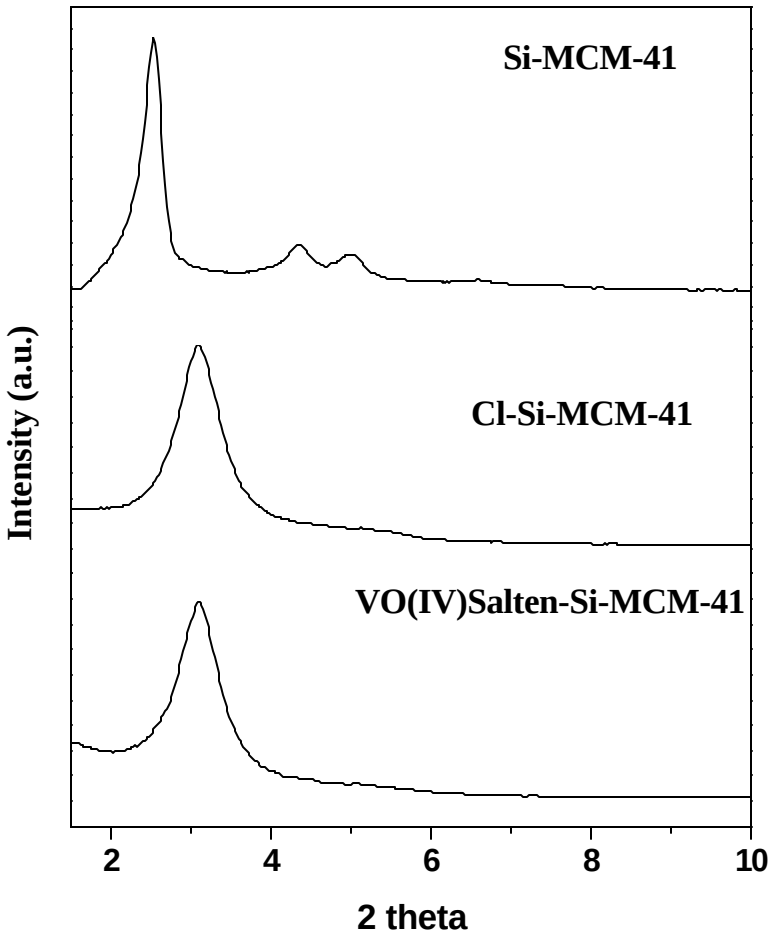

Figure 3.2 XRD patters of (a) Si-MCM-41, (b) Cl-Si-MCM-41, (c) VO(IV)Salten-Si-MCM-41.

(100) reflection was observed on immobilizing VO(IV)Salten complex onto Si-MCM-41-VO(IV)Salten (Figure 3.2 c). However the peaks at (110) and (200) reflections were not observed upon modification.

Figure 3.3 (a-e) shows the XRD patterns of Si-MCM-41, NH_2-MCM-41, [RuHCl(CO)(PPh_3)$_2$]-NH_2-MCM-41, physical mixture of Si-MCM-41 and [RuHCl(CO)(PPh_3)$_3$] and "neat"-[RuHCl(CO)(PPh_3)$_3$]. The XRD pattern of Si-MCM-41 (Figure 3.3 a) shows peaks typical of Si-MCM-41. It is seen that upon functionalization with APTES the intensities of the peaks decrease significantly (Figure 3.3 b). No significant further loss in the intensities is observed after immobilization of the ruthenium complex (Figure 3.3 c). However the peaks at (110) and (200) reflections were not observed upon immobilization of complex. However the XRD pattern of the physical mixture of Si-MCM-41 and the ruthenium complex shows some peaks other than that of MCM-41 which can be indexed to that of the neat complex (Figure 3.3 d). The XRD pattern of "neat"-[RuHCl(CO)(PPh_3)$_3$] is depicted in (Figure 3.3 e).

The XRD patterns on Si-SBA-15, NH_2-SBA-15 and [RuHCl(CO)(PPh_3)$_2$]-NH_2-SBA-15 are depicted in the Figure 3.4 (a-c). The XRD diffraction pattern of Si-SBA-15 shows a very intense peak (100) and two additional high order peaks with lower intensities (Figure 3.4 a), indicating a significant degree of long range ordering of the structure and well formed hexagonal pore arrays. Some loss in the intensities of the peaks was observed upon modification with APTES revealing that silylation has indeed occurred inside the mesopores of Si-SBA-15 (Figure 3.4 b). However it is evident from XRD that in addition to the very intense peak (100) the two higher order peaks were still observed indicating that the silylation procedure did not diminish the structural ordering of Si-SBA-15. No

significant loss in the intensity was observed on immobilizing the ruthenium complex (Figure 3.4 c). This indicates that the structure of Si-SBA-15 is retained when the ruthenium complex is dispersed in the channels.

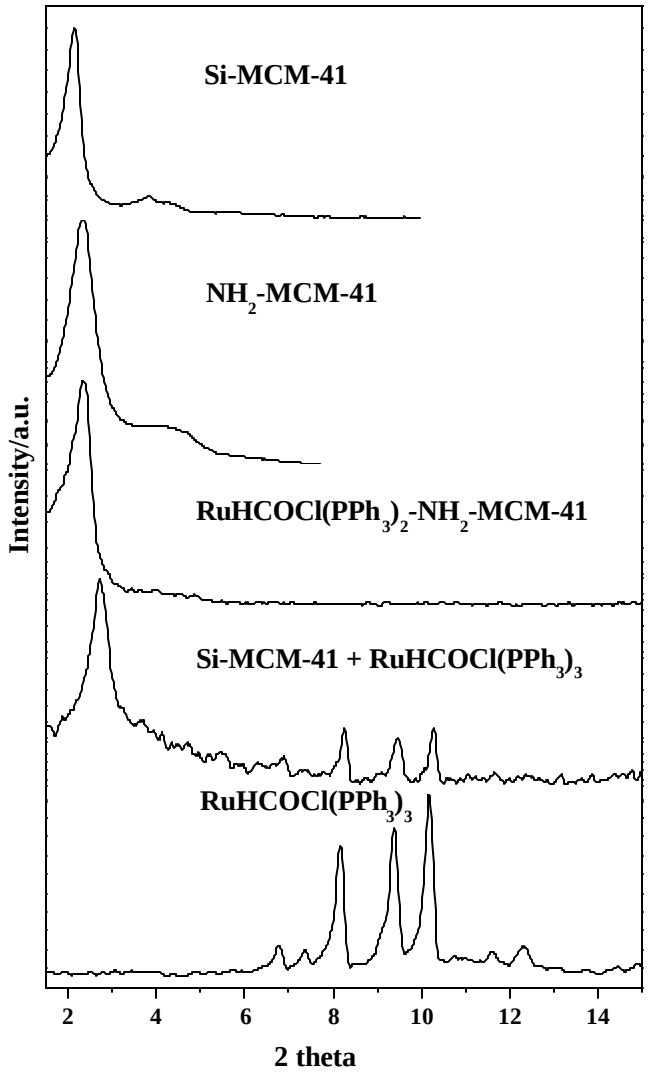

Figure 3.3 XRD profiles of (a) Si-MCM-41, (b) NH_2-MCM-41, (c) [$RuHCl(CO)(PPh_3)_2$]-NH_2-MCM-41, (d) Si-MCM-41+[$RuHCl(CO)(PPh_3)_3$], and (d) "neat" [$RuHCl(CO)(PPh_3)_3$].

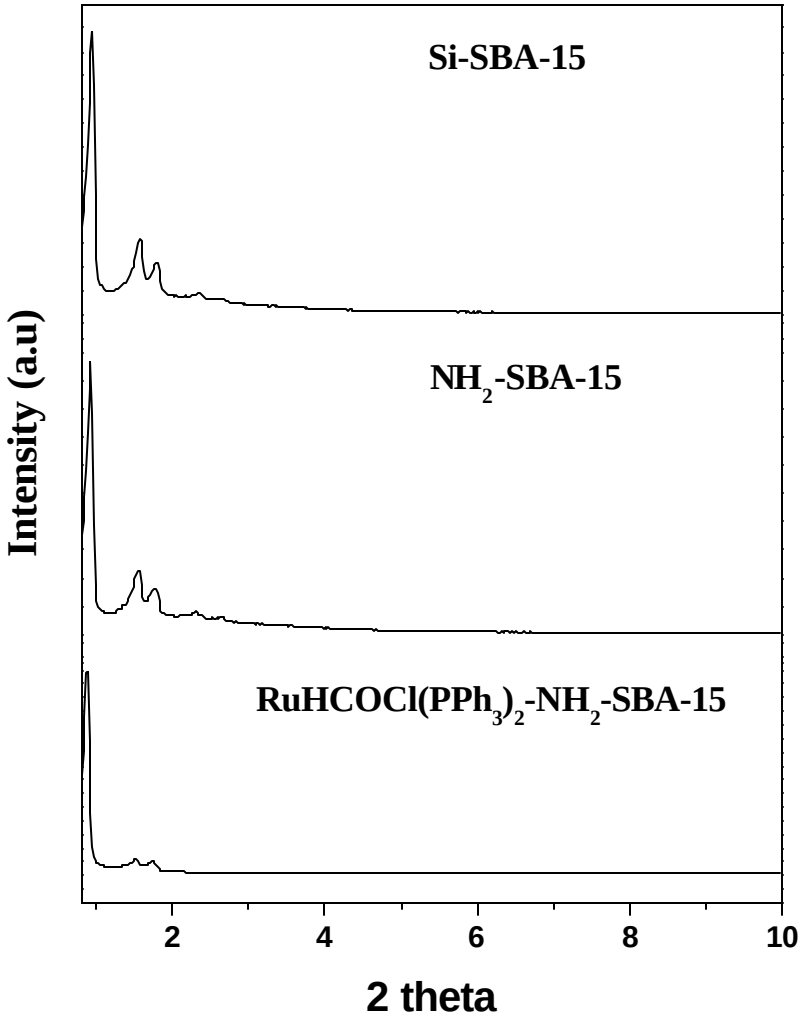

Figure3.4 XRD profiles of (a) Si-SBA-15, (b) NH_2-SBA-15, and (c) [RuHCl(CO)(PPh_3)$_2$]-NH_2-SBA-15.

3.3.3 Sorption studies

The textural properties (surface area, pore volume and average pore diameter) of the encapsulated/immobilized complexes can be determined from the N_2-sorption studies.

A significant reduction in the adsorption capacity should follow immobilization. If the complexes are merely adsorbed on the external surface of the support there may not be significant difference in the surface area/pore volume values. Similarly, reduction in the surface area and pore volume is observed on encapsulation of phthalocyanines and porphyrin complexes in zeolite-X and Y [2-3].

Nitrogen adsorption data for the various immobilized complexes onto microporous and mesoporous materials is presented in the table 3.2

Table 3.2

Surface area and pore volume of catalysts

Catalyst	Surface area ($m^2\ g^{-1}$)	Pore volume(ml g^{-1}) Pore Diameter (Å)
Na-Y	836.3	0.42
Co(II)-Y	554.0	0.23
Ru(III)-Y	546.0	0.24
VO-Y	549	0.31
Al-MCM-41	950	23 (Å)
Si-MCM-41	1000	33 (Å)
Si-SBA-15	980	90 (Å)
Cl-MCM-41	850	24 (Å)
Cl-SBA-15	820	80 (Å)
NH_2-MCM-41	600	20 (Å)

NH_2-SBA-15	800	80(Å)
Co(II)Saloph -Y	442	0.21
Co(II)Cl-Saloph - Y	484	0.20
Co(II)Br-Saloph - Y	475	0.20
Co(II)Nitro-Saloph -Y	369	0.17
Ru(III)Saloph-Y	458	0.23
VO(IV)Saloph-Y	473	0.24
VO(IV)Saloph-Al-MCM-41	540	11 (Å)
VO(IV)Salten-MCM-41	700	16 (Å)
VO(IV)Salten-SBA-15	660	76 (Å)
[RuHCl(CO)(PPh_3)$_2$]-NH_2-MCM-41	260	11 (Å)
[RuHCl(CO)(PPh_3)$_2$]-NH_2-SBA-15	630	73 (Å)

Upon encapsulating VO(IV)Saloph, the surface area of zeolite-Y and Al-MCM-41 decreased from 836 to 473 m^2/g and from 950 to 540 m^2/g, respectively. Also a decrease in pore volume of zeolite-Y from 0.42 to 0.24 ml/g was observed. The average pore diameter of Al-MCM-41 decreased from 23 (in Al-MCM-41) to 11 Å. The reduction in the pore diameter is due to pore blockage by VO(IV)Saloph molecules. The N_2 adsorption and XRD studies confirm the formation and presence of VO(IV)Saloph in the cages of zeolite-Y and Al-MCM-41.

On modifying Si-MCM-41 with 3-CPTES the surface area of Si-MCM-41 decreased from 1000 to 850 m^2/g and the pore size reduced from 33 (Å) to 24 (Å). Upon immobilizing VO(IV)Salten, a further reduction in the surface area from 850 to 700 m^2/g

and pore size from 2.4 to 1.6 nm was observed. The reduction in the surface area and pore size is due to the lining of the walls of Si-MCM-41 with the organic moieties. Similar trend has also been observed previously [4].

In the case of SBA-15 a decrease in the surface area from 980 m^2/g to 800 m^2/g and decrease in pore size from 90 Å to 80 Å was observed on modification with APTES. Further decrease in the surface area from 800 to 630 m^2/g and pore size from 80 Å to 73 Å was observed upon immobilization of NH_2-SBA-15 with the ruthenium complex. The N_2 adsorption and XRD studies confirm the presence of ruthenium complex inside the channels of NH_2-MCM-41 and NH_2-SBA-15.

3.3.4 Infrared spectroscopy

The FT-IR spectra (Figure 3.5) confirmed the formation and integrity of VO(IV)Saloph complexes inside zeolite-Y and Al-MCM-41. The assignments of a few representative bands are given in Table 3.3. In the spectra of zeolite-encapsulated complexes the bands due to VO(IV)Saloph were weak and masked by the zeolite bands due to the low concentration of the former. However, in VO(IV)Saloph -Al-MCM-41 the ligand vibrational bands were comparatively more intense. The marginal shift in the position of the bands corresponding to C=N, C-O and C=C (Table 3.3) indicates changes in the geometry of VO(IV)Saloph as a consequence of encapsulation. Such shift in band positions due to encapsulation was reported earlier also in other Schiff base and phthalocyanine complexes [5-7]. In case of Cu(Saloph) and Mn(Saloph) complexes the bands due to ν(C-O) occurred at 1339 and 1284 cm^{-1} [8].

Table 3.3

FT-IR bands of VO(IV)Saloph complexes

Catalyst	FT-IR bands (cm^{-1})			
	ν(C=N)	ν(C=C)	ν(C-O)	Ring
"neat"VO(IV)Saloph	1600	1572	1370	1530, 1456
VO(IV)Saloph-Y	1572	1577	1377	1527, 1461
VO(IV)Saloph-Al-MCM-41	1604	1578	1377	1531, 1458

However, in VO(IV)Saloph this band appeared at 1370 cm^{-1} (Table 3.3). The shift in the band position towards lower energy side (VO(IV)Saloph >Cu(Saloph)>Mn(Saloph) suggests that the metal-ligand bond is more covalent in VO(IV)Saloph than in Cu(Saloph) and Mn(Saloph) complexes. Further, appearance of ν(C-O) at still higher frequencies (1377 cm^{-1}) in encapsulated complexes points out a greater amount of charge delocalization onto the ligands.

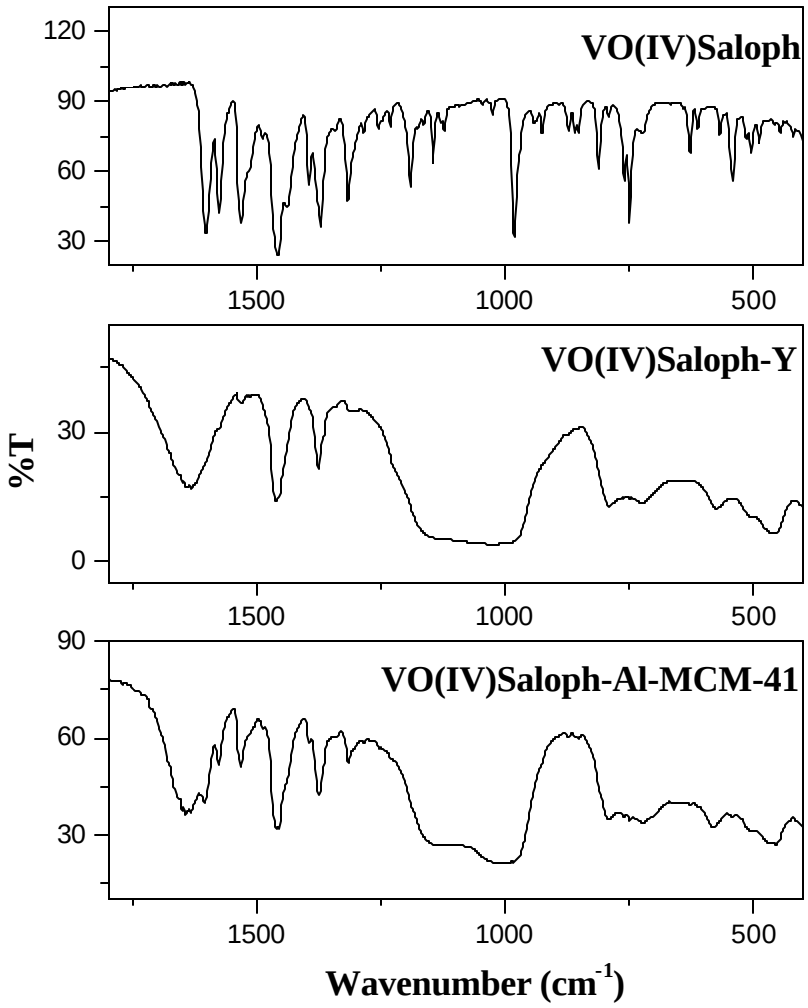

Figure 3.5 FT-IR spectra (Nujol mull): (a) "neat" VO(IV)Saloph, (b) VO(IV)Saloph-Y and (c) VO(IV)Saloph-Al-MCM-41.

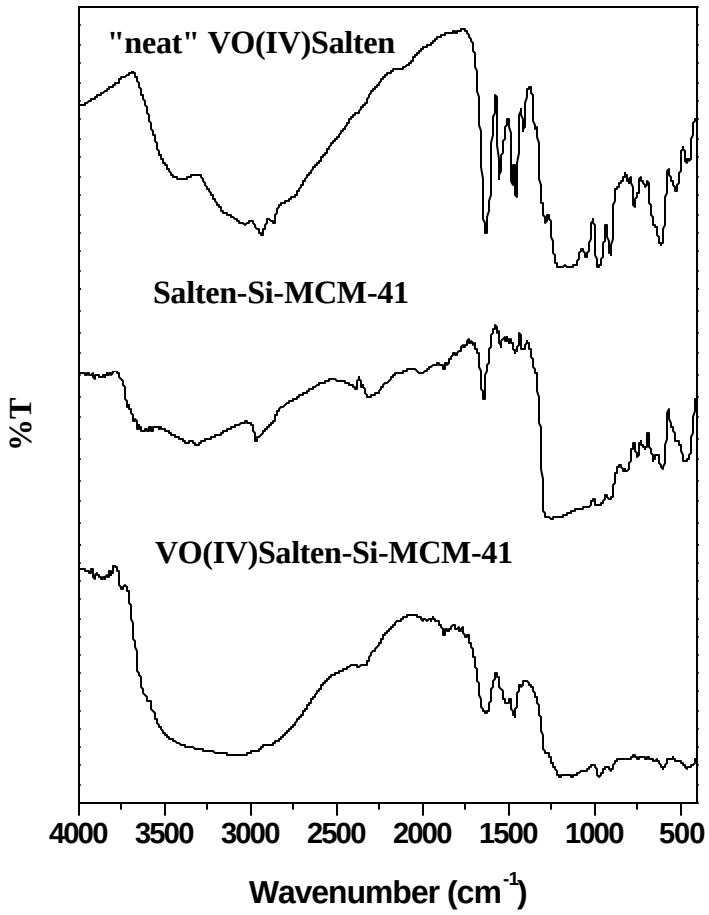

Figure 3.6 FT-IR spectra (a) "neat" VO(IV)Salten, (b) Salten-Si-MCM-41, (c) VO(IV)Salten-Si-MCM-41.

The FTIR spectra (Figure 3.6) confirms the formation and integrity of VO(IV)Salten complex inside the channel of Si-MCM-41. The assignments of a few representative bands for "neat" VO(IV)Salten and immobilized VO(IV)Salten-MCM-41 are 1623 and 1624 (C=N), 1449 and 1455 (C=C) and 1376 and 1394 (C=O). The marginal shift in the positions of the bands corresponding to C=N, C=C and C=O is due to

immobilization of the complex. In the spectra of the immobilized complex the bands due to VO(IV)Salten are weak due to their low concentration and are masked by Si-OH bands.

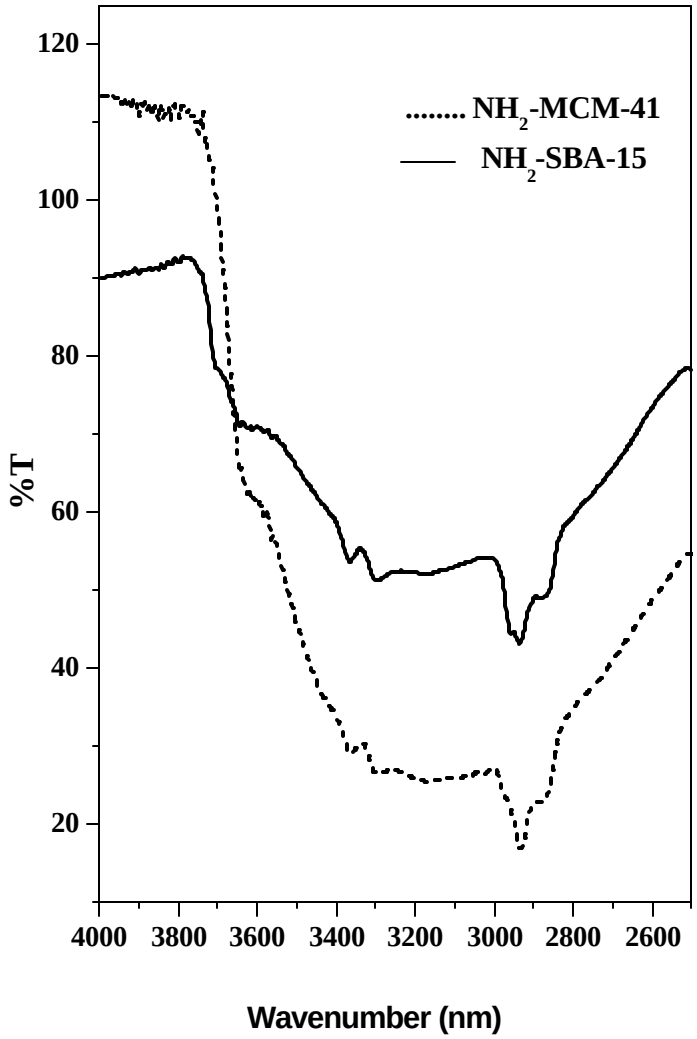

Figure 3.7 FT-IR spectra of (…..) NH_2-MCM-41, and (___) NH_2-SBA-15.

The amine modified and [$RuHCl(CO)(PPh_3)_3$] immobilized MCM-41/SBA-15 materials were characterized by IR spectroscopy. The FT-IR spectra of NH_2-MCM-41/ NH_2-SBA-15 showed two bands at 3365 and 3298 cm^{-1} characteristic of the NH_2 groups (NH vibrations) and two bands at 2935 and 2872 cm^{-1} characteristic of asymmetric and symmetric vibrations of the CH_2 groups of the propyl chain of the silylating agent (Figure 3.7). These results are quite consistent with the results previously reported [9].

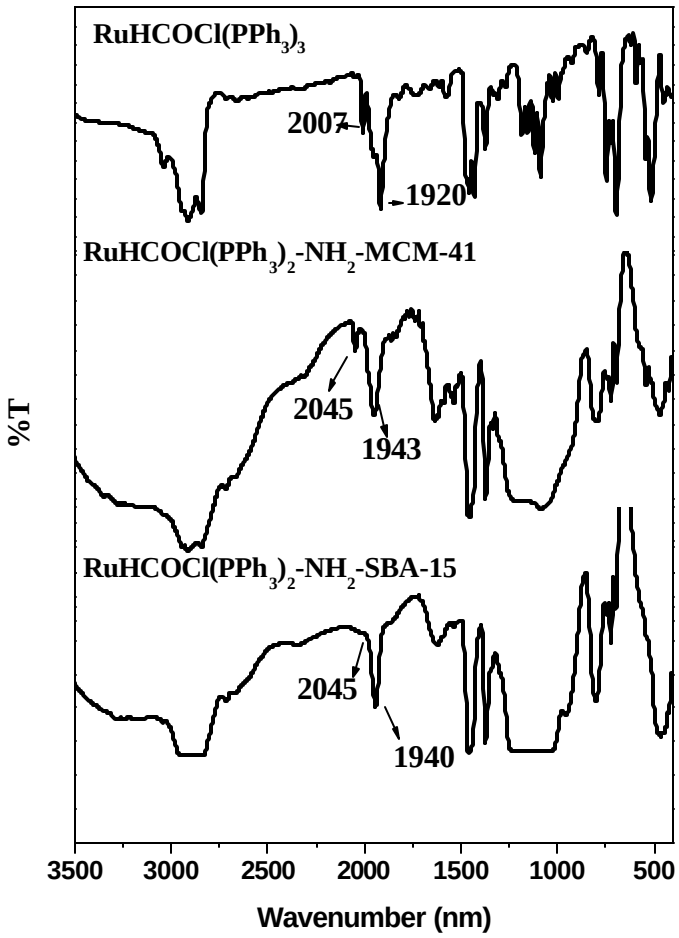

Figure 3.8 FT-IR spectra of (a) "neat" [$RuHCl(CO)(PPh_3)_3$] (b) [$RuHCl(CO)(PPh_3)_2$]-NH_2-MCM-41and (c) [$RuHCl(CO)(PPh_3)_2$]-NH_2-SBA-15.

The FT-IR spectra of "neat" [RuHCl(CO)(PPh_3)$_3$] and [RuHCl(CO)(PPh_3)$_2$]-NH_2-MCM-41and [RuHCl(CO)(PPh_3)$_2$]-NH_2-SBA-15 are shown in the Figure 3.8. The spectra of immobilized complex showed characteristic peaks of the neat complex indicating the retention of the structure of the complex upon immobilization. The neat complex showed a medium band for ν RuH at 2007 cm^{-1} and a strong band due to ν(C≡O) at 1919 cm^{-1}, which is shifted to 2045 and 1940 cm^{-1} upon immobilization. This increase in ν(C≡O) could be attributed ϖ the presence of a strong electronegative atom like nitrogen, which is a strong σ donor. In the immobilized complexes the decrease in the intensity of bands due to phosphine at 3000, 742, 717 and 692 indicates that one phosphine molecule has been knocked out during the coordination of ruthenium to nitrogen. The unusual trans bond weakening effect of the hydride ligand in [RuHCl(CO)(PPh_3)$_3$] complex accounts for the ready displacement of trans phosphine by strong bonding Lewis base [27]. The nitrogen can easily replace trans phosphine giving a anchored [RuHCl(CO)(PPh_3)$_3$] complex.

[RuHCl(CO)(PPh_3)$_3$] + NH_2-MCM/SBA ⟶ *NH_2-MCM/SBA-[RuHCl(CO)(PPh_3)$_2$] + PPh_3*

3.3.5 Nuclear Magnetic Resonance (NMR) Spectroscopy

The ^{1}H NMR spectrum of the "neat" [RuHCl(CO)(PPh_3)$_3$] and the Solid State-MAS-NMR spectrum of NH_2-MCM-[RuHCl(CO)(PPh_3)$_2$] and NH_2-SBA-[RuHCl(CO)(PPh_3)$_2$] were taken. The ^{1}H NMR spectrum of the neat complex shows that the aromatic protons resonate in the range of 7 to 7.7 ppm with an intensity of 45. While in the immobilized complex of the same the intensity of the aromatic protons reduces to 31 which confirms the knocking out of one PPh_3 during immobilization. The ^{1}H NMR spectrum of the same exhibits two triplets with 1 : 2 : 1 intensity at –7.2 ppm due to

coupling of hydridic proton with phosphorous nuclei indicating that the complex contains two equivalent PPh_3 cis to hydrogen with coupling constant $^2J(P\text{-}H)_{cis}$ = 22 Hz and one PPh_3 trans to hydrogen with large coupling constant $^2J(P\text{-}H)_{trans}$ = 105 Hz. The ^{31}P NMR of "neat" $[RuHCl(CO)(PPh_3)_3]$ shows four peaks at 39, 29.1, 13.45 and 12.4 ppm indicating the presence of three PPh_3 groups. However in the case of immobilized complexes the ^{31}P NMR shows a singlet at 32 and 34 ppm in NH_2-MCM-$[RuHCl(CO)(PPh_3)_2]$ and NH_2-SBA-$[RuHCl(CO)(PPh_3)_2]$ respectively suggesting the presence of only two PPh_3 groups trans to each other.. The high field shift in the ^{31}P NMR from 39 ppm in the neat complex to 32 and 34 ppm in the immobilized complexes is due to the presence of electron donating NH_2 group of the silylating agent, which increases the electron density at ruthenium by $d\pi(P) \leftrightarrow d\pi(Ru)$ bonding as reported earlier [10].

3.3.6 ESR spectroscopy

Frozen acetonitrile solutions of VO(IV)Saloph at 77 K exhibited an axial-type ESR spectrum (Figure 3.9 a). The hyperfine features due to vanadium (I = 7/2) are well resolved both in the parallel and perpendicular regions. The spin Hamiltonion parameters ($g_{||}$ = 1.955, $g_{\perp}$ = 1.980, $A_{||}$ = 178 G and $A_{\perp}$=60 G), obtained by spectral simulations, reveal a square pyramidal geometry for vanadium [11-12].

VO(IV)Saloph -Y (Figure 3.9 b) showed spectra attributable to two types of V(IV) species. Species I, characterized by an axial spectrum with spin Hamiltonian parameters $g_{||}$ = 1.936, $g_{\perp}$ = 1.980, $A_{||}$ = 185 G and $A_{\perp}$ = 72 G, is attributed to encapsulated VO(IV)Saloph complexes and species II, characterized by $g_{||}$ = 1.944, $g_{\perp}$ = 1.980, $A_{||}$ = 188 G and $A_{\perp}$ = 68 G, is due to uncomplexed VO^{2+} ions located in the sodalite cages. In VO(IV)Saloph-Al-

MCM-41, the signals were broad and the vanadium hyperfine features could be barely seen (Figure 3.9 c; $g_{||}$ = 1.938, $g_{\perp}$ = 1.980 and $A_{||}$ = 198 G). The difference in ESR spectra of "neat" VO(IV)Saloph, VO(IV)Saloph -Y and VO(IV)Saloph-Al-MCM-41 are consistent with the increasing vanadium content in the samples (VO(IV)Saloph-Al-MCM-41 contains 2.14% V while VO(IV)Saloph -Y has 1.46% V).

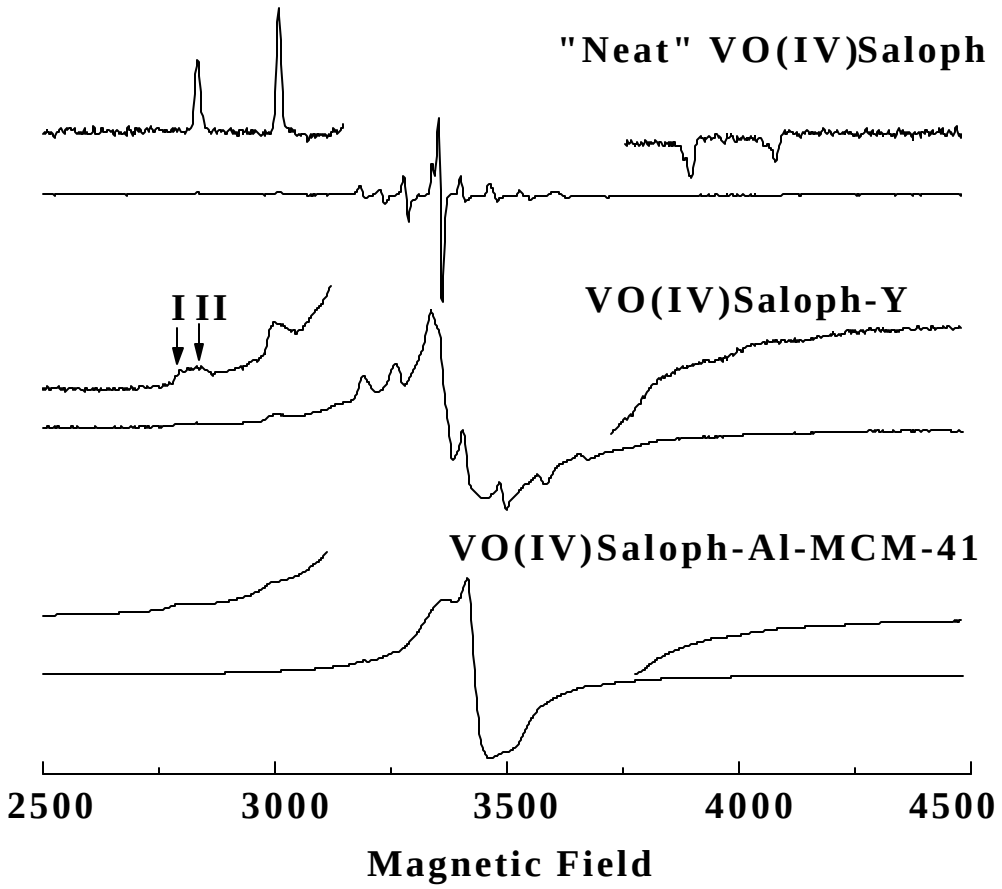

Figure 3.9 ESR spectra at 77 K: (a) frozen VO(IV)Saloph in acetonitrile, (b) VO(IV)Saloph-Y and (c) VO(IV)Saloph-Al-MCM-41.

While the complexes are isolated and confined in the supercages of zeolite-Y, they exhibit weak intermolecular interactions in VO(IV)Saloph-Al-MCM-41, resulting in broad ESR signals (Figure 3.9 c). Distinct variations in g and vanadium hyperfine parameters were observed upon encapsulation (Table 3.4). These parameters suggest a distorted octahedral geometry for vanadium in the encapsulated complexes. Perhaps, the zeolites/silica framework provides the sixth-coordination to VO(IV)Saloph. Such interactions were observed also in Cu(Salen) [13] and Cu(phthalocyanine) [14] encapsulated in zeolite-Y.

Table 3.4

ESR parameters of VO(IV)Saloph complexes

Catalyst	ESR parameters (at 77 K)			
	$g_{\|\|}$	$g_{\perp}$	$A_{\|\|}$ (G)	$A_{\perp}$ (G)
VO(IV)Saloph-"neat"	1.955	1.980	178	60
VO(IV)Saloph-Y	1.936	1.980	185	75
VO(IV)Saloph-Al-MCM-41	1.938	1.980	198	-

3.3.7 X-ray photoelectron spectroscopy (XPS)

XPS was used for surface characterization of the immobilized metal complexes. The relative elemental concentration at the surface and oxidation states of the central metal atom can be found out by using XPS. A shift in the binding energy of the central metal atom and the nitrogen indicate encapsulation [15-18].

The homogeneous distribution of the complex inside the zeolite framework can be estimated from the surface metal/Si or metal/Al ratios. In the present work XPS was used to elucidate the oxidation state of the metals, the effect of encapsulation and to estimate the surface enrichment of the metals.

Figure 3.10 (A) shows the Ru 3p core levels of neat and encapsulated Ru(III)Saloph complexes. The binding energy of Ru 3p levels are very close to the BE of Ru^{3+} reported [19]. However upon encapsulation a clear shift towards higher BE is seen compared to the neat complex. It is attributed to the complexation of Ru with Saloph ligand inside the zeolite cages. Additionally a clear satellite is seen at 473 eV for encapsulated complex and this is due to charge transfer from ligand to metal as observed in transition metal compounds.

Figure 3.10 (B) shows the Co 2p core levels of "neat" and encapsulated Co(II)Saloph complexes. In Co-complexes also similar experimental trend has been observed, as in Ru cases. Cobalt remains in the 2+ oxidation state in both the "neat" and encapsulated state and it matches well with the reported values for similar systems [19]. There is a strong increase in satellite intensity for Co 2p levels and a large energy gap (16.3 eV) between them is observed from encapsulated complex, which results in higher catalytic activity than "neat" complex. Table 3.5 lists the relevant parameters for Ru and Co complexes.

Figure-3.10 A XPS of Ru

Figure-3.10 B XPS of Co

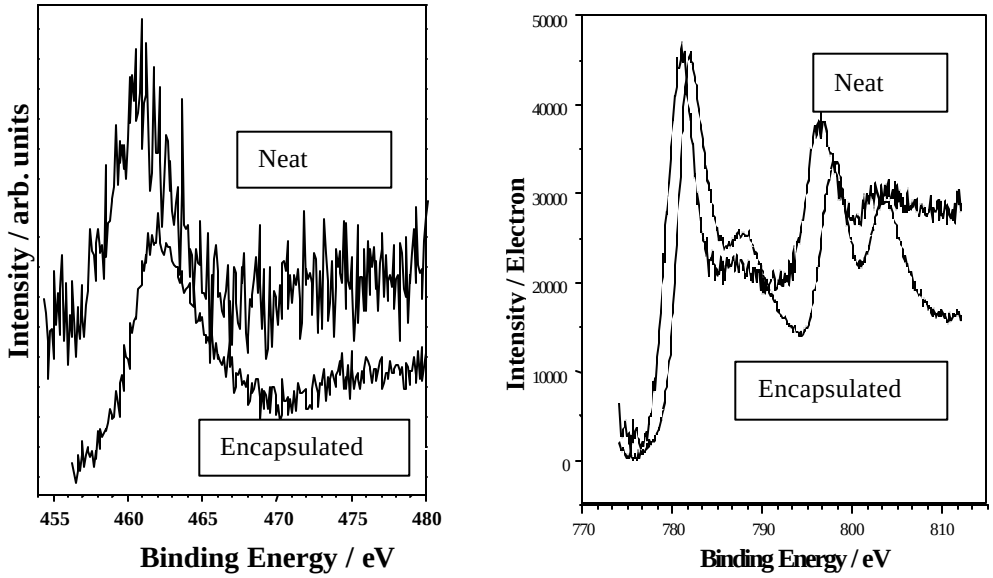

Figure 3.10 (A) XPS of Ru in "neat" and encapsulated complex (B) XPS of Co in "neat" and encapsulated complex

Table 3.5

XPS data of Ru(III)Saloph and Co(II)Saloph Complexes

Catalysts	BE, Ru $3p_{3/2}$ or Co $2p_{3/2}$ (eV)	$p_{3/2}$ and $p_{1/2}$ separation (eV)
"neat" Ru(III) Saloph	461.4	22.4
Ru(III)Saloph-Y, Encapsulated	462.2	22.3
"neat" Co(II)Saloph	781.0	15.5
Co(II)Saloph-Y, Encapsulated	781.9	16.3

Even though lot of spectroscopic work has been done on Vanadium complexes very few data are available on XPS of vanadium compounds because of the overlap of the

V 2p signal with reasonably intense satellites of O 1s line [20-21]. This problem in the past has been managed by using monochromatized radiation or by commercially available satellite subtraction software [21]. Monochromatization leads to huge reduction in signal intensity and makes this method unviable to the analysis of materials with small amount of metal ions. However, our results clearly demonstrate that at least V $2p_{3/2}$ line is not affected when Mg Kα is employed. The X-ray photoemission spectra of "neat" VO(IV)Saloph, VO(IV)Saloph -Y, VO(IV)Saloph-Al-MCM-41 from the V 2p level are shown in Figure 3.11. The inset shows the spectra from the O 1s core level of SiO_2. VO(IV)Saloph exhibits V $2p_{3/2}$ core level peak at a binding energy of about 516 eV consistent with the +4 oxidation state of vanadium (Table 3.6). This BE compares well with that of V^{4+} compounds reported in the literature such as V in zeolite-Y [20], vanadyl sulphate and vanadyl acetyl acetate [22]. The peak from V $2p_{1/2}$ core level overlaps with the satellite peak from O 1s of SiO_2 (Figure 3.11). In encapsulated complexes, the spectra were weak and indicate the location of the complex inside the cages.

Table 3.6

XPS data of VO(IV)Saloph complexes

Catalyst	BE (in eV)		
	$V2p_{3/2}$	N1s	O1s
VO(IV)Saloph-"neat"	515.7	399.0	530.8
VO(IV)Saloph-Y	515.7	398.8	531.8
VO(IV)Saloph-Al-MCM-41	516.1	399.0	531.8

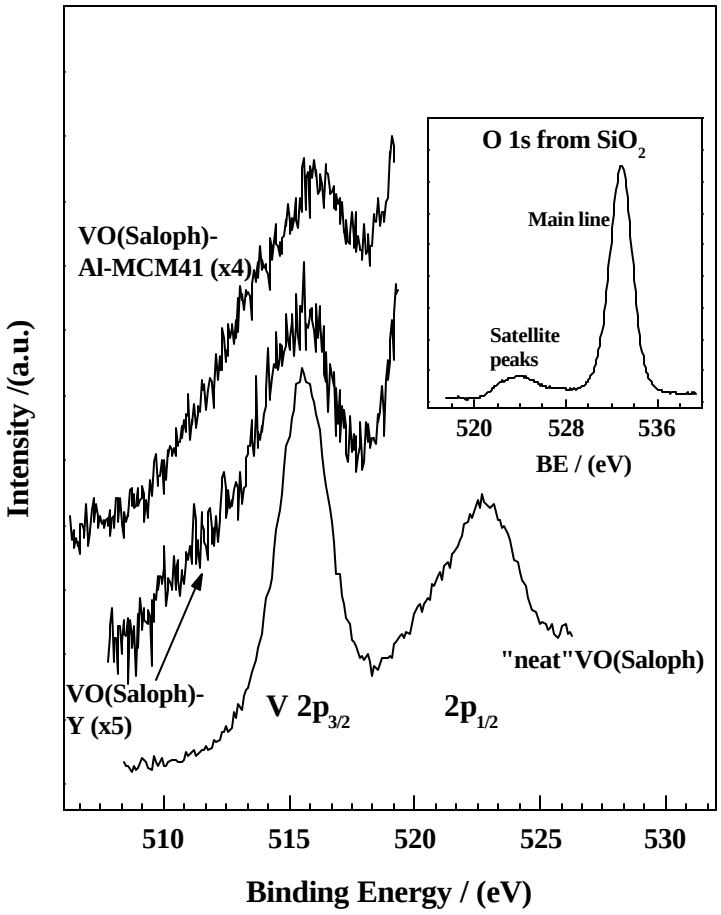

Figure 3.11 XPS of "neat" VO(IV)Saloph, VO(IV)Saloph -Y and VO(IV)Saloph -Al-MCM-41 from V 2p core level. Inset shows the peaks from O1s core level of SiO_2.

Both encapsulated complexes exhibits larger full width at half maximum (FWHM) compared to the neat complex. Additionally, V 2p core level in MCM-41 is broadened and non-symmetrical than that of VO(IV)Saloph-Y. The reason could be that in the case of zeolite Y, the vanadyl complex is packed from all sides inside the zeolite cavity and it is experiencing almost a uniform secondary effect due to the interaction between zeolite and

VO(IV)Saloph. In other words the size of the VO(IV)Saloph and zeolite cavity is very close. However, in the case of VO(IV)Saloph-Al-MCM41, size of the complex is smaller than the pore size of MCM-41 so the complex might be attached to the pores in more than one style. Interaction between VO(IV)Saloph and MCM-41 pores may not be uniform, as may be the case in VO(IV)Saloph -Y. In addition to the above, there is a possibility that relaxation effect [23], which is contributing to the final state of V 2p photoemmision due to the above interaction between the metal ion and the support, ie zeolite or MCM-41. The above relaxation effect due to support mainly lowers the photoelectron energy and broadens the peak depending on the extent of interaction between vanadyl complex and support. Larger broadening with MCM-41 indicates that the degree of metal support interaction is high compared to zeolite –Y. By employing non-monochromatised Mg Kα radiation a satellite is observed due to the secondary radiation for O 1s core level between 8-10.5 eV below the actual BE of O 1s core level. However, this satellite overlaps only with V $2p_{1/2}$ level and does not contribute to V $2p_{3/2}$ level as can be seen in Figure 3.11. To demonstrate clearly a V free pure SiO_2 is analyzed and its O 1s spectrum is given in the inset in Figure 3.11. Satellite contribution occurs only above 520 eV and V $2p_{3/2}$ peak occurs well below that limit, which clearly demonstrates that V $2p_{3/2}$ level, is not contaminated by O1s satellites in the present case. Broadening due to O 1s satellites can be clearly seen with V $2p_{1/2}$ level in neat complex, but not with V $2p_{3/2}$ level. However, in the case of Al Kα radiation the O 1s satellite appears between 8.5 and 13 eV below O 1s core level and hence affects both V $2p_{3/2}$ and 2 $p_{1/2}$ core levels [21]

The X-ray photoemission spectra of the Ru 3p core level of "neat" $[RuHCl(CO)(PPh_3)_3]$ and $[RuHCl(CO)(PPh_3)_2]$-NH_2-MCM-41are shown in the Figure

3.12. The neat ruthenium complex exhibits Ru 3p core level peak at a binding energy of 464 eV consistent with the +2 oxidation state of ruthenium. In the case of the immobilized complex a shift in the binding energy of the Ru 3p core level to 465 eV was observed.

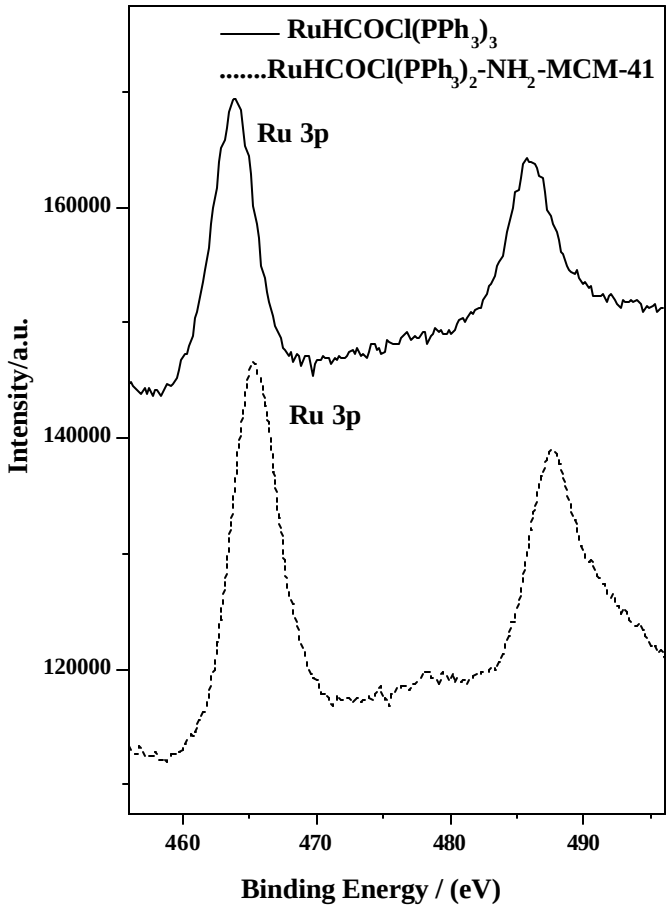

Figure 3.12 XPS of (a ——) "neat" [RuHCl(CO)(PPh_3)$_3$], and (b …..) [RuHCl(CO)(PPh_3)$_2$-NH_2-MCM-41] from Ru3p core level.

3.3.8 Transmission electron microscopy

The topographic information obtained by TEM at near atomic resolution has been a key method for the structural characterization and identification of MCM-41 and metal

complex immobilized inside the channels of MCM-41. TEM can detect the presence of transition metal complexes or oxides deposited on the outer surface of the mesoporous materials. The hexagonal pore structures with similar XRD patterns as that of MCM-41 materials have been observed by high resolution TEM. These structures were also observed in the mesoporous materials after modification with APTES and after immobilization with the complex (Figure – 3.13 a-c). It also provides information about the pore size and wall thickness of the materials before and after immobilization.

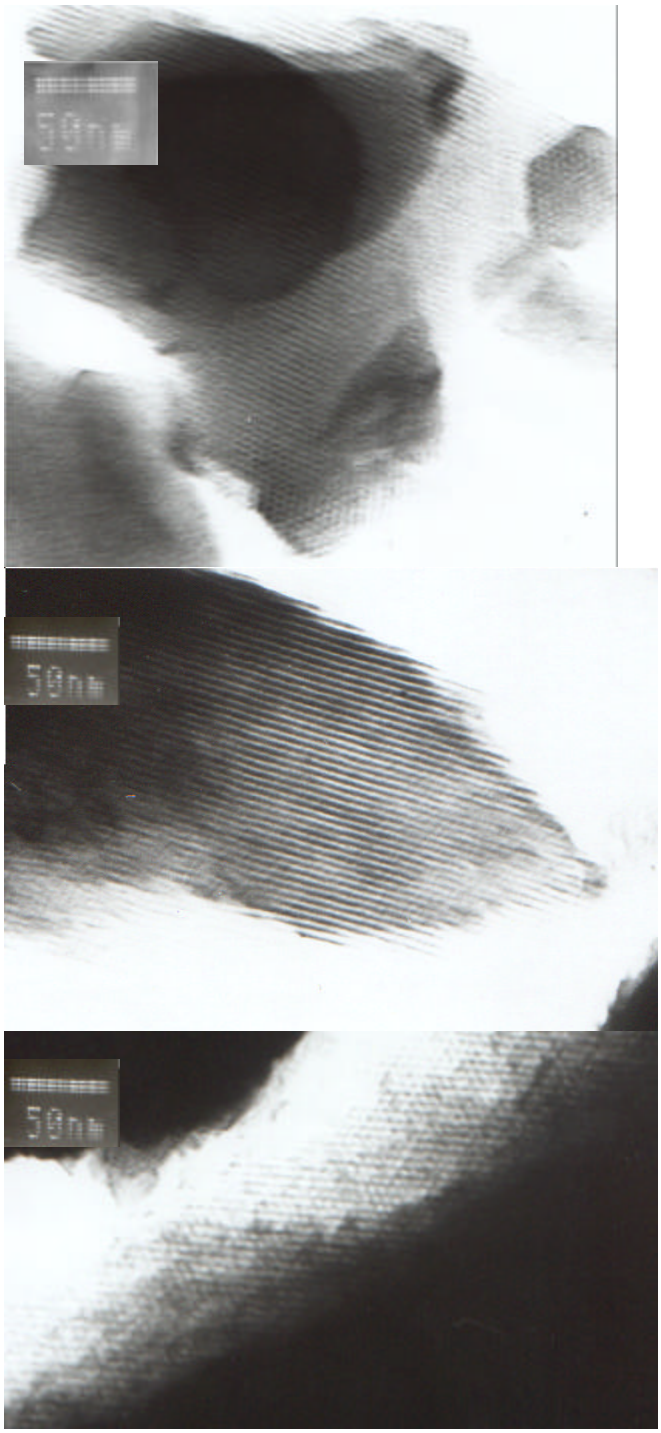

Figure 3.13 Transmission electron micrographs of a) Si-MCM-41 b) Cl-Si-MCM-41 c) VO(IV)Salten-MCM-41

3.3.9 Thermal analysis

Differential thermal (DTA) and thermogravimetric analysis (TGA) has been used to characterize metal complex immobilized onto microporous and mesoporous materials [24]. The metal complex loading can also be estimated form the weight loss. Hence this technique can also be used to ascertain the amount of uncomplexed ligand.

DTA and TGA data with respect to the catalysts studied are presented in Figures 3.14 (A) – (D). The "neat" Co complex showed weight loss at (600 K). However, for the corresponding encapsulated complex weight loss occurs in two stages. In the first stage up to 423 K due to desorption of water. In the second stage weight loss is observed in the range iof 573 to 723 K due to decomposition of the complex (Figures 3.14 B). In the case of "neat" ruthenium complex there is a continuous weight loss up to 773 K due to desorption of water and decomposition of the complex. But in the case of encapsulated comple even though weight loss is observed up to 823 K the % weight loss is less compared to "neat" complex. Thus thermal analysis data shows that the encapsulated complexes are generally more stable (to thermal decomposition) than the free complexes [7, 25-26].

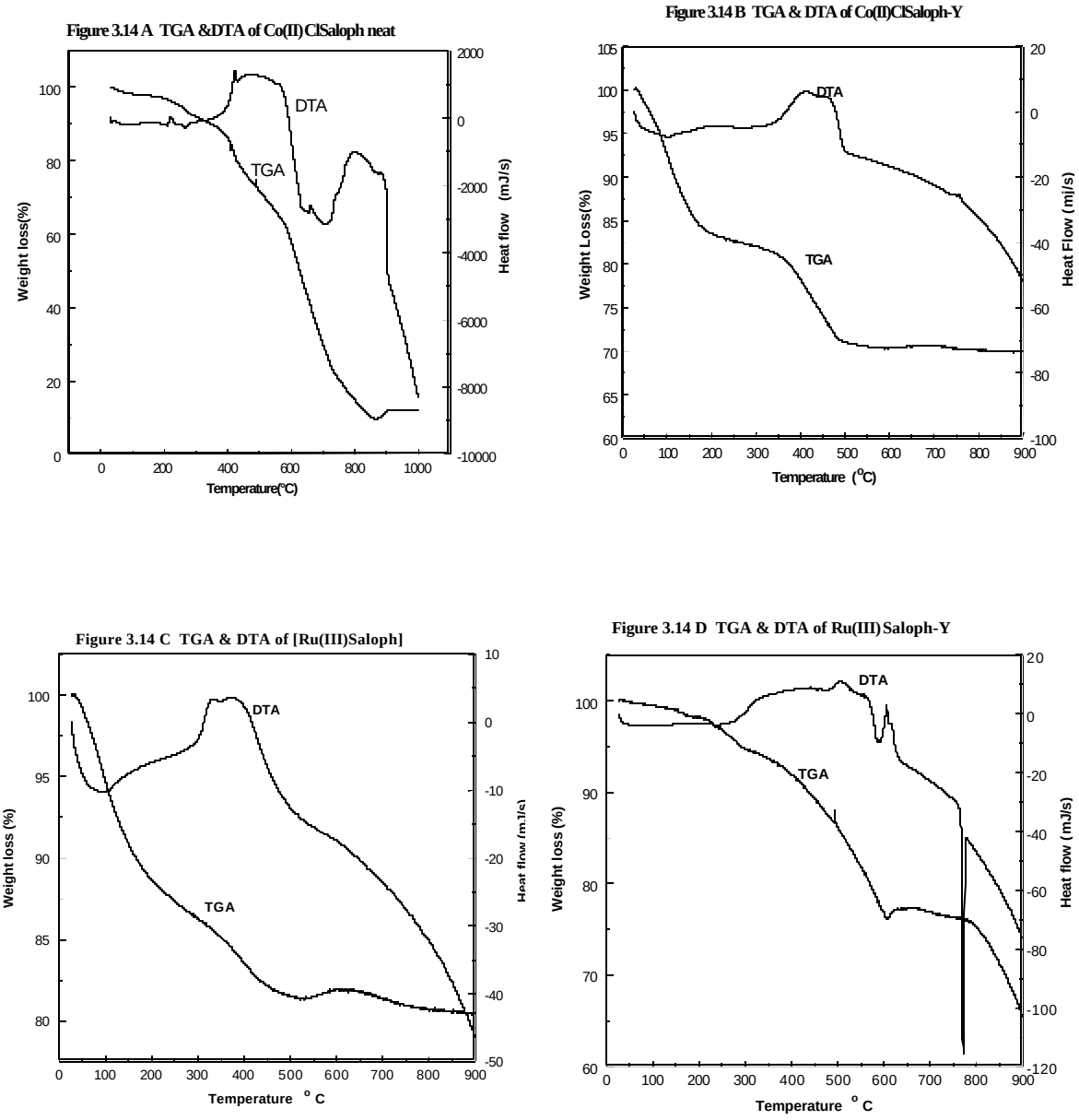

Figure 3.14 TG and DTA of (A) Co(II)ClSaloph neat; (B) Co(II)ClSaloph-Y; (C) Ru(III) Saloph neat and (D) Ru(III)Saloph-Y

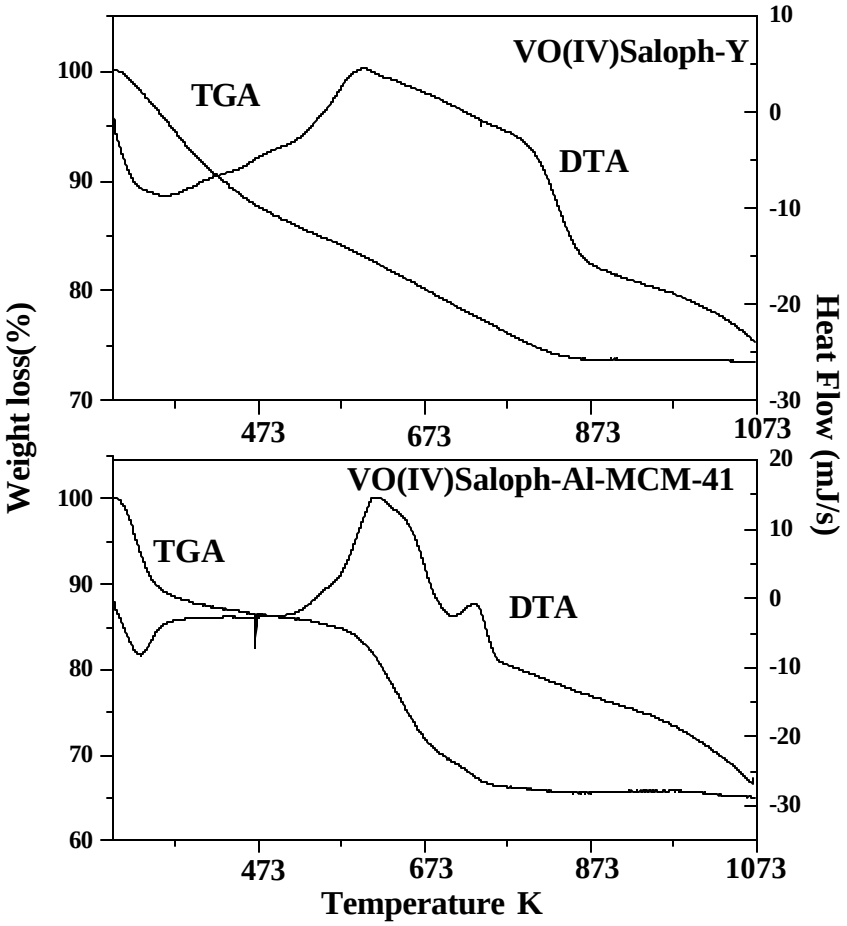

Figure 3.15 TG (__) and DTA (----) profiles of (a) VO(IV)Saloph-Y and (b) VO(IV)Saloph-Al- MCM-41.

VO(IV)Saloph-Y exhibited weight loss in two stages. In the first stage the weight loss is up to 473 K and in the second stage the weight loss is between 473 to 823 K (Figure 3.15). The former is due to desorption of water while the latter is due to decomposition of Saloph complex. In the case of VO(IV)Saloph-Al-MCM-41 sample the desorption of water

takes place up to 373 K and decompostion starts at 573 K (Figure 3.15). The difference in the thermal behavior in microporous zeolite-Y and mesoporous MCM-41 samples is attributed to constrained molecular geometry and cage effects.

The thermal decomposition of the VO(IV)Salten-Si-MCM-41 complex was observed in two steps. The former (<373 K) is due to desorption of water while the latter is due to decomposition/combustion of Salten complex. The decompostion of VO(IV)Salten takes place in a temperature range in VO(IV)Salten-Si-MCM-41 complex at 623 to 873 K.

3.4 REFERENCES

1 A. Kozlov, K. Asakura, Y. Iwasawa Microporous Mesoporous Mater. 21 (1998) 571.

2. H. Diegruber, P. J. Plath, E. G. Schulz-Elkoff and M. Mohl, J. Mol. Catal. 24 (1984) 15.

3. N. Herron, G. D. Stucky and C. A. Tolman, J. Chem. Soc., Chem. Commun., (1986) 1521.

4. D. Brunel, N. Bellocq, P. Sutra, A. Cauvel, M. Laspéras, P. Moreau, F. Di Renzo, A. Galarneau and F. Fajula, Coord. Chem. Rev. 180 (II) (1998) 1085.

5. K.J. Balkus Jr., A.K. Khanmamedova, K.M. Dixon, F. Bedioui, Appl. Catal. A: 143 (1996) 159.

6. S. Deshpade, D. Srinivas and P. Ratnasamy J. Catal. 188 (1999) 261.

7. K. J. Balkus Jr., A.G. Gabrielov J. Incl. Phenom. Mol. Recog. Chem. 21 (1995) 159.

8. T.H. Bennur, D. Srinivas and P. Ratnasamy Microporous Mesoporous Mater. 48 (2001) 111.

9. M. J. Verhoef, J. A. Peters and H. van Bekkum, Stud. Surf. Sci. Catal., 125 (1999) 465.

10. K. Mukhopadhyay, B. R. Sarkar and R. V. Chaudhari, J. Am. Chem. Soc., 124 (2002) 9692.

11. K. P. Callhan and P. J. Durand Inorg. Chem. 19 (1980) 3211.

12. B. R. McGarvey Trans. Metal Chem. 3 (1969) 89.

13. S. Deshpade, D. Srinivas and P. Ratnasamy J. Catal. 188 (1999) 261.

14. S. Seelan, A.K. Sinha, D. Srinivas and S. Sivasanker J. Mol. Catal. A: 157 (2000) 163.

15. B. V. Romanovsky and A. G. Gabrielov, Stud. Surf. Sci. Catal., 72 (1992) 443.

16. B. V. Romanovsky and A. G. Gabrielov, J. Mol.Catal., 74 191992) 293.

17. G. Meyer, D. Wohrle, D. Mohl and G. Schultz-Ekloff, Zeolites, 4 (1984) 30.

18. K. Putyera, G. Plesch, L. Benco, J. Dobrovodsky, A. V. Tchuvaev, V. I. Nefedov and M. Zikmund, Proc. 12th Conf. Coord. Chem., (1990) 295.

19. L. Guczi, R. Sundararajan, Zs. Koppany, Z. Zsoldos, Z. Schay, F. Mizukami, S. Niwa. J. Catal. 167 (1997) 482.

20. A. Kozlov, K. Asakura, V. Iwasawa, J. Chem. Soc., Faraday Trans. 94(6) (1998) 809.

21. M. Wark, M. Koch, A. Brückner, W. Grünert, J. Chem. Soc., Faraday Trans. 94(14) (1998) 2033.

22. R. Larsson, B. Folkessen, G.Schön, Chem. Scr. 3 (1973) 88.

23. R. Ganesan, B. Viswanathan, Bull. Catal. Soc. India. 10 (5) (2000) 1.

24. K. J. Balkus Jr. and A. G. Gabrielov, J. Inclusion Phenomena and molecular Recognition in Chemistry, 21 (1995) 173.

25. K. J. Balkus Jr. and J. P. Ferraris, J. Phys. Chem., 94 (1990) 8019

26. C. Ratnasamy, A. Murugkar, S. Padhye and S. A. Pardhy, Indian J. Chem., 35A (1995) 1.

27. S. Gopinathan, S. S. Deshpande, I. R. Unny and C. Gopinathan, Ind. J. Chem. 25A (1986) 1015.

CHAPTER 4

CATALYTIC ACTIVITY

4.1 OXIDATION OF *p*-CRESOL

4.1.1 INTRODUCTION

p-Hydroxybenzaldehyde (PHBA) is obtained as a by-product from the Reimer-Tiemann reaction of salicylaldehyde with phenol. PHBA is a chemical, which is used as an additive for metal plating, brighteners, perfumes, as well as a source for the production of pharmaceutical intermediates. Cobalt salts are frequently used as catalysts in oxidation reactions [1-4]. Recently many attempts to produce PHBA from *p*-cresol through liquid-phase oxidation have been reported. The liquid-phase oxidation of *p*-cresol was reported by Sharma et al. using cobaltous chloride as catalyst in presence of excess sodium hydroxide to give an overall *p*-cresol conversion of 90 % with 60 % selectivity to PHBA [5]. Other by-products included p-hydroxybenzyl alcohol (PHBAlc.), p-hydroxybenzoic acid (PHBAcid), p- hydroxybenzyly methyl ether (Ether) and minor quantities of tarry materials. The catalytic oxidation of *p*-cresol to PHBA using cobalt chloride catalyst in methanol in the presence of three moles of sodium hydroxide is a potentially interesting route [6-7]. The selective catalytic oxidation of *p*-cresol with molecular oxygen is a viable proposition due to the fact that the phenolic hydroxyl group acts as a built-in inhibitor to further oxidation of the aldehyde group under mild reaction conditions. However the process reported by Nishizawa and co-workers [6] apart from the use of large amounts of sodium hydroxide suffers from a major drawback that it produces large amount of by-products and the catalyst undergoes deactivation due to the formation of inactive, hydroxyl-bridged, cobalt complexes. An increased yield of PHBA has been achieved using

heterogeneous catalysts such as CoAPO-5 and CoAPO-11 [8]. Recently, compounds like hydrotalcite also have been used as catalysts to get a high *p*-cresol conversion [9].

This part of the thesis deals with the oxidation of *p*-cresol under alkaline conditions using "neat" and zeolite-Y encapsulated cobalt(II) Salen complexes with a view to obtain an increased selectivity towards PHBA. The oxidation of *p*-cresol gave the following products (Scheme-4.1.1).

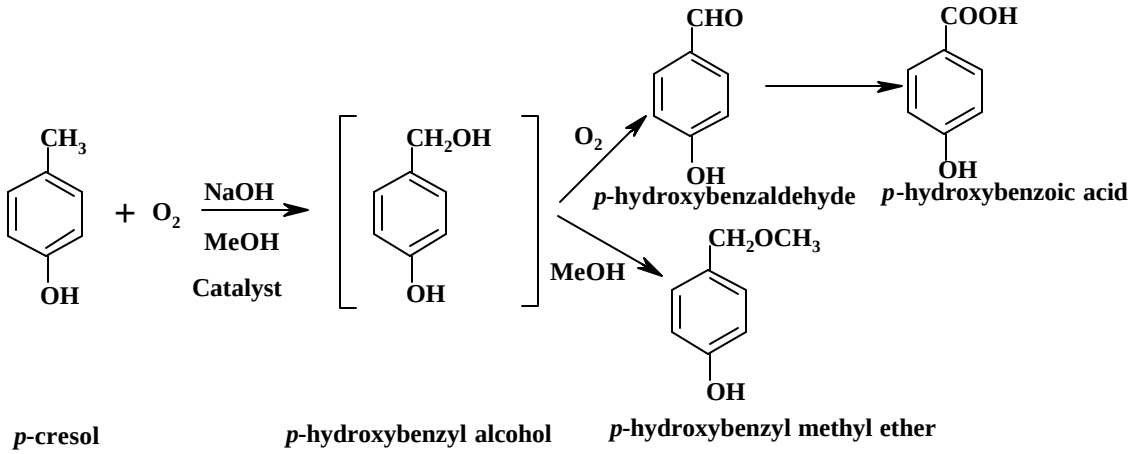

Scheme-4.1.1 Products of *p*-cresol oxidation

4.1.2 EXPERIMENTAL

4.1.2.1 Materials

Salicyladehyde, ethylenediamine, 5-chlorosalicylaldehyde, 5-bromosalicylaldehyde, 5-nitrosalycylaldehyde, *p*-cresol and Na-Y were procured from Aldrich Chemicals. Cobalt acetate, NaOH, MeOH and ethanol were procured from Loba Chemicals India.

4.1.2.2 Procedure

p-Cresol (6 g) was added to a warm methanolic solution (25 ml) of sodium hydroxide (6.2 g) in a Parr autoclave of 300 ml capacity and to that was added Cobalt(II)Salen catalyst ("neat" = 0.7 mg and encapsulated 0.175 mg). The autoclave was then pressurized with air up to 600 psig and heated to 353 K with stirring. A drop in the pressure suggested commencement of the reaction, which was continued over a period of 3 h. After the reaction, the autoclave was cooled, gases were released and the product was obtained as brown solid slurry. It was homogenized by dissolving in water and analyzed by HPLC (Shimadzu liquid chromatograph (Model LC-9A) equipped with Chrompak C18 15 cm column) using a water methanol elluent (75 : 25) by external standard method. The products were detected using a UV detector operating at 210 nm.

4.1.3 RESULTS AND DISCUSSION

The aerial oxidation of *p*-cresol was carried out using "neat" as well as zeolite encapsulated cobalt (II)Salen catalysts. The *p*-cresol conversion and the corresponding product selectivities are given in the table 4.1.1. Earlier studies using homogeneous cobalt catalysts have showed that the oxidation state of cobalt changed reversibly between 2+ and 3+. Hence the encapsulated cobalt systems will also have the same ability. Apart from this the encapsulated systems will evade the disadvantage of catalyst deactivation due to the dimerization of cobalt complex. The zeolite encapsulated catalysts are found to be superior to the corresponding "neat" complexes. The TOF for these catalysts is also increased by a factor of ~ 4. This increased conversion and selectivity could be attributed to an optimum residence time for the substrate near site isolated active catalyst intermediate in the

supercages of zeolite. Substitution of electron withdrawing groups like the halogen or -nitro group enhances the conversion and turnover frequency, (TOF). Among the catalyst studied, the chloro-Salen derivative gave maximum substrate conversion and PHBA selectivity. The bromo- and nitro-Salen derivatives also showed marginally better performance compared to the unsubstituted cobalt(II)Salen. Substitution of electron withdrawing groups on the ligand enhances the electrophilic character of the active oxygen species and consequently its reactivity.

Table 4.1.1

Catalytic activities of "neat" and zeolite encapsulated complexes in *p*-cresol oxidation

Catalyst	*p*-cresol	Product Selectivity (%)					
	Conv. (%)	PHBA	Ether	PHBAlc.	PHBAcid	Others	TOF
Co(II)Salen	90	85	8	2	4	1	235
Co(II)Salen-Y	96	90	5	2.5	1.5	1	982
Co(II)Cl-Salen	98	96	1.5	1.5	0.5	0.5	254
Co(II)Cl-Salen-Y	100	97	1	1	0.5	0.5	1049
Co(II)Br-Salen	94	92	5	2.5	1.5	1	245
Co(II)Br-Salen-Y	98	95	3	2	1.5	0.5	1011
Co(II)NO_2-Salen	92	89	3.5	2.5	3.6	1.4	240
Co(II)NO_2-Salen-Y	97	93	4.5	2.5	1	2	1049

Reaction conditions: p-cresol = 6 g, NaOH = 6.2 g, temp.= 353 K, catalyst "neat" Co(II)Salen= 0.7 mg of cobalt/6 g of *p*-cresol, encapsulated catalyst = 0.175 mg of cobalt/6 g of *p*-cresol and time = 3 h.

Table 4.1.2

Effect of temperature on the catalytic activities of "neat" and zeolite encapsulated cobalt(II)Cl-Salen complexes

Temperature (K)	*p*-cresol	Product Selectivity (%)				
	Conv. (%)	PHBA	Ether	PHBAlc.	PHBAcid	Others
313 "neat" complex	30	65	25	5	4	1
333	70	80	9.5	4.5	4.5	1.5
343	88	89	5	2.5	2.5	1
353	98	96	1.5	1.5	0.5	0.5
313 "encapsulated"	63	70	20	4	4	2
333	85	82	8.5	3.5	4	2
343	93	93	2	1.5	2.5	1
353	100	97	1	1	0.5	0.5

Reaction conditions: p-cresol = 6 g, NaOH = 6.2 g, catalyst "neat" Co(II)Cl-Salen = 0.6 mg of cobalt/6 g of *p*-cresol, encapsulated = 0175 mg of cobalt/6 g of *p*-cresol, time = 3 h..

Table 4.1.3

Effect of cobalt content on the catalytic activities of "neat" cobalt(II)Cl-Salen complex

Amt. of Co (mg)	*p*-cresol Conv. (%)	Product Selectivity (%)				
		PHBA	Ether	PHBAlc.	PHBAcid	Others
1.02	83	79	10	5	4	2
2.1	90	90	4	3	2	1
4.2	98	96	1.5	1.5	0.5	0.5

Reaction conditions: p-cresol = 6 g, NaOH = 6.2 g, temperature = 353 K, catalyst "neat" Co(II)Cl-Salen, time = 3 h..

4.1.3.1 *Effect of temperature*

The reactions have been conducted using "neat" and encapsulated chloroSalen catalysts in the temperature range of 313-353 K to study the effect of temperature on the rate of reaction and PHBA selectivity. The results are furnished in table 4.1.2. The reaction was found to be incomplete at lower temperature (313 K) even after increasing the reaction time up to 5 h. The selectivity towards PHBA is also decreased considerably due to unwanted benzyl methyl ether formation. An enhancement of reaction rate has been observed with an increase in reaction temperature between 333 and 343 K.

4.1.3.2 Effect of cobalt content

Reactions have been carried out at different *p*-cresol to catalyst ratio at 353 K. The results show (Table-4.1.3) that on increasing the amount of catalyst, the percentage conversion of *p*-cresol increases.

4.1.4 CONCLUSIONS

Catalytic behaviour of "neat" and encapsulated cobalt(II)Salen complexes in the reaction of *p*-cresol oxidation was studied. Results show that encapsulated complexes have higher TOF than "neat" complexes. The cobalt content has an obvious effect on the catalytic activity. Choice of a suitable reaction temperature and reaction time improves the selectivity towards the desired product. Encapsulated cobalt Schiff base complexes are expected to be novel and efficient catalysts for selective oxidation of *p*-cresol to PHBA.

4.1.5 REFERENCES

1. E. Marko and L. Triendl, Catal Lett., 46 (1992) 345.
2. P. Lin and H. Alper, J. Mol. Catal., 72 (1992) 143.
3. A. T. Au, US Pat. 4 471 140 (1984).
4. J. Dakka, A. Zoran and S. Yoel, Eur. Pat. 00 300 921 (1989).
5. S. N. Sharma and S. B. Chandalia, J. Chem. Tech. Biotechnol 49 (1990) 141.
6. K. Nishizawa, K. Hamada and T. Aratani, Eur. Pat. 0 012 939 (1979).
7. P. Campo, P. Cocolios, P. Dognin and H. Ledon, Eur. Pat. 0 323 290 (1987).
8. M. P. J. Peeters, M. Busio and P. Leijten, Appl. Catal. A. : General, 118 (1994) 51.
9. L. Yumin, L. Shetian, Z. Kaizheng, Y. Xingkai and W. Yue, Appl. Catal. A. : General, 169 (1998) 127.

4.2 OXIDATION OF b-ISOPHORONE

4.2.1 INTRODUCTION

Allylic oxo-functionalization of cyclic olefins is an attractive process transforming cheap and readily available substrates to valuable intermediates for the fine chemical industry. Allylic oxo-functionalization is defined, for the purpose of this chapter, as the preparation of α,β-unsaturated ketones of cyclic olefins using primarily dioxygen as oxidant. Allylic oxidation and epoxidation (Refer Chapter 4 Part C) are two competing processes both in vivo and in vitro [1]. Typically, allylic oxidation products are formed when hydrogen abstraction is the dominant reaction. In contrast to epoxidation, allylic oxidation retains the olefinic functionality in the product allowing further useful transformations. Allylic oxidation is a process involving free radicals and is most likely to occur in the presence of low oxidation state transition metal species [1].

β-Isophorone (βIP) to keto-isophorone (KIP) is an important reaction, since KIP is known as a key intermediate for the synthesis of caratenoids [2-4], flavoring substances [5-8] and is also used for producing compounds of vitamin A, E series and hence, the above study has been aimed at providing a heterogeneous catalyst system for the above reaction. The oxidation of βIP gave KIP as the major product along with side products A and B, as shown in the following reaction Scheme – 4.2.1.

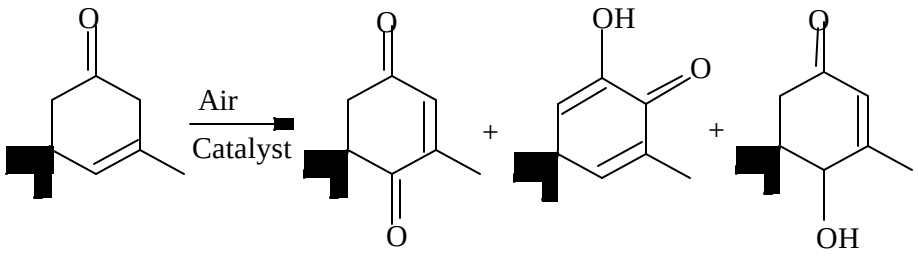

A= 4,4,6-Trimethyl-2-hydroxy-cyclohex-2,5-dien-1-one

B = 3,5,5-Trimethyl-4-hydroxy-cyclohex-2-en-1-one

Scheme 4.2.1 Reaction scheme of oxidation of β-isophorone

A broad range of homogeneous catalysts have been reported in literature, some of them affording over 90 % yield to the desired α,β-unsaturated ketone [9-10]. The search for a heterogeneous system has been less successful. Conventional gas phase allylic oxidation catalysts are non-selective at the typical high operating temperatures [11-12]. At lower operational temperatures (ca 473 K), which are necessary in the selective oxidation of thermally sensitive substrates, the conventional gas phase catalysts do not function properly. Liquid phase oxidation with solid catalysts, such as Cr-pillared clays and molecular sieves, suffer from metal leaching. Apparently, the search for a heterogeneous catalyst for allylic oxo-functionalization is not a trouble free route to replace homogeneous catalysts. At present, the most attractive solution appears to be the heterogenization of proven homogeneous catalysts.

Utilizing molecular oxygen as oxidant is particularly attractive for economic reasons. In addition, air and oxygen/nitrogen mixtures as oxidants in the presence of true heterogeneous catalysts fulfill the demands of non-polluting oxidizing agents. When such systems can be employed, replacing for example highly toxic chromium oxidizing

reagents the benefits to the society is clear. In the production of commodity chemicals the price of oxidant may determine the economic viability of the entire process.

Keeping in view of the above goals, here we attempt to trace the development from homogeneous to heterogeneous catalysis in the allylic oxofunctionalization of cyclic olefins. The utility of this oxidative conversion is highlighted succinctly in the allylic oxidation of βIP to KIP, which is a useful intermediate in the synthesis of carotenoids and fragrances. This chapter deals with the catalytic activities in aerobic oxidation of βIP to KIP using air as an oxidant by Co(II)Saloph-Y and its "neat" derivatives containing substituted electron withdrawing groups, such as, -Cl, -Br or -NO_2 in Saloph ligand

4.2.2 EXPERIMENTAL

4.2.2.1 Materials

NaY (Si/Al = 2.3), $Co(OAc)_2.4H_2O$, salicylaldehyde, 5-chlorosalicylaldehyde, 5-bromosalicylaldehyde, 5-nitrosalicylaldehyde and o-phenylenediimine were procured from Aldrich Co. β-isophorone (βIP) and keto-isophorone (KIP) were procured from Herdillia, India. Triethyl amine, acetyl acetone, methyl ethyl ketone (MEK), and the solvents were of AR grade and were procured from s.d. fine Chemicals, India.

4.2.2.2 Procedure

The catalytic runs for the oxidation of βIP were carried out in a two-necked round bottom flask fitted with a water condenser connected to a balloon filled-with air and kept in a thermostatic oil bath. Reaction mixture containing known amounts of βIP (1 g), catalyst ("neat" Co(II) catalysts = 0.015 g and encapsulated Co(II) catalysts = 0.2 g), MEK (8 g), acetyl acetone (0.12 g) and trimethyl amine (0.12 g) was placed in the flask. The flask was then connected to balloon filled with air. The reaction was initiated by

stirring the reaction mixture with a magnetic needle. The progress of the reactions was monitored by withdrawing the samples at different times and analyzing them by a gas chromatograph (Shimadzu 14B; FID detector; SE-52 capillary column). The identities of the products were confirmed by GC-MS (Shimadzu GCMS QP 5000).

4.2.3 RESULTS AND DISCUSSION

The zeolite encapsulated Co(II)Salo ph and their "neat" complexes oxidized βIP to KIP at ambient temperature and pressure. The oxidation of βIP to KIP is negligible in the absence of cobalt Saloph catalysts confirming that under the conditions of the experiments, the oxidation is indeed catalytic in nature. In the case of the encapsulated catalysts, cobalt was not detected in the reaction products at the end of the reaction (atomic absorption spectroscopy) indicating that oxidation of βIP by dissolved cobalt Saloph complexes leached out from the zeolite matrix is negligible. Also no reaction took place over CO(II)-Y. The oxidation of βIP to KIP gave 90% selectivity for KIP at βIP conversion of 60 % over a period of 16 h. However, the selectivity for KIP was highest i.e. 95 % at βIP conversion in the range up to 30 % in 3 h and then decreases at higher conversions of βIP. The experimental conditions and the results obtained are presented in Table 4.2.1.

Table 4.2.1.

Catalytic activities of "neat" and zeolite encapsulated complexes

"Neat" Complexes	βIP Conv. (Wt.%)	TON*	Encapsulated complexes	βIP Conv. (Wt. %)	TON*
Co(II)Cl-Saloph	15.3	29.8	Co(II)Cl-Saloph-Y	25.8	50.3
Co(II)Br-Saloph	12.5	24.2	Co(II)Br-Saloph-Y	23.4	45.5
Co(II)nitro-Saloph	10.8	21.0	Co(II)nitro-Saloph-Y	20.6	40.1
Co(II)Saloph	7.4	14.3	Co(II)Saloph-Y	15.7	30.5

Reaction conditions: βIP = 1 g, acetyl acetone = 0.12 g, triethyl amine = 0.12 g, MEK = 8.0 g, temperature = 298 K, Co(II) catalysts, "neat" = 0.015 g, Co(II) encapsulated = 0.2 g, oxidant, Air = 1 atm. and reaction time = 1.0 h.

* = mole βIP converted per mole of cobalt.

From the catalytic activities data (Table 4.2.1 and Figure 4.2.1), it is found that zeolite encapsulated catalysts gave higher conversions of βIP (TON's) than their corresponding "neat" complexes. The higher activity of encapsulated complexes is because of site isolation of the complexes inside the zeolite cages. Among the catalysts studied, Co(II)Cl-Saloph gave the maximum βIP conversion followed by bromo and nitro substituted Salophs. The same trend is seen with their corresponding encapsulated catalysts. The increase in activities shown by the catalysts containing electronegative substituents on the Saloph ligand is due to the enhancement of the electrophilic character of the cobalt superoxo radical.

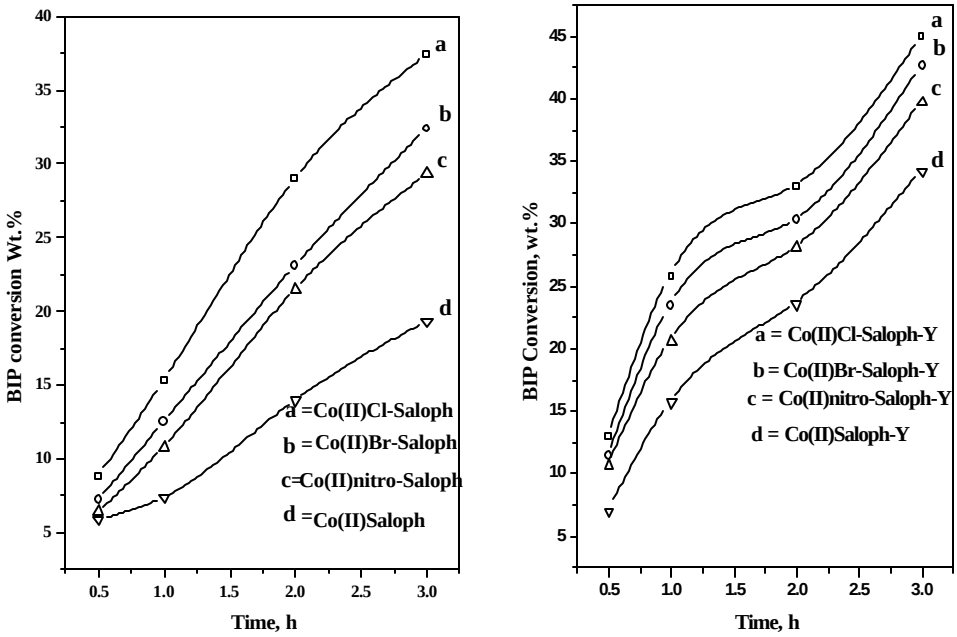

Figure 4.2.1 Conversion of β IP vs. Time plot for "neat" and encapsulated Co(II) complexes

Reaction conditions: β IP = 1 g, acetyl acetone = 0.12 g, triethyl amine = 0.12 g, MEK = 8.0 g, temperature = 298 K, Co(II) catalysts, "neat" = 0.015 g, Co(II) encapsulated = 0.2 g, air = 1 atm.

4.2.3.1 Kinetic study of Co(II)Cl-Saloph-Y "neat" complex catalyzed oxidation of bIP

The Co(II)Cl-Saloph-Y catalyst was chosen for kinetic investigation as it is the most reactive catalysts system in the oxidation reaction. The kinetics of the oxidation of β IP to KIP catalyzed by Co(II)Cl-Saloph-Y was investigated by varying the concentrations of catalyst, substrate, oxidant (air), and temperature. The effect of air pressure was studied by carrying the reaction in a Parr reactor. The rates of oxidation of β IP were evaluated graphically from the moles of β IP converted as a function of time in all the experiments. The kinetic rate data is presented in Table 4.2.2

Table 4.2.2

Kinetic results of Co(II)Cl-Saloph-Y catalyzed oxidation of βIP to KIP

Run No.	Co(II)Cl-Saloph-Y Conc.(mmol)	βIP Conc. (mol)	O_2 (Air) (atm.)	Temp. (K)	Rate of oxidation - x 10^4(mol h^{-1})
Effect of catalyst concentration					
1	0.0370	0.0072	1.0	303	1.75
2	0.0305	0.0072	1.0	303	1.40
3	0.0204	0.0072	1.0	303	1.00
4	0.0100	0.0072	1.0	303	0.41
Effect of BIP concentration					
5	0.0370	0.0145	1.0	303	18.0
6	0.0370	0.0217	1.0	303	22.0
7	0.0370	0.0290	1.0	303	27.0
8	0.0370	0.0360	1.0	303	36.0
Effect of temperature					
9	0.0370	0.0145	1.0	293	10.0
10	0.0370	0.0145	1.0	303	18.0
11	0.0370	0.0145	1.0	313	32.0
Effect of Air (O_2) pressure (volume reaction mixture =30 ml)					
12	0.11	0.0217	1.0	303	22.0
13	0.11	0.0217	7.0	303	28.0
14	0.11	0.0217	14.0	303	34.0

Reaction conditions: acetyl acetone = 0.12 g, tiethyl amine = 0.12 g and MEK = 8.0 g.

4.2.3.2 Rate law

From, the results presented in Table 4.2.2, it is found that, the rates of oxidation of βIP to KIP had a first order dependence with respect to catalyst and βIP concentrations (determined graphically) and half order dependence with respect to oxygen concentration. Based on kinetic dependence studies and the mechanism shown in Scheme – 4.2.2, the overall rate equation for the oxidation of βIP to KIP catalyzed by LCo (II) catalyst systems could be represented as:

$$\text{rate} = k_r K_1 K_2 [\text{Catalyst}][\beta\text{IP}][O_2]^{1/2} \qquad (1)$$

Where, the concentrations of the reactants are represented in square brackets and k_r is rate constant. The order of the reaction is 2.5. The values of k_r, K_1 and K_2 were calculated graphically by a standard method using steady state conditions of the oxidation reaction. These values are k_r = 20.8 $mol^{-3/2} lit^{3/2} s^{-1}$, K_1 = 80.5 M^{-1} and K_2 = 154.6 M^{-1}, respectively.

From the temperature dependence study, the rates of oxidation of βIP determined were plotted as -ln rate vs.1/T (Arrhenius plot, Figure 4.2.2) and from the slope of the straight line; the activation energy evaluated was 12.3 kcal mol^{-1}.

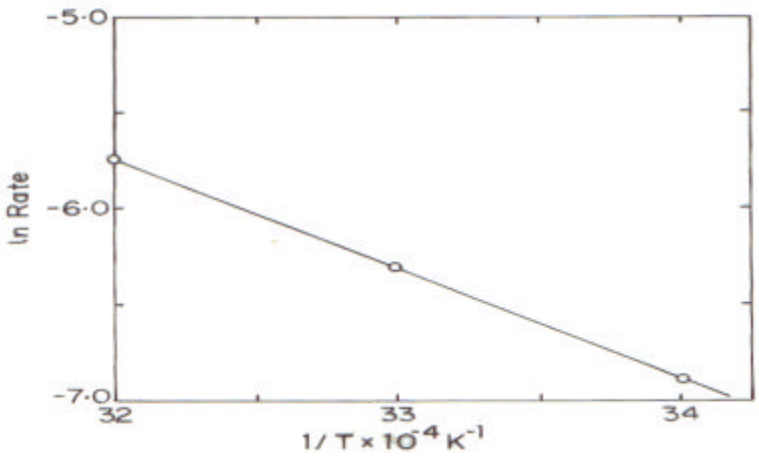

Figure 4.2.2 Arrhenius plot

Thermodynamic activation parameters are of importance in knowing the influence of temperature over the performance of the catalyst in any catalytic transformations. Standard thermodynamic relations were used to calculate thermodynamic activation parameters and these are:

1. Slope of the Arrhenius graph = $- E_a/RT$ (2)

2. Enthalpy of activation, $\Delta H^{\#} = Ea - RT$ (3)

3. Entropy of activation

$$e^{\Delta S\#/R} = h/(k_B T)\,(k_r)\, e^{\Delta H\#/RT} \quad (4)$$

4. Gibb's Free-energy of activation, $\Delta G^{\#} = (\Delta H^{\#} - T\,\Delta S^{\#})$ (5)

Where, E_a = Energy of activation, $\Delta H^{\#}$ = Enthalpy of activation, $\Delta S^{\#}$ = Entropy of activation, $\Delta G^{\#}$ = Free energy of activation, R = gas constant, T = temperature in K, h = Planck's constant, k = Boltzman's constant and k_r = rate constant of the reaction.

Thermodynamic activation parameters evaluated for Co(II)Cl-Saloph-Y catalyzed oxidation of βIP to KIP are; E_a = 12.3 kcal mol^{-1}, $\Delta H^{\#}$ = 11.7 kcal mol^{1}, $\Delta S^{\#}$ = + 40.5 cal deg^{-1} mol^{-1} and $\Delta G^{\#}$ = - 0.57 kcal mol^{-1}.

4.2.3.3 Mechanistic studies

Mechanistic studies of oxidation of βIP were performed using neat Co(II)Saloph by UV-Visible spectroscopy. The UV-Visible spectra of Co(II)Saloph was taken in MEK solvent and it showed an absorption maximum at 450 nm (Figure 4.2.3), which is characteristic of Co(II) species having a square planar configuration. When the catalyst solution was interacted with air, the absorption maximum was shifted to higher wavelength 456 nm, showing the formation of new Co(III)-O-O· superoxo species. When, the substrate was added to this solution, the absorption maximum shifted further to 500 nm, suggesting a complex formation through peroxo linkage. The mechanism proposed for the oxidation of βIP to KIP catalysed by Mn(III)Cl-Salen under homogeneous conditions was similar to the one proposed in Scheme – 4.2.2, wherein, Mn(IV) metalloperoxy intermediate has been proposed as the intermediate species in the oxidation of βIP catalyzed by Mn(III)Cl-Salen under homogeneous conditions [13].

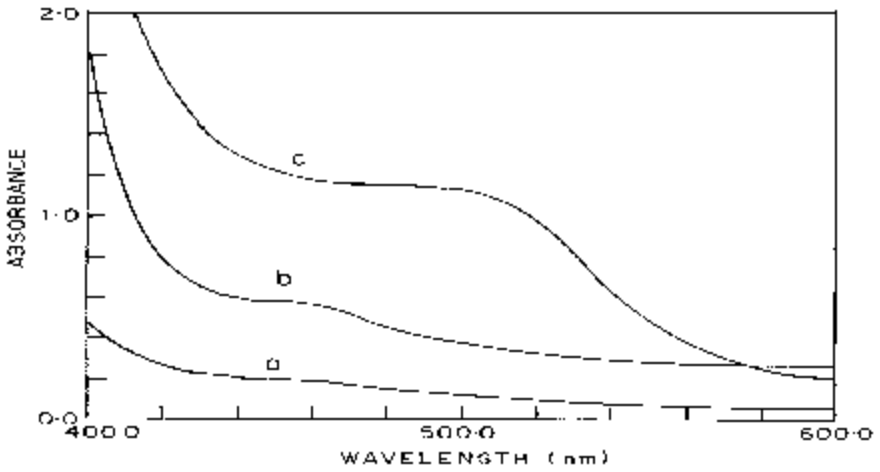

Figure 4.2.3 UV-Visible spectra: (a) "neat" Co(II)Saloph in solvent, (b) Co(II)Saloph + air and (c) Co(II)Saloph + air + BIP.

Based on the mechanistic studies carried out by UV-Visible spectroscopy, a probable mechanism for Co(II) catalyzed oxidation of βIP to KIP has been given in Scheme – 4.2.2.

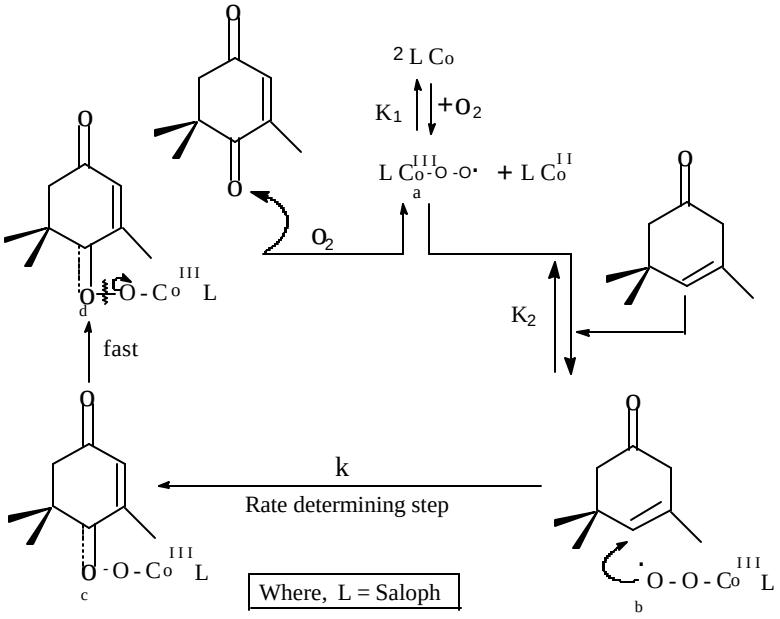

Scheme – 4.2.2 Mechanism

The mechanism in Scheme – 4.2.2, involves the reaction between two moles of LCo(II) catalyst precursor with one mole of oxygen in a equilibrium step to give LCo(III)-O-O· superoxo intermediate species *a* and LCO(II). The formation of species *a* is well established in literature [14]. Species *a* being reactive, it immediately takes up a mole of βIP in another equilibrium step to form a π bonded intermediate species *b*. In a rate-determining step, cyclic peroxometallation takes place to form cyclometalloperoxo species *c*. This in a fast step forms species *d*, which under goes homolytic cleavage by transfer of oxygen and double bond migration to give KIP, while regenerating the active catalytic species *a* in presence of air to continue the catalytic cycle. Similar mechanisms have been proposed for the oxidation of styrene [15] and octene [16] and the oxidation of βIP to KIP [13].

4.2.4 CONCLUSIONS

Zeolite encapsulated Co(II)Saloph complexes catalyzed the oxidation of βIP with molecular oxygen to KIP with higher selectivity (90 %) at BIP conversion (60 %) for a period of 16 h. Encapsulated catalyst systems showed higher activities than their homogeneous analogues in the oxidation reaction. Mechanism of oxidation catalyzed by LCo(II) revealed that the transfer of oxygen to βIP to form KIP took place via LCo(III)-O-O· superoxo intermediate species. The encapsulated catalysts were recycled with Co(II)Cl-Saloph-Y catalyst as a representative and were found that the catalyst was active in the oxidation reaction in three cycles studied. Various parameters of Co(II)Cl-Saloph-Y catalyzed aerial oxidation of βIP was investigated and the rates of oxidation have been obtained for variations made in reaction parameters.

4.2.5 REFERENCES

1. R. A. Sheldon and K. K. Kochi, Metal Complex Catalyzed Oxidation of Organic Compounds, Academic Press, New York, 1981.
2. H. Mayer, Pure Appl. Chem., 51 (1979) 535.
3. O. Isler, Carotenoids, Birkhauser, Basel, 1971.
4 K. K. Light, B. M. Spencer, J. F. Vinals, J. Kiwala, M. H. Vock and E. J. Shuster, US patent 4076854, Chem Abstract 89 11(1978) 23843d.
5. P. Weyerstahl, T. Meisel, K. Mewes, S. Negahdari and Liebigs Ann, Chem. (1991) 19.
6. M. Shibagaki, S. Shibata and H. Kaneko, Agric. Biol. Chem. 45 (1981) 2911.
7. J. N. Marx, Tertrahedron 31 (1975) 1251.
8. E. Demole and P. Enggist, Helv. Chim. Acta 57 (1974) 2087.
9. N. Ito, K. Kinoshita, K. Suzuki, T. Eto, Soda Aromatic, JP Patent 1 175955, Chem. Abstract 112 (1987) 76460.
10. M. Constantini, A. Dromard, M. Jouffret, B. Brossard and J. Varagnat, J. Mol. Catal. 7 (1980) 89.
11. G. S. Selvapati, K. V. Ramanamurty, V. Khandavel, M. J. Rao, R. Vaidyeswaran, IN Patent 167 840, Chem. Absract 118 (1987) 61910.
12. H. Strickler, J. J. Becker, G. Ohloff, Firmenich, US Patent 3931 327, 1973.
13 S. B. Halligudi, N. K. Kala Raj, S. S. Deshpande and S. Gopinathan, J. Mol. Catal. 157 (2000) 9.
14. El-saied A. Aly, J.Mol.Catal., 78 (1993) L1.
15. A. Nishinaga, T. Yamada, H. Fujisawa, K. Ishizaki, H. Ihara and T. Matsuura., J.Mol.Catal. 48 (1988) 249.

16. O. Brotolini, F.D. Furia, G. Modena, R. Seraglia. J. Mol.Catal., 22 (1984) 313.

4.3 OXIDATION OF a -PINENE

4.3.1 INTRODUCTION

Allylic oxofunctionalization of terpenes to oxygenated products is of interest since these products find their use in the preparation of natural product [1]. Allylic oxidation (refer- Oxidation of BIP, chapter 4 part B) and epoxidation are often competitive processes in the oxidation of cyclic olefins and frequently both processes occur simultaneously. The dominance of one or the other process depends on the nature of olefin used and the relative stability of the intermediate allylic radical formed [2]. The epoxidation of bicyclic α-pinene to D-Verbenone using dioxygen as oxidant takes place by the electrophilic attack at the double bond of cyclic olefin leading to epoxidation or ring cleavage [3].

Historically, the autoxidation of pinenes has been known for two centuries, however, high selectivity to a single product in the catalytic oxidation of pinenes has alluded the chemist. The allylic oxidation of α-pinene gives various products (Scheme-4.3.1) out of which D-Verbenone is important because it is considered a suitable precursor in the preparation of taxol, which has recently been introduced as a therapeutic agent [4-5].

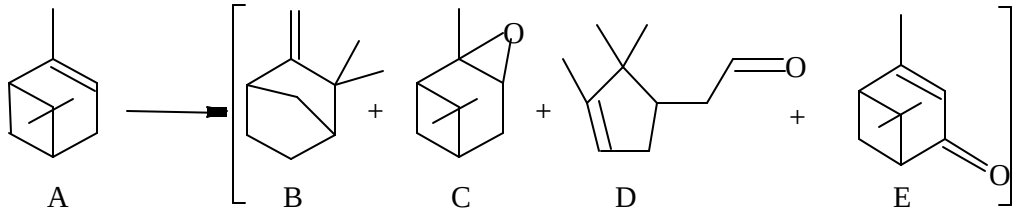

A = α-Pinene, B = Camphene, C = Epoxy, D = Campholene aldehyde and E = D-verbenone

Scheme – 4.3.1 Products of catalytic oxidation of α-pinene

Cobalt and palladium catalysts systems have been reported in the literature for the oxidation of α-pinene [6-7]. Pd/C promoted with Co, Mn, Bi, Cd and Zn has also been used for the oxidation of α-pinene with molecular oxygen to give verbenol and D-Verbenone [8]. Cobalt salts such as cobalt dibromide containing bipyridyl ($Co(C_2H_5N)_2Br_2$ and $Co(4\text{-}Me(C_5H_4N)_2Br_2)$ or fatty acids and chromium salts of fatty acids have been reported as catalysts for the selective oxidation of α-pinene to D-Verbenone [9-10] and these catalysts have been now rejected because of the stoichiometric amounts required and toxicity of waste products, which are not preferred from environmental view point. There is still a scope to develop efficient catalysts for the oxidation of α-pinene to achieve commercially viable and environmentally acceptable reaction conditions. The aim of the present study is to encapsulate the metal complexes in the zeolite and investigate the catalytic and mechanistic studies of α-pinene oxidation using Co(II)Saloph-Y and Ru(III)Saloph-Y and to optimize the condition to get higher yields of epoxy and D-Verbenone.

4.3.2 EXPERIMENTAL

4.3.2.1 Materials

Salicyladehyde, *o*-Phenylene diamine, 5-chlorosalicylaldehyde, 5-bromosalicylaldehyde, 5-nitrosalycylaldehyde, α-pinene and Na-Y were procured from Aldrich Co. Cobalt acetate, ethanol, acetonitrile, *tert*-butanol, concentrated HCl, azo-bis-isobutyronitrile (Azobis) and KCl were procured from Loba Chemicals India and $RuCl_3.3H_2O$ was procured from Arora Mathey Ltd., India.

4.3.2.2 Procedure

The α-pinene oxidation experiments were carried out in a 300 ml Parr autoclave under (O_2) air pressure. In a typical experiment, reaction mixture containing α-pinene (2 g), catalyst, acetonitrile (30 g) and Azobis (0.05 g) (a radical initiator) were placed into the autoclave. The autoclave was then pressurized with air (30 atm.) and was then heated to a temperature of 373 K and kept at that temperature under constant stirring. The reaction mixtures were withdrawn at fixed time intervals and analyzed by gas chromatography (Shimadzu 14B) using FID detector and a SE-52 capillary column. From the gas chromatographic analysis, the conversions of α-pinene and the selectivity of the oxidation products were estimated. The identities of the products were confirmed by GC-MS (Shimadzu GCMS QP 5000).

4.3.3 RESULTS AND DISCUSSION

The "neat" and zeolite encapsulated Co(II)Saloph and Ru(III)Saloph catalysts were used for the aerial oxidation of α-pinene and the experimental conditions and the results are presented in Table 4.3.1. The encapsulated catalyst systems were more active than the corresponding "neat" complexes. The reason being the site isolation of the metal complex molecules from each other within the supercages of the faujasites. The "neat" complexes as catalysts undergo irreversible deactivation due to the formation of μ- peroxo dimeric and other polymeric species and hence cannot be recycled even once as they loose their catalytic activity after use. By contrast, the encapsulated catalysts could be filtered, washed and reused without major loss in activity. Ligand tuning as demonstrated in the Table 4.3.1 for cobalt complexes play a significant role. Substitution of electron withdrawing groups like the halogen or - nitro group enhances the conversion and turnover

frequency, (TOF). Among the Co(II) complexes, Co(II)nitro-Saloph (converted α-pinene = 23.0 %) was more active than Co(II)Cl-Saloph (converted α-pinene = 20.3 %) and Co(II)Br-Saloph (converted α-pinene = 18.7 %) complexes. Substitution of electron withdrawing groups on the ligand enhances the electrophilic character of the active oxygen species and consequently its reactivity. This is comparable with what is reported in literature for porphyrinns [11]. Similar trend in activity is also observed for the encapsulated systems. The Saloph ligand alone in the absence of the metals was not catalytically active.

Table 4.3.1

Catalytic activities of neat and zeolite encapsulated complexes in α-pinene oxidation

Neat Complex (0.004 g)	α-pinene, Conv. (Wt%)	TOF*	Encapsulated Complex (0.04 g)	α-pinene, Conv. (Wt%)	TOF*
Co(II)Saloph	13.2	3524	Co(II)Saloph-Y	30.4	7826
Co(II)Br-Saloph	18.7	6864	Co(II)BrSaloph-Y	31.8	11153
Co(II)Cl-Saloph	20.3	6394	Co(II)ClSaloph-Y	33.8	11868
Co(II)NO_2Saloph	23.0	7402	Co(II) NO_2Saloph-Y	39.7	15341
Ru(III)Saloph	29.4	9044	Ru(III)Saloph-Y (0.02 g)	49.5	18210

Reaction conditions:α-pinene = 2 g (0,0146 mol), Acetonitrile = 30 g, Azobis = 0.05 g, Temperature = 373 K, Air = 30 atm. and Time = 1 h. * = mol ∝-pinene oxidized per mol metal per hour.

Ru(III)Saloph-Y and Co(II)Saloph-Y were tested in the oxidation of α-pinene under similar reaction conditions and the reaction was monitored as a function of time. The conversion of α-pinene as a function of time is shown in Fig. 4.3.1. It is seen from the figure that Ru(III)Saloph-Y was found to be more active than Co(II)Saloph-Y.

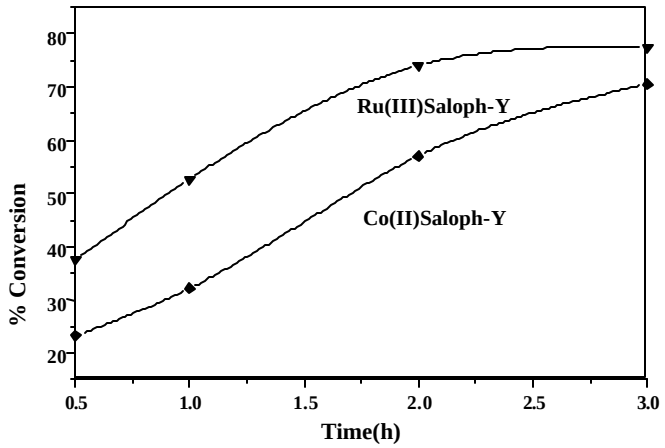

Figure 4.3.1 Conversion as a function of time

Reaction conditions: α-pinene = 2 g, Acetonitrile = 30 g, Ru(III)Saloph-Y = 0.02 g, Co(II)Saloph-Y = 0.050 g, Air = 30 atm, Azobis = 0.05 g and Temp = 373 K.

A highest conversion (75 %) of α-pinene is obtained with Ru(III)Saloph-Y in a contact time of 3 h. The effect of temperature on conversion of α-pinene monitored as a function of time with Ru(III)Saloph-Y catalyst is shown in Fig.4.3.2. At 343 K, the conversion of α-pinene was low and at 373 K and above, conversion of α-pinene was enhanced considerably with time. The effect of solvent on the α-pinene oxidation reaction was carried out with Ru(III)Saloph-Y. Under the reaction conditions studied, the catalyst showed higher activity with acetonitrile solvent compared to acetone and benzene. The

higher catalytic activity in acetonitrile is attributed to the polarity of solvent. Hence, the solvent effect in the oxidation of α-pinene decreased in the order, acetonitrile > acetone > benzene.

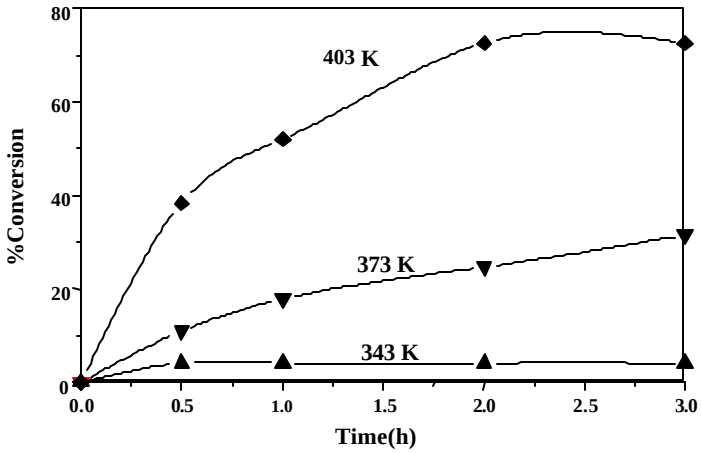

Figure 4.3.2 Effect of reaction temperature on the performance of Ru(III)Saloph-Y. *Reaction conditions*: α-pinene = 2 g, Acetonitrile = 30 g, Ru(III)Saloph-Y = 0.02 g, Air = 30 atm. and Azobis=0.05 g.

The product selectivities of α-pinene oxidation catalyzed by Ru(III)Saloph-Y monitored as a function of time is shown in Fig.4.3.3. It is seen from the figure that the selectivities for epoxy were higher throughout the reaction and the maximum selectivity for epoxy was 35 % in 3 h. The selectivity for D-Verbenone increases marginally with time. On continuing the reaction for a period of 7 h, the selectivity for D-Verbenone increases to 60 % for a conversion of 93 % for α-pinene. Similarly, the graph of selectivity for products *vs.* time for Co(II)Saloph-Y is shown in Fig 4.3.4. The selectivity for D-

Verbenone increases to 40 % for a conversion of 80 % for α-pinene. The mechanisms for the formation of epoxy from α-pinene and D-Verbenone from epoxy are shown in Scheme- 4.3.3 and 4.3.4 respectively.

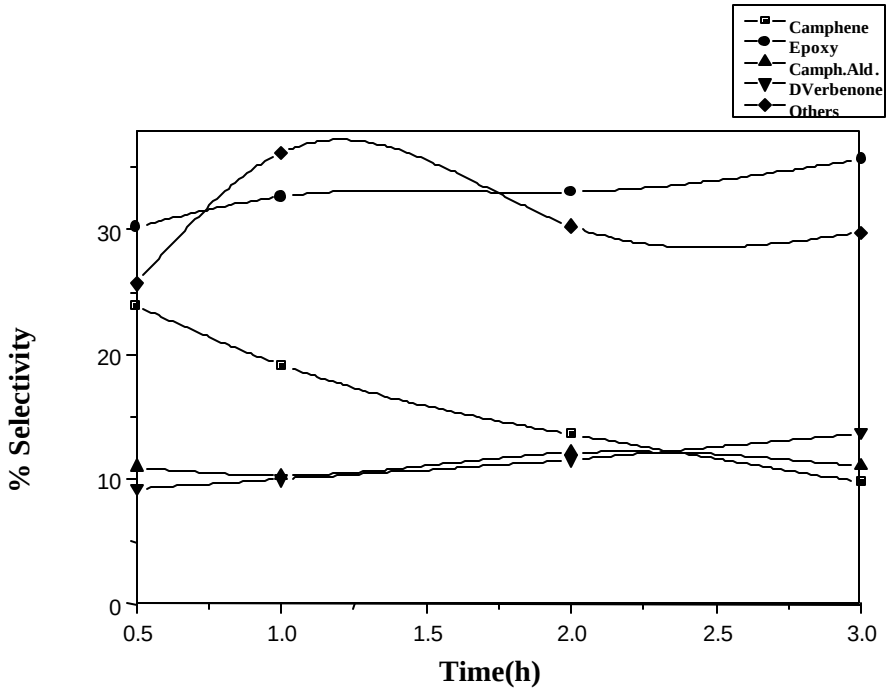

Figure 4.3.3 Products selectivity as a function of time with Ru(III)Saloph-Y.

Reaction conditions: α-pinene = 2 g, Acetonitrile = 30 g, Azobis = 0.05 g, Ru(III)Saloph-Y = 0.02 g, Air = 30 atm. and Temp. = 373 K.

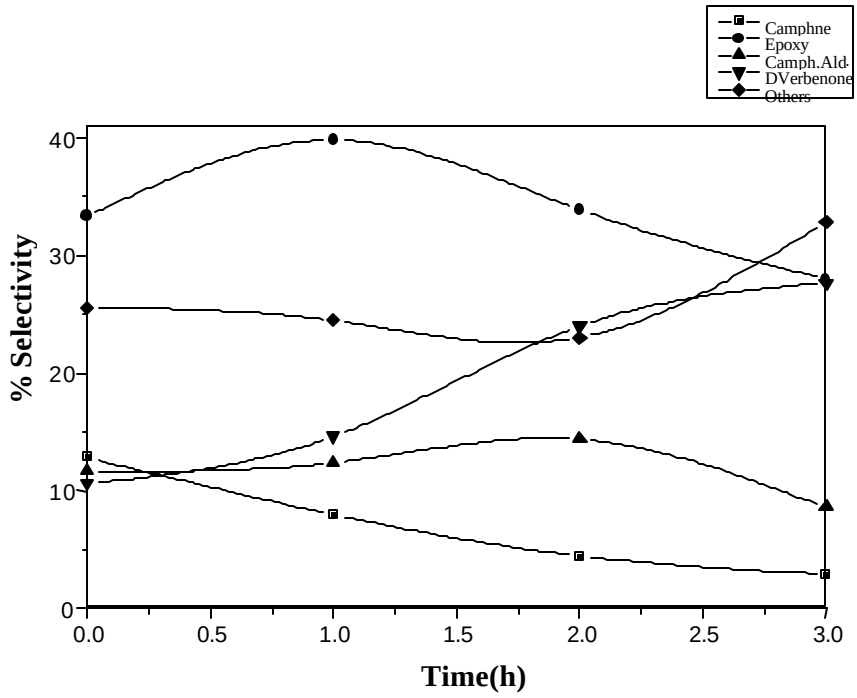

Figure 4.3.4 Products selectivity as a function of time with Co(II)Saloph-Y.

Reaction conditions: α-pinene = 2 g, Acetonitrile = 30 g, Azobis = 0.05 g, Co(II)Saloph-Y = 0.05 g, Ai r = 30 atm and Temp = 373 K.

4.3.3.1 Mechanistic studies

"Neat" Ru(III)Saloph complex was used to study the mechanism of oxidation of α-pinene to epoxy derivatives. The reaction mixture was monitored by UV-Vis spectrophotometer and the absorption spectra are shown in Figure 4.3.5. "Neat" complex in acetonitrile showed absorption maximum at 391 nm, which is a characteristic LMCT absorption band corresponding to Ru^{III} species. The absorption at 391 nm shifted to 400 nm when the above solution was interacted with O_2 (air). This shift could be due to the formation of peroxo ruthenium species $Ru^{IV}O_2^-$ via one electron transfer oxidation. When

α-pinene was added to the above solution the absorption at 400 nm shifted to 402 nm with a reduction in the intensity. This has been attributed to the transfer of oxygen to olefin bond of α-pinene to give epoxy in rate determining step, while Ru^{V}=O species in presence of O_2 active peroxo species is regenerated in a catalytic cycle.

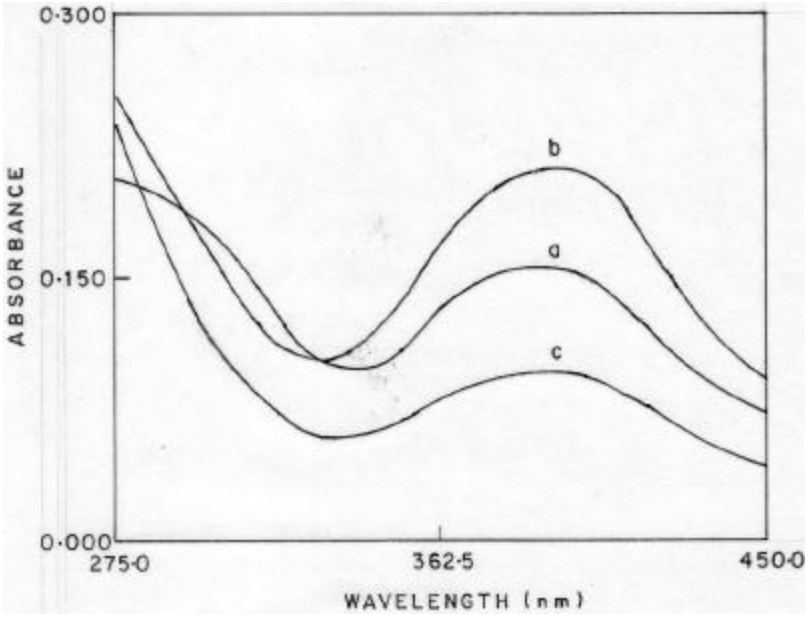

Figure 4.3.5 UV-Vis Spectrophotometric study a) Ru(III)Saloph neat in acetonitrile; b) Ru(III)Saloph neat in acetonitrile + air ; c) Ru(III)Saloph neat in acetonitrile + air + α-pinene.

Based on the above study, the mechanism proposed for [Ru(III)Saloph] neat catalyzed oxidation of α-pinene is shown in Scheme 4.3.2.

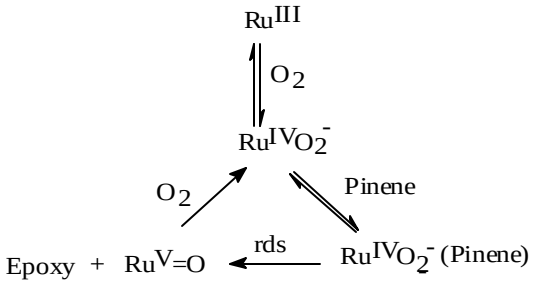

Scheme–4.3.2 Mechanism for α-pinene oxidation using neat [Ru(III)Saloph] complex

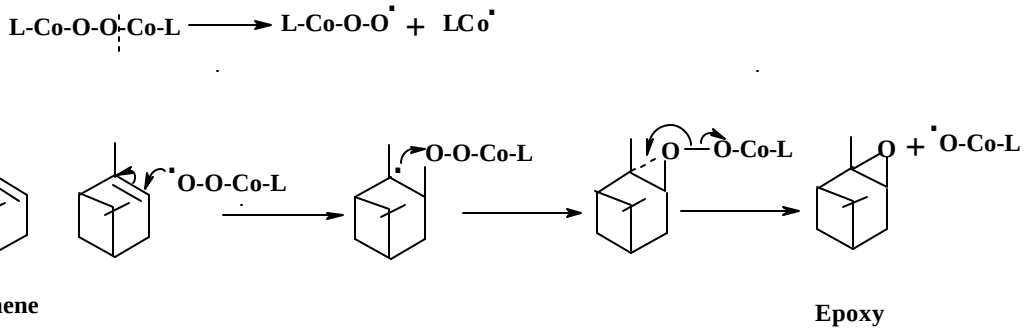

Scheme – 4.3.3 Mechanism for oxidation of α-pinene to epoxy

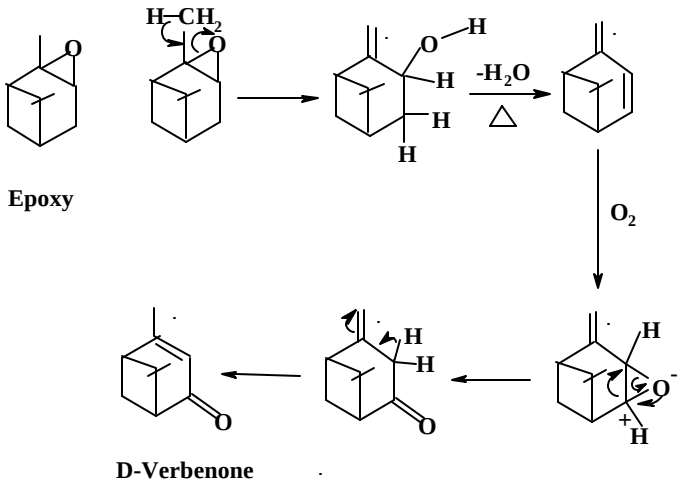

Scheme – 4.3.4 Mechanism for oxidation of epoxy to D-Verbenone

Since zeolite encapsulated metal complexes were used the separation of the catalyst from the reaction mixture was carried out by simple filtration. The mechanism for bicyclic olefins takes place via epoxidation and allylic oxidation [12-13]. The first step in epoxidation ie the attack of double bond and the second step is allylic oxidation i.e abstraction of allylic hydrogen. It is proposed that in case of α-pinene, epoxidation take place other than hydrogen abstraction (HA). For HA, the conformational flexibility of α-pinene molecule should be similar to the transition state but owing to the rigidity of the structure of α-pinene the orbital overlapping required for HA does not take place. This results in easy attack on the double bond, which leads to the formation of epoxide, a primary product in the oxidation of α-pinene.

4.3.4 CONCLUSIONS

The allylic oxidation of α-pinene to its oxygenated products has been investigated using Saloph and substituted (Cl, Br and NO_2) Salophs of cobalt in zeolite-Y. The oxidation of α-pinene resulted in various products like camphene, epoxy, campholene aldehyde and D-Verbenone. Ru(III)Saloph-Y showed higher catalytic activity than Co(II)Saloph-Y with a turn over frequency >18000 at 373 K and 30 atm air. The selectivity for epoxy and D-Verbenone was found to be higher in α-pinene oxidation with both Ru and Co catalyst systems. The catalytic performance of the encapsulated complexes was better than the "neat" complexes. Air was a convenient oxidant than H_2O_2 and TBHP. No leaching of the metal complex in encapsulated systems was observed in the oxidation reaction. Electronic spectra of the reaction mixture indicated that the oxidation of α-pinene proceeds through a free radical mechanism involving peroxoruthenium species as an active intermediate.

4.3.5 REFERENCES

1. G. Rothenberg, Y. Yatziv, Y. Sasson. Tetrahedron. 54 (1998) 593.
2. R. A. Sheldon and K. K. Kochi, Metal Complex Catalyzed Oxidation of Organic Compounds, Academic Press, New York, 1981.
3. K. Kaneda, S. Haruna, T. Imanaka, K. Kawamoto, J. Chem. Soc., Chem. Commun. (1990) 1467.
4. P. A. Wender and T. P. Mucciaro. J. Am. Chem. Soc. 114 (1992) 5878.
5. M. R. Sivik, K. J. Stanton, L. A. Paquette. Org. Synth. 72 (1994) 57.
6. J. Kizlink, M. Hronec, Z. Cvengrosova, M. Harustiak, A. Oblozinsky, J. Ilavsky CS Patent 268 571, Chem. Abstract 116, 214747m (1987).
7. Z. Cvengrosova, M. Hronec. CS Patent 270 180, Chem. Abstract 116, 41802v (1988).
8. Z. Cvengrosova, M. Hronec. CS Patent 270 181, Chem. Abstract 116, 6775s (1988).
9. J. Kizlink, M. Hronec, Z. Cvengrosova, M. Harustiak, J. Ilavsky, Chem. Perum. 39 (1989) 576.
10. M. Lajunen, A. M. P. Koskinen, Tetrahedron Lett. 35 (1994) 4461.
11. Mather et al; 1987; Pessiki and Dismukes.
12. R. S. Drago, Activation of Molecular Oxygen by Transition Metal Complexes. In Dioxygen Activation and Homogenous Catalytic Oxidation; Simandi, L. I., Ed.; Elsiver: Amsterdam, 1991; 83.
13. T. Punniyamurthy and J. Iqbal, Tetrahedron Lett. 35 (1994) 4007.

4.4 OXIDATION OF STYRENE AND *trans*-STILBENE

4.4.1 INTRODUCTION

Catalytic oxidation of olefins to epoxides, carbonyl compounds, diols, cleavage of the olefinic bond etc, is an important area in the preparation of bulk and fine chemicals. Epoxidation of olefins or substituted olefins is a very important and sometimes a necessary step in a number of important organic transformation reactions. Epoxides are industrially important bulk chemicals. These materials are largely used for the synthesis of several perfume materials, antihelminthic preparations, epoxy resins, plasticizers, drugs, sweeteners, etc. Therefore the synthesis of an epoxide by an easier method and a low cost route is of great interest to researchers working in this field.

Homogeneous vanadium complexes have been used in the oxidation of hydrocarbons using oxidants H_2O_2 and *tert*-butylhydroperoxide (TBHP) [1-3]. The vanadium(IV) complex of Salen forms an oxo bridged dimer in solution which inhibits the catalytic activity [4]. This problem may be avoided, in principle, by isolating the vanadium complexes from each other by encapsulation in the cavities of zeolite. Vanadium Salen encapsulated in Y type zeolite was found to be an effective catalyst for the room temperature epoxidation of cyclohexene using TBHP as the oxidant [5]. Upon encapsulation the coordination of VO(IV)Saloph changes from a square pyramidal to an octahedral geometry. Efforts are being made to encapsulate metal complexes in mesoporous silicate, to develop materials capable of catalyzing organic transformations with bulkier substrates [6-10]. It is interesting to investigate the effect of pore size on the structure and activity of the encapsulated metal complex in epoxidation reactions. The epoxidation of styrene has been studied; so far, mostly in homogeneous systems [11-12], or over titanosilicate zeolites [13-14], or heteropolytungstates [15]. Styrene oxide is

manufactured industrially by the reaction of benzene with ethylene oxide or by the epoxidation of styrene by NaOCl. Styrene oxide is an intermediate for the manufacture of the perfumery chemical, phenylethyl alcohol.

In this chapter we describe the studies on the epoxidation of *trans*-stilbene and styrene to corresponding oxygenated products with TBHP using VO(IV)Saloph complex encapsulated in microporous zeolite NaY and mesoporous Al-MCM-41 molecular sieves (refer chapter 2 and 3 for synthesis and characterization). The effect of the two supports on the catalytic activity and selectivity of products is also discussed.

4.4.2 EXPERIMENTAL

4.4.2.1 Materials

NaY (Si/Al = 2.3), tetraethylorthosilicate (TEOS), cetyltrimethylammonium bromide (CTAB), salicylaldehyde, *trans*-stilbene and styrene were procured from Aldrich Co. Tetramethylammonium hydroxide (TMAOH), *tert*-butylhydroperoxide (TBHP) and *ortho*-phenylenediamine were obtained from Merck. All the solvents were of AR grade and were procured from s.d. fine Chemicals, India.

4.4.2.2 Procedure

A known amount of substrate (1.8 g *trans*-stilbene or 1.05 g styrene), catalyst ("neat"- VO(IV)Saloph = 5 mg; VO(IV)Saloph -Y = 50 mg, VO(IV)Saloph-Al-MCM-41 = 20 mg), TBHP (70% solution in water; 2.56 g) and acetonitrile (15 g) were taken in a 50 ml round bottom flask immersed in an oil bath and fitted with a water cooled condenser. The reactions were conducted at 363 K. The progress of the reactions was monitored by withdrawing the samples at different times and analyzing them by a gas chromatograph

(Shimadzu 14B; FID detector; SE-52 capillary column). The identities of the products were confirmed by GC-MS (Shimadzu GCMS QP 5000).

4.4.3 RESULTS AND DISCUSSION

The catalytic activities of "neat" and encapsulated VO(IV)Saloph complexes in the epoxidation of *trans*-stilbene and styrene are presented in Table 4.4.1. The reactions did not proceed in the absence of VO(IV)Saloph confirming that, under the conditions of the experiments, the oxidation is indeed catalytic in nature. Also no reaction took place over Al-MCM-41, VO-Y and VO-Al-MCM-41. The encapsulated complexes exhibited higher activity and selectivity compared to "neat" VO(IV)Saloph. The comparative catalytic activity and selectivity of "neat" and encapsulated complexes are shown in Figure 4.4.1.

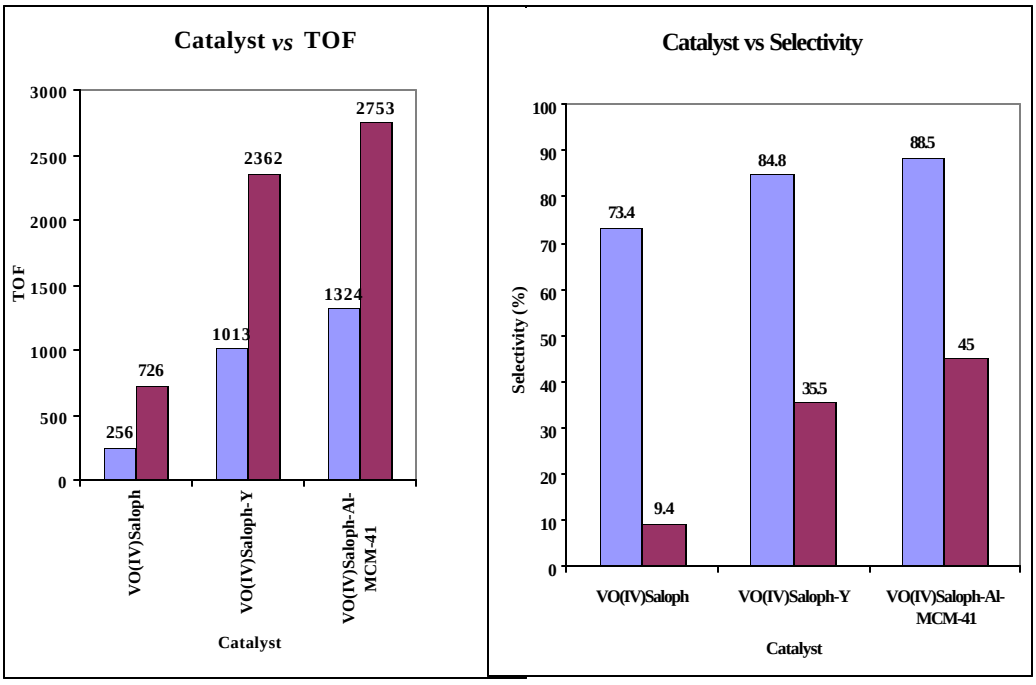

Figure 4.4.1 Catalytic activities of "neat" and encapsulated VO(IV)Saloph complexes

Blue = *t*-stilbene, Brown = styrene

The turnover frequency (TOF) of VO(IV)Saloph-Y and VO(IV)Saloph-Al-MCM-41 were about 4 and 5 times greater than that of "neat" VO(IV)Saloph (Table 4.4.1; Figure 4.4.1). The reaction was selective (73 – 88 mol%) for epoxide in *trans*-stilbene oxidation. However, in styrene epoxidation, double bond cleavage products (e.g., benzaldehyde, etc.) were obtained in significant amounts in addition to epoxide (Table 4.4.1). The encapsulated complexes did not undergo any color change during the reaction and were recovered by filtration and used again for the oxidation of styrene and *trans*-stilbene using TBHP as oxidant. In contrast, the neat complexes were completely destroyed during the first run while changing the color from green to pale yellow. The catalytic activity of the 1st recycles of VO(IV)Saloph-Y and VO(IV)Saloph-Al-MCM-41 is reported in the Table 4.4.1.

Table 4.4.1

Catalytic activities of "neat", zeolite-Y and Al-MCM-41-encapsulated VO(Saloph) in epoxidation of trans-stilbene and styrene with TBHP[a]

Catalyst (weight -mg)	*trans*-stilbene epoxidation			styrene epoxidation				
	conversion (wt.%)	TOF[b]	-epoxide (%)	conversion (wt.%)	TOF[b]	product selectivity (%) -ald	-epoxide	others
VO(Saloph) (5)	9.3	256	73.4	10.7	726	32.3	9.4	58.3
VO(Saloph)-Y (50)	36.8	1013	84.8	34.8	2362	11.5	35.5	53.0
VO(Saloph)-Al-MCM-41 (20)	48.1	1324	88.5	40.6	2753	7.7	45.0	47.3
VO(Saloph)-Y (50)-1st recycle	28.2	-	83	30.1	-	13.8	27.6	58.6
VO(Saloph)-Al-MCM-41 (20) 1st recycle	32.7	-	87.1	28.9	-	7.5	37.2	55.3

[a]*Reaction conditions*: trans-stilbene epoxidation: trans-stilbene = 1.8 g (10 mmol), acetonitrile = 15 g, TBHP = 2.56 g (20 mmol) temp.=363 K, reaction time = 5 h; styrene epoxidation:styrene = 1.04 g (10mmol), acetonitrile (20g), TBHP = 2.56 g (20 mmol), temp.= 363 K and reaction time = 2 h ,[b]TOF = mole substrate oxidized per mole of metal per hour.

Encapsulation has a marked effect on the product selectivity. This is more obvious, particularly, in styrene epoxidation. Yield of styrene epoxide was 4 to 5 times greater over the encapsulated complexes than with "neat" VO(IV)Saloph (Table 4.4.1). Among the encapsulated complexes, VO(IV)Saloph-Al-MCM-41 was more active than VO(IV)Saloph-Y. The difference in activity is perhaps due to diffusion limitations in Y-type zeolites or the cage effect. In the reactions with metal Schiff base complexes in homogeneous medium one often encounters catalyst deactivation due to formation of oxo-bridged dimer complexes. However, such a deactivation is suppressed on heterogenizing the Schiff base complexes (Table 4.4.1; Figure 4.4.1). This is evident from the spectroscopic studies (*vide infra*).

The effect of catalyst, substrate and oxidant concentrations and temperature on *trans*-stilbene epoxidation over VO(IV)Saloph-Al-MCM-41 were investigated. The kinetics data were interpreted using the initial rate approach model. The studies were carried out at the following reaction conditions:

(i) The concentration of the catalyst was varied between 9.7 to 38.9 mM by keeping the temperature (363 K) and concentrations of *trans*-stilbene (1 mM), and TBHP (2 mM) constant.

(ii) The substrate to catalyst mole ratio was varied between 13 – 39, by keeping the temperature (363 K) and concentrations of TBHP (2 mM) and catalyst (20 mM) constant.

(iii) TBHP to substrate (mM) ratio was varied between 1 and 3, by keeping substrate to catalyst mole ratio (19.5) and temperature (363 K) constant.

(iv) By keeping substrate to catalyst and substrate to oxidant ratio constant, reaction temperature was varied between 343 and 363 K.

The results revealed a first order reaction rate dependence with the catalyst and substrate and half-order dependence with the oxidant. From the plot of ln(rate) versus 1000/T, the thermodynamic parameters were evaluated to be E_a = 6.7 kcal.mol^{-1}, $\Delta H^{\#}$ = 5.7 kcal.mol^{-1}, $\Delta S^{\#}$ = 15.8 cal.deg^{-1}.mol^{-1} and $\Delta G^{\#}$ = -0.0042 kcal.mol^{-1}.

Based on the kinetic data, the rate of epoxidation of *trans*-stilbene could be written as:

$$\text{rate} = k\,[\text{catalyst}][\textit{trans}\text{-stilbene}][\text{TBHP}]^{1/2}. \qquad (2)$$

where k is the rate constant. Substituting [catalyst] in terms of its total concentration ($[\text{catalyst}]_T$), eq. (2) can be rewritten as:

$$[\text{catalyst}]_T\,[\textit{trans}\text{-stilbene}]/\text{rate} = 1/k\,[\text{TBHP}]^{1/2} + 1/k \qquad (3)$$

The plot of the left-hand side of the eq. (3) verses $[\text{TBHP}]^{1/2}$ gave a straight line with a finite intercept. From the slope and intercept of the straight line, the value of k was determined to be 0.11mol$^{-3/2}$lit$^{3/2}$s^{-1}.

The mechanism of epoxidation over "neat" and encapsulated VO(IV)Saloph catalysts with TBHP was investigated by *in situ* ESR and UV-Vis spectroscopies. In the reactions with "neat" VO(IV)Saloph, a known quantity of the reaction mixture was taken out at different time intervals and subjected for the spectroscopic studies. However, with the solid, encapsulated catalysts, the reactions were performed for a specific period of time and then the catalyst was separated by filtration, dried and characterized by ESR. Representative spectra of "neat" and encapsulated VO(IV)Saloph as a function of reaction time are shown in Figure 4.4.2 (i – iii). For reactions in homogeneous medium using "neat" VO(IV)Saloph, the intensity of vanadium ESR signals decreased with time and disappeared at 135 min (Figure 4.4.2 (i); trace d). In the absence of substrate (stilbene) the signals disappeared at 105 min

itself. Interestingly, the encapsulated catalysts (VO(IV)Saloph-Y and VO(IV)Saloph-Al-MCM-41) were ESR active even after 24 h (Fig. 4.4.2 (ii and iii); trace d).

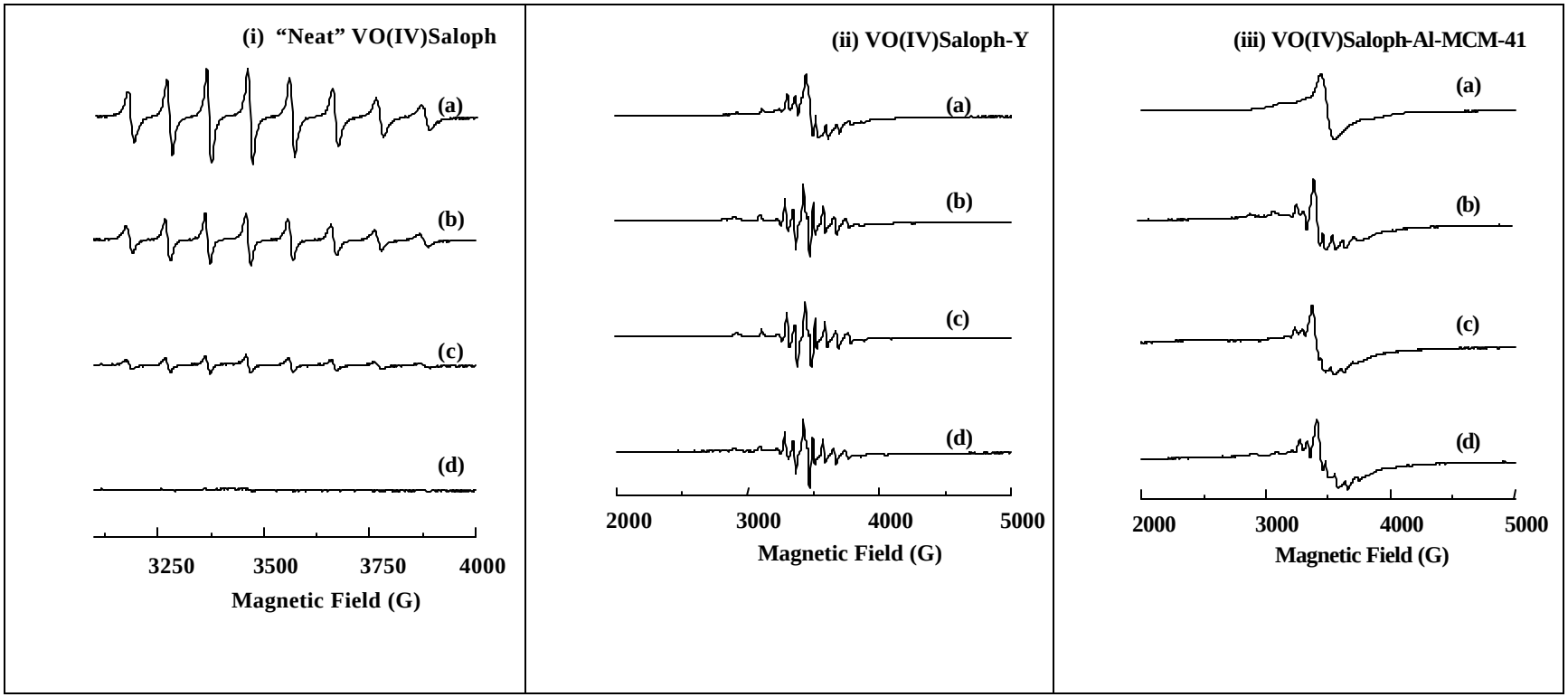

Figure 4.4.2 ESR spectra (at 298 K) of reaction mixtures in *trans*-stilbene oxidation:

(i) over "neat" VO(IV)Saloph: reaction time – (a) 0, (b) 30, (c) 60 and (d) 135 min; (ii) VO(IV)Saloph-Y: reaction time - (a) 0, (b) 2 (c) 4 and (d) 6-24 h. (iii) VO(IV)Saloph-Al-MCM-41: reaction time - (a) 0, (b) 2 (c) 4 and (d) 6-24 h.

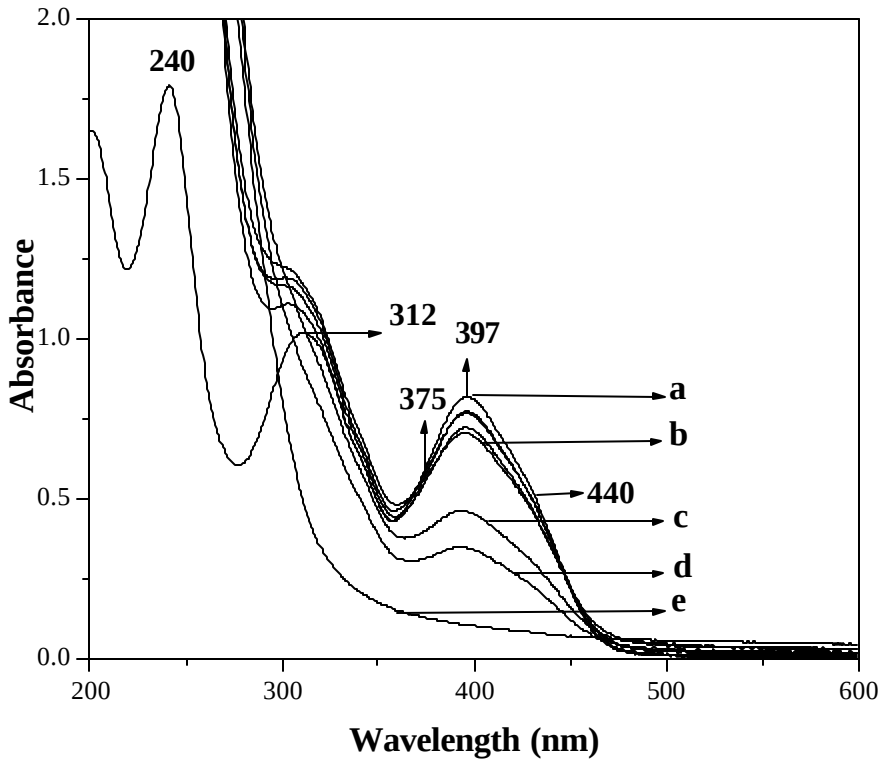

.

Figure 4.4.3 *In situ* UV-Vis studies of *trans*-stilbene oxidation using "neat" VO(IV)Saloph.

a) VO(IV)Saloph + acetonitrile, b) 30 min. after adding TBHP, c) 1 h. after adding TBHP, d) 1.15 h. after adding TBHP, e) 2 h. after adding TBHP.

VO(IV)Saloph in acetonitrile showed characteristic UV-Vis bands at 240 and 312 nm, respectively due to π-π^* and n-π^* transitions of Saloph and at 397 nm with shoulder at 440 nm attributable to O$\rightarrow$V charge transfer/d-d transitions (Figure. 4.4.3). On interaction with TBHP (in the absence of substrate) the intensity of 397 nm band decreased and that of 312 nm increased and shifted to higher energy side with an

isosbestic point at 375 nm (Figure 4.4.3). These bands (312 and 397 nm) disappeared after 1.15 h. These spectral variations reveal instability of "neat" VO(IV)Saloph in the homogeneous reaction conditions and formation of new oxo-vanadium species. The results are in agreement with the *in situ* ESR studies (Figure 4.4.2 (i)) where a transformation of paramagnetic vanadium to an ESR-silent vanadium species was noted. VO(IV)Saloph forms vanadium peroxo complexes on interaction with TBHP. The peroxo complex transfers one of its oxygen atoms to the substrate and itself gets converted into an oxo-hydroxo or dioxo-vanadium species. In the homogenous medium these species can further react forming ultimately an ESR inactive μ-oxo-vanadium(IV) complexes [16-17]. The latter are catalytically inactive. However, in the solid catalysts, VO(IV)Saloph molecules are well separated due to confinement in the cages or interactions with the support as revealed from ESR studies and remain active throughout the reaction (Figure 4.4.2 (ii and iii); trace d). Although the formation of such catalytically inactive, μ-oxo complexes during the reaction and the advantage of heterogenizing metal complexes in suppressing the formation of such inactive species was postulated earlier, it has not been proved, so far, experimentally. Site isolation of the complex inside Na-Y and Al-MCM-41 stabilizes the monomeric complex and prevents the conversion of catalytically active oxo-hydroxo or dioxo-vanadium species to catalytically inactive μ-oxo brided dimer and hence giving high TOF. The *in situ* spectral characterizations unequivocally establish this hypothesis. The encapsulated VO(IV)Saloph complexes are advantageous over the "neat" VO(IV)Saloph in that they can be easily separated and reused.

4.4.4 CONCLUSIONS

VO(IV)Saloph complexes encapsulated in zeolite-Y and Al-MCM-41 exhibited high catalytic activity and selectivity in the epoxidation of *trans*-stilbene and styrene. Encapsulation and the pore size have marked effects on the *trans*-stilbene and styrene epoxidation activities of VO(IV)Saloph, with *tert*-butylhydroperoxide as oxidant. The encapsulated complexes are more active (by 4 to 5 times) than the "neat" complexes. Among the encapsulated complexes, VO(IV)Saloph-Al-MCM-41 was more active than VO(IV)Saloph-Y. This difference in activity is attributed to diffusional limitations and cage-size effect. *In situ* ESR and electronic spectroscopic studies revealed that encapsulation enhances the stability of VO(IV)Saloph complexes during the oxidation reaction by suppressing the formation of inactive μ-oxo-vanadium species.

4.4.5 REFERENCES

1. A. Kozlov, K. Asakura, Y. Iwasawa, Microporous Mesoporous Mater. 21 (1998) 571.
2. C.J. Chang, J.A. Labinger, H.B. Gray Inorg. Chem. 36 (1997) 5927.
3. P.P. Knops-Gerrits, C.A.Trujillo, B.Z.Zhan, X.Y.Li, P. Rouxhet and P. A. Jacobs, Topics Catal. 3 (1996) 437.
4. E. Tsuchida, K. Yamamoto, K. Oyaizu, N. Iwasaki and F.C. Anson, Inorg. Chem. 33 (1994) 1056.
5. K. J. Balkus Jr., A. K. Khanmamedova, K. M. Dixonand, F. Bedioui, Appl. Catal. A: 143 (1996) 159.
6. S. Ernst and M. Selle, Microporous Mesoporous Mater. 27 (1999) 355.
7. C. Liv, Y. Shan, X. Xang, X. Ye, Y. Wu, J. Catal. 168 (1997) 35.
8. B.M. Choudhary, M.L. Laxmikantam, B.Bharathi, P.Sreekanth, F. Figueras, J. Mol. Catal. A: 159 (2000) 417.
9. S.-S.Kim, W.Zhang and T.J. Pinnavaia, Catal. Lett. 43 (1997) 149.
10. M. Eswaramoorthy, Neeraj and C.N.R. Rao, Chem. Commun. (1998) 615.
11. P. P. Knops-Gerrits, D. de Vos, F. T. Starzyk and P. A. Jacobs, Nature, 369 (1994) 543.
12. K. Srinivasan, P. Michaud and J. K. Kochi, J. Am. Chem. Soc., 108 (1986) 2309.
13. R. Irie, Y. Ito and T. Katsuki, Syn. Lett., (1991) 265.
14. S. B. Kumar, S. P. Mirajkar, G. C. G. Pais, P. Kumar and R. Kumar, J. Catal., 156 (1995) 163.
15. J. S. Reddy, U. R. Khire, P. Ratnasamy and R. B. Mitra, J. Chem. Soc., Chem. Commun., (1992) 1234.

16. K. Oykizu, K. Yamamoto, K. Yoneda and E. Tsuchida, Inorg. Chem. 35 (1996) 6634.

17. E. Tsuchida, K. Oyaizu, E.L. Dewi, T. Imai and F.C. Anson, Inorg. Chem. 38 (1999) 3704.

4.5 OXIDATION OF ADAMANTANE

4.5.1 INTRODUCTION

Metal complexes have been recognized as potential catalysts for the oxidation of hydrocarbons. The desire of higher TON and reusability of the catalyst have lead to the development of heterogenizing metal complexes in microporous materials such as zeolite-Y [1-3]. However due to the size restrictions in zeolite-Y the encapsulation of large complexes is difficult, as it imposes some geometrical restrictions on the complexes to accommodate it and makes it difficult for substrates to diffuse and access the active sites and for products to diffuse out of the pores [4-5]. Hence the focus has been shifted to mesoporous materials having bigger pores and higher surface area [6-7]. Since direct immobilization of such complexes by impregnation into the mesoporous support is not advantageous due to the possibilities of leaching, the anchoring of these metal complexes through an organic spacer to the support is preferred. These inorganic-organic hybrid materials offer great scope for the development of new catalysts [8-12]. Brunel has reported immobilization of large number of complexes inside the channels of these materials [13]. The amine functions of triazocyclonane (TACN) was reacted with the epoxy groups of MCM-41 grafted (3-glycidyloxypropyl)-trimethoxy silane and was used to anchor 2-hydroxyalkyl-substituted TACN ligands to MCM-41 and its manganese complex was used for the epoxidation of styrene with H_2O_2 [14]. Similarly ruthenium (II)mesotetrakis(4-chlorophenyporphyrin) was anchored on to the walls of MCM-41 modified with 3-aminopropyl triethoxysilane (APTES) and was used for the alkene oxidation by TBHP [15].

Adamantane has been used in the literature as a model to probe into the mechanistic aspects of C-H activation reactions [16-21]. D. Mansuy *et al* has reported the hydroxylation of adamantane with H_2O_2 using iron polynitroporphyrins as catalyst [22].

This chapter deals with the catalytic studies for the oxidation of adamantane using anhydrous urea hydrogen peroxide (UHP) as oxidizing agent. The result obtained with the immobilized catalyst is compared with those obtained with the corresponding homogeneous catalyst.

4.5.2 EXPERIMENAL

4.5.2.1 Materials

Tetraethylorthosilicate (TEOS), cetyltrimethylammoniumbromide (CTAB), 3-chloropropyl triethoxysilane (CPTES), salicylaldehyde, di-ethylene triamine, $VOSO_4$ and adamantane were procured from Aldrich Co. Tetramethylammonium hydroxide (TMAOH), urea and H_2O_2 were obtained from Merck. All the solvents were of AR grade and were procured from s.d. fine Chemicals, India and were distilled and dried before use.

4.5.2.2 Procedure

A known amount of substrate (1.36 g adamantane), catalyst ("neat"-VO(Salten) = 3 mg and VO(IV)Salten-Si-MCM-41 = 50 mg), UHP = 1.88 g and acetonitrile = 40 g were taken in a 100 ml round bottom flask immersed in an oil bath and fitted with a water cooled condenser. The reactions were conducted at 333 K. The progress of the reactions was monitored by withdrawing the samples at different times and analyzing them by a gas chromatograph (Shimadzu 14B; FID detector; SE-52 packed column). The identities of the products were confirmed by GC-MS (Shimadzu GCMS QP 5000).

4.5.3. RESULTS AND DISCUSSION

The catalytic oxidation of adamantane was investigated in non-aqueous medium using urea hydrogen peroxide as the oxidant and with "neat" VO(IV)Salten

and VO(IV)Salten-Si-MCM-41 complex. The two major products obtained were 1-adamantanol (1-ol) and 2-adamantanone (2-one)(Scheme – 4.5.1). Ganeshpure *et al* have reported similar product pattern for adamantane oxidation [23]. The kinetics data were interpreted using the initial rate approach model. The kinetic investigations results revealed a first order reaction rate dependence with the catalyst and substrate and half-order dependence with the oxidant. The reactions did not proceed in the absence of VO(IV)Salten. Also no reaction took place over Si-MCM-41 and Cl-Si-MCM-41. The reaction conditions have been optimized towards maximum conversion by varying different parameters.

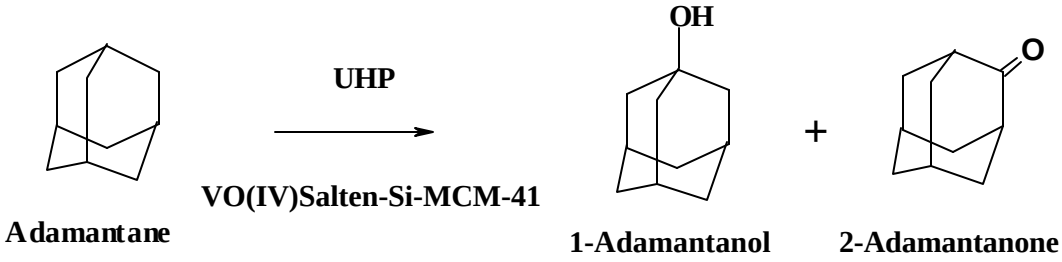

Scheme – 4.5.1 Reaction scheme for oxidation of adamantane

4.5.3.1 Effect of oxidants

The effect of different sources of the oxidizing agents on the conversion of adamantane (wt. %) and product selectivity (wt. %) was studied (Table-4.5.1) for comparison keeping other parameters (adamantane : UHP mole ratio, temperature, catalyst concentration and solvent) constant. It is observed that the adamantane conversion in the case of UHP is more than that of TBHP and aqueous H_2O_2. As evident from the table that air and TBHP are not good oxidants in the case of

adamantane oxidation under this reaction condition. In the case of aqueous H_2O_2 the conversion was found to be lower than that of solid UHP. This is because of the slow release of hydrogen peroxide from the urea hydrogen peroxide adduct [24]. The reaction stops almost after 3 h. due to the complete consumption of peroxide.

Table-4.5.1

Effect of Different Oxidants on the oxidation of adamantane

Oxidant	Conversion, wt. %	Product distribution, wt. %		
		1-ol	2-one	Others
UHP	22.7	55.6	43.2	1.2
H_2O_2	14	61.7	38.3	nil
TBHP	2	75	25	nil
O_2(air)	nil			

Reaction conditions: Catalyst wt.% = 50 mg, Adamantane : oxidant (mol/mol) = 1 : 2, Temp. = 333 K, solvent (acetonitrile) = 40 g and reaction time = 2.5 h.

4.5.3.2 Effect of UHP concentration

In Figure 4.5.1 the effect of adamantane/UHP mole ratio on the adamantane conversion and selectivity as a function of reaction time is plotted. The conversion increases with time with the increase in the mole ratio of adamantane/UHP and almost attains a steady state after 2 h. This increase in conversion becomes marginal beyond adamantane/UHP ratio 1:5 (data not shown) and no significant change in the selectivity is observed with the increase in the ratio.

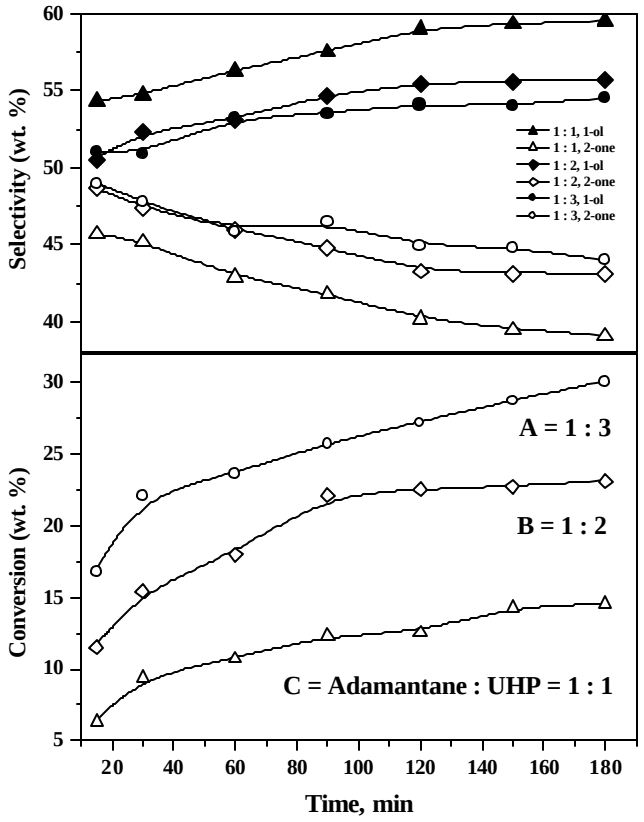

Figure 4.5.1 Effect of adamantane to UHP mole ratio on the oxidation of adamantane.

Reaction conditions: catalyst = VO(IV)Salten-Si-MCM-41 = 50 mg, Temp. = 333 K, (acetonitrile)= 40 g and reaction time = 3 h.

4.5.3.3 Effect of temperature

The effect of temperature on the adamantane conversion and selectivity is shown in Figure 4.5.2. The adamantane conversion first increases linearly with time up to 90 min. in the temperature range of 323 – 333 K. This is because of the slow decomposition of UHP and thus making hydrogen peroxide available for a longer time. On further increasing the temperature (343 K) there is a sudden increase in conversion up to 15 min. and then it attains a steady state.

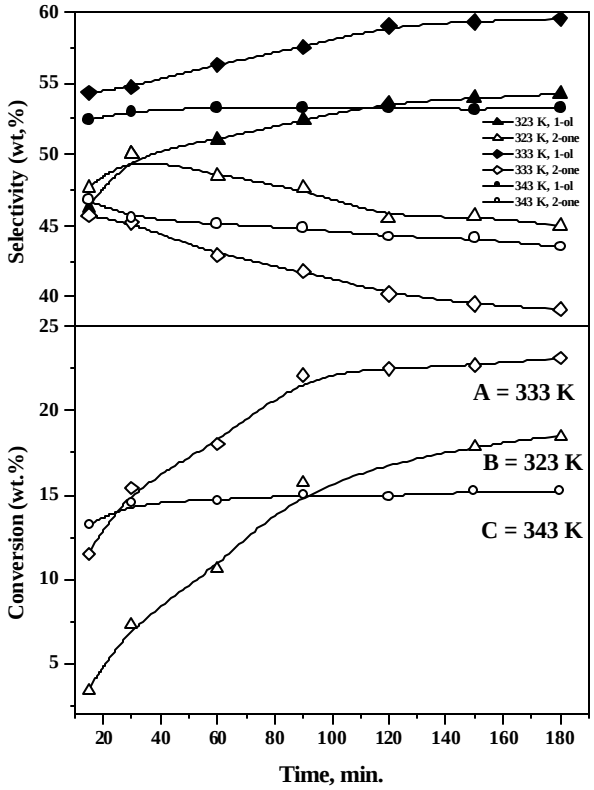

Figure 4.5.2 Effect of reaction temperature on the oxidation of adamantane.

Reaction conditions: catalyst = VO(IV)Salten-Si-MCM-41 = 50 mg, adamantane = 1.36 g, UHP = 1.88 g, acetonitrile = 40 g and reaction time = 3 h.

This may be due to the fast decomposition of UHP since the stability of urea hydrogen peroxide adduct decreases on increasing the temperature which facilitates the

faster decomposition of peroxide. Therefore from the Figure 4.5.2 it is clear that increasing the temperature above 333 K does not enhance the percentage conversion of adamantane using UHP as oxidant.

4.5.3.4 Effect of catalyst concentration

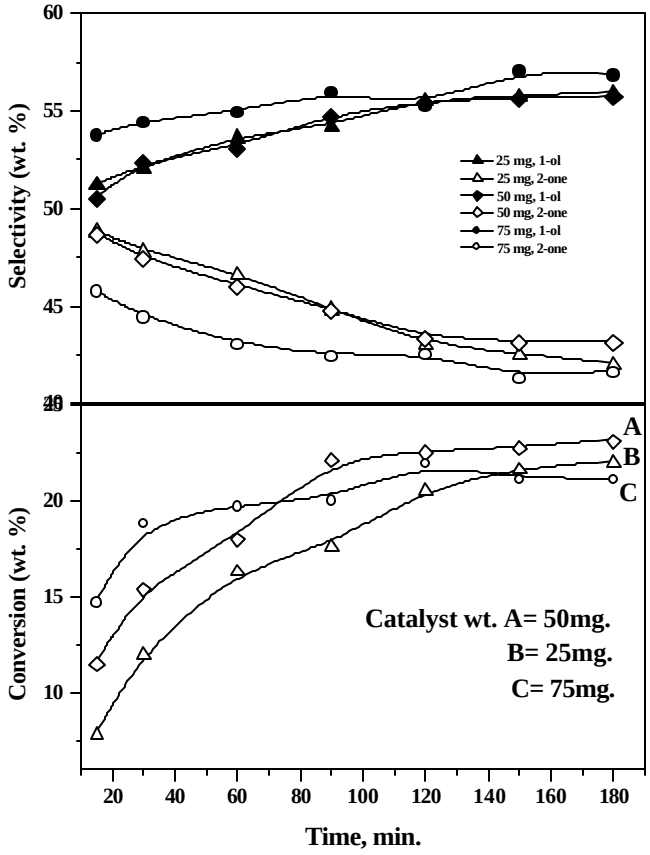

Figure 4.5.3 Effect of catalyst concentration on the oxidation of adamantane.

Reaction conditions: adamantane = 1.36 g, UHP = 1.88 g, Temp. = 333 K, acetonitrile = 40 g and reaction time = 3 h.

Figure 4.5.3 depicts the effect of catalyst concentration on the oxidation of adamantane. The amount of catalyst was varied in the range of 25 mg-75 mg. It is observed that an increase in the catalyst concentration with respect to adamantane resulted in an increase in the conversion of adamantane initially, and then attained a

steady state after 1h of the reaction time. This could be because of the decomposition of peroxide by excess catalyst.

4.5.3.5 Effect of anchoring

Oxidation of adamantane was also carried out using "neat" VO(IV)Salten containing the same amount of vanadium as in the case of anchored complex. The results are stated in Table-4.5.2. It is evident from the table that the conversion increases on anchoring the complex. Earlier studies reveal that the "neat" Vanadium (IV)complexes of Schiff bases like Salen tends to form oxo-bridged dimer in solution [4, 25-26] thus inhibiting the catalytic activity. Therefore in the present study it is evident that the higher conversions for adamantane is because the VO(IV)Salten molecules are isolated and well separated from each other since they are anchored to the walls of MCM-41.

Table 4.5.2

Catalytic activities of "neat" and VO(IV)Salten-Si-MCM-41 in oxidation adamantane with UHP[a]

Catalyst (weight -mg)	Adamantane oxidation				
	Conv. (wt.%)	TOF[b]	Product selectivity (wt.%)		
			1-ol	2-one	Others
"Neat" VO(IV)Salten (3)	5	31	56	44	1.58
VO(IV)Salten-Si-MCM-41 (50)	22	141	55.7	43.2	1.1

[a]*Reaction conditions* : adamantane = 1.36 g, UHP = 1.88 g, acetonitrile = 40 g, temp.=333 K, reaction time = 2 h and [b]TOF = mole substrate oxidized per mole of metal per hour.

From the above study it is evident that the reaction rate enhances in the beginning with time and then becomes constant after 2h. The conversion of adamantane attains a maximum level after 3h. A conversion of 23% and a selectivity of 56% and 43% are obtained with the immobilized catalyst.

4.5.4 CONCLUSIONS

A significant increase in the conversion of adamantane was observed on anchoring the complex inside the mesopores of Cl-Si-MCM-41. The conversions were low in the case of homogeneous complex compared to that of anchored complex. The formation of catalytically inactive μ-oxo-bridged complexes with "neat" VO(IV)Salten complex has been speculated as the cause of catalyst deactivation. When UHP was used as an oxidant for adamantane oxidation a significant increase in the conversion was observed compared to the use of aqueous H_2O_2. This is because of the slow release of peroxide from the urea-hydrogen peroxide adduct. These inorganic-organic hybrid materials have proved to be efficient catalysts as the active species are covalently bound to the support and place no restrictions on the pore size.

4.5.5 REFERENCES

1. N. Herron, Inorg. Chem., 25 (1986) 4714.
2. C. Bowers, P.K. Dutta, J. Catal., 122 (1990) 271.
3. K.J. Balkus Jr., A.K. Khanmamedova, K.M. Dixon, F. Bedioui, Appl. Catal. A: General 143 (1996) 159.
4. R.F. Parton, D.R.C. Huybrechts, P. Buskens, P.A. Jaccobs, Zeolites as Catalysts For Alkane Oxidations in Catalysis and Adsorption by Zeolites, Elsevier, Amsterdam (1991).
5. N. Herron, J. Coord. Chem., 19 (1988) 25.
6. S.-S. Kim, W. Zhang, T.J. Pinnavaia, Catal. Lett. 43 (1997) 149.
7. G-J Kim, D-W Park, Catalysis Today, 63 (2000) 537.
8. C. Huber, K. Moeller, T. Bein, Chem. Commun. (1994) 2619.
9. J. Diaz, S.G. Li, W.Q. Pang, C.M. Che, Chem. Commun. (1997) 641.
10. J.H. Clerk D.J. Macquarrie, Chem. Commun (1998) 853.
11. P. Sutra, D. Brunel, Chem. Commun (1996) 2485.
12. J. Chisem, I.C. Chisem, J.S. Rafelt, D.J. Macquarrie, J.H. Clerk Chem. Commun. (1997) 2203.
13. D. Brunel, Microporous Mesoporous Mat. 27 (1999) 329.
14. Y. V. S. Rao, D. E. De Vos, T. Bein, P. A. Jacobs, Chem. Commun. (1997) 355.
15. C-J. Liu, S-G. Li, W-Q. Pang, C-M. Che, Chem. Commun. (1997) 65.
16. D. H. R. Barton, M. J. Gastiger, W. B. Motherwell, Chem. Commun. (1983) 41.
17. D. H. R. Barton, D. Doller, Acc. Chem. Res. 25 (1992) 504.
18. I. Tabushi, T. Nakajima, K. Seto, Tetrahedron Lett. 21 (1980) 2565.
19. D. H. R. Barton, Ammerican Chemical Society: Washington, DC (1991) 103.

20. A. E. Tapper, J. R. Long, R. J. Staples, P. Stavropoulos, Angew. Chem. Int. Ed. 39 (2000) No. 13h, 2343.

21. P. Stavropoulos, R. C-Cetin, A. E. Tapper, Acc. Chem. Res. 34 (2001) 745.

22. J-F. Bartoli, K. Le Barch, M. Palacio, P. Battioni, D. Mansuy, Chem. Commun. (2001) 1718.

23. G. L. Tembe, P. A. Ganeshpure, S. Satish, J. Mol. Catal. A: Chemical 121 (1997) 17.

24. A. M. A. R. Gonsalves, R. A. Johnstone, M. M. Pereira, J. Shaw, J. Chem. Res.(S), (1991) 208.

25. E. Tsuchida, K. Yamamoto, K. Oyaizu, N. Iwasaki, F. C. Anson, Inorg. Chem., 33 (1994) 1056.

26. T. Joseph, D. Srinivas, C. S. Gopinath, and S. B. Halligudi, Catal. Lett., 83, 3-4 (2002) 209.

4.6 HYDROGENATION OF OLEFINS

4.6.1 INTRODUCTION

Since the discovery of the M41S family of materials by Mobil Corporation scientists in 1992 [1,2], much attention has been paid to the synthesis and applications of mesoporous molecular sieves. In 1998 Stucky and co-workers [3] synthesized a new ordered hexagonal mesoporous silica with much thicker walls named SBA-15 using triblock co-polymer; poly(ethylene oxide)-poly(propylene oxide) poly(ethylene oxide) [EO_n-PO_m-EO_n] as the structure directing agent. These mesoporous materials because of their high surface area, tunable pore size and well modified surface properties [4-5] are finding use as adsorbents for the removal of toxic heavy metal ions from waste water [6], enzyme carriers [7], catalysts [8] and materials to sequester and release proteins [9].

The chemical reactivity of these mesoporous materials facilitates the co-valent anchoring of various functional groups to the walls. The preparation of such inorganic-organic hybrid materials is of growing interest [10-11] especially for the attachment of various metal complexes. Brunel and co-workers have reported the anchoring of Mn(III)Salpr complex through covalently linked organic moieties [12]. Brunel and co-workers have also reported the grafting of TEMPO to organically modified MCM-41 [13]. Ruthenium(II)meso tetrakis(4-chloro phenyl)porphyrin has been encapsulated in MCM-41 modified with 3-aminopropyl triethoxysilane for alkene oxidation by Chi-Ming Che and co-workers [14]. Crudden and co-workers have anchored a bidentate rhodium phosphine complex on to MCM-41 and used as catalyst for hydrogenation of alkenes [15]. We have developed a covalently anchored Vanadium Schiff's base complex onto the walls of functionalized MCM-41 for the oxidation of adamantane using urea hydroperoxide as oxidant [16].

In this chapter we have described the catalytic activity of immobilized octahedral hydrido chlorocarbonyl tris-(triphenylphosphine) ruthenium(II)complex [$RuHCl(CO)(PPh_3)_3$] on inorganic-organic hybrid (APTES modified mesoporous) materials like NH_2-MCM-41/ NH_2-SBA- 15 for hydrogenation of olefins. The complex gets attached to the amine modified Si-MCM-41 and Si-SBA-15 by displacement of a phosphine ligand. The trans bond weakening effect of the hydride ligand in [$RuHCl(CO)(PPh_3)_3$] accounts for the ready displacement of trans phosphine by strongly bonding amine (base).

4.6.2 EXPERIMENTAL

4.6.2.1 Materials

Tetraethylorthosilicate (TEOS), cetyltrimethylammoniumbromide (CTAB), poly(ethylene oxide)-poly(propylene oxide) poly(ethylene oxide), Pluronic P123 [EO_{20}-PO_{70}-EO_{20}], triphenylphosphine (TPP), 3-aminopropyl triethoxysilane (APTES), styrene, α-methyl styrene, trans-stilbene, cis-stilbene and limonene were procured from Aldrich Co. Tetramethylammonium hydroxide (TMAOH) was obtained from Merck. All the solvents were of AR grade and were procured from s.d. fine Chemicals, India and were distilled and dried before use.

4.6.2.2 Procedure

A known amount of substrate (1g), catalyst "neat"-[$RuHCl(CO)(PPh_3)_3$] = 4.14 mg/ -[$RuHCl(CO)(PPh_3)_2$]-NH_2-MCM-41= 50 mg/ [$RuHCl(CO)(PPh_3)_2$]-NH_2-SBA-15= 33.85 mg, acetonitrile (30 ml) were taken in a 300 ml stainless steel Parr autoclave, was pressurized to 400 psig hydrogen and was heated to a temperature of 333K. The progress of the reaction was monitored by withdrawing samples at different time

intervals and analyzing by gas chromatograph (Shimadzu 14B, FID detector, SE-52 30 m capillary column). The identities of the products were confirmed by GC-MS (Shimadzu GCMS QP 5000).

4.6.3 RESULTS AND DISCUSSION

The hydrogenation of olefins was carried out with neat and immobilized catalysts. The catalytic activity was found to be more in the case of immobilized catalysts than that of the neat complex (Table-4.6.1). The improvement in the catalytic activity for the catalyst immobilized by functionalization of ruthenium complex can be attributed to the chemical coordination of the ruthenium complex to APTES over Si-MCM-41and electron transfer from APTES to ruthenium.

The enhanced catalytic activity in the case of the complex immobilized on functionalized SBA-15 than on MCM-41 could be because of the easy access of the active site to the reactant molecules due to the large pore diameter of SBA-15 compared to MCM-41. The large decrease in the surface area and pore size of MCM-41 upon functionalization with APTES and on immobilizing the complex may be due to partial collapse of the walls of MCM-41 during the modification procedure. The XRD results support this conclusion (Refer chapter 3). But in the case of SBA-15 due to the higher hydrothermal stability and thicker pore walls than MCM-41 these modification procedures have very little effect on the walls of SBA-15 as evident from the XRD profiles.

Table -4.6.1

Hydrogenation of olefins by "neat" and immobilized hydrido chlorocarbonyl tris-triphenylphosphine ruthenium (II) complex.

Catalyst (weight -mg)	Substrate	Conversion (wt.%)
"neat" $[RuHCl(CO)(PPh_3)_3]$ (4.14)	Styrene	9
$[RuHCl(CO)(PPh_3)_2]$- NH_2-MCM-41 (50)	Styrene	43
$[RuHCl(CO)(PPh_3)_2]$-NH_2-SBA-15 (33.85)	Styrene	66
"neat" $[RuHCl(CO)(PPh_3)_3]$	t-stilbene	10
$[RuHCl(CO)(PPh_3)_2]$- NH_2-MCM-41	t-stilbene	82
$[RuHCl(CO)(PPh_3)_2]$-NH_2-SBA-15	t-stilbene	93
"neat" $[RuHCl(CO)(PPh_3)_3]$	cis-stilbene	12
$[RuHCl(CO)(PPh_3)_2]$-NH_2-SBA-15	cis-stilbene	95
"neat" $[RuHCl(CO)(PPh_3)_3]$	α-methyl styrene	18
$[RuHCl(CO)(PPh_3)_2]$-NH_2-SBA-15	α-methyl styrene	97
"neat" $[RuHCl(CO)(PPh_3)_3]$	limonene	15
$[RuHCl(CO)(PPh_3)_2]$-NH_2-SBA-15	limonene	89

Reaction conditions: Substrate = 1 g, methanol = 30 g, temp. = 333 K, H_2 pressure= 400 psig and reaction time = 12 h.

4.6.4 CONCLUSIONS

Hydrido chlorocarbonyl tris- triphenylphosphine ruthenium (II) complex has been immobilized on amine functionalised MCM-41 and SBA-15 by the displacement of one PPh_3 group. Immobilization and the pore size of the support have marked effects on the activity of $[RuHCl(CO)(PPh_3)_3]$ complex in the hydrogenation of olefins.. The complexes immobilized on functionalized mesoporous materials are more active than the "neat" complex. The immobilized complexes can be reused. $[RuHCl(CO)(PPh_3)_3]$

complexes immobilized on NH_2-SBA-15 are relatively more active than that immobilized on NH_2-MCM-41. The easy access of the active site to the substrate molecules is perhaps responsible for the higher activity of the SBA-15 catalysts.

4.6.5 REFERENCES

1. C. T. Kresge, M. E. Leonowicz, W. J. Roth, J. C. Vartuli and J. S. Beck, Nature 359 (1992) 710.
2. J. S. Beck, J. C. Vartuli, W. J. Roth, M. E. Leonowicz, C. T. Kresge, K. D. Schmitt, C. T.-W. Chu, D. H. Olson, E. W. Sheppard, S. B. McCullen, J. B. Higgins and J. L. Schenker, J. Am. Chem. Soc. 114 (1992) 10834.
3. D. Y. Zhao, J. L. Feng, Q. S. Huo, N. Melosh, G. H. Fredrickson, B. F. Chmelka and G. D. Stucky, Science, 279 (1998) 548.
4. X. Feng, G. E. Fryxell, L.-Q. Wang, A. Y. Kim, J. Liu and K. M. Kemner, Science, 276 (1997) 923.
5. L. Mercier and T. J. Pinnavia, Adv. Mater., 9 (1997) 500.
6. A. M. Liu, K. Hidajat, S. Kawi and D. Y. Zhao, Chem. Commun (2000) 1145.
7. H. Takahashi, Bo Li, T. Sasaki, C. Miyazaki, T. Kajino and S. Inagaki, Microporous Mesoporous Mater. 44-45 (2001) 755.
8. C. Huber, K. Moller and T. Bein, J.Chem.Soc. Chem. Commun. (1994) 2619.
9. Y-J Han, G. D. Stucky and A. Butler, J. Am. Chem. Soc., 121 (1999) 9897.
10. T. Asefa, M. J. Maclachlan, N. Coombs, G. A. Ozin, Nature, 402 (1999) 867.
11. B. F. G. Johnson, S. A. Raynor, D. S. Shephard, T. Mashmeyer, J. M. Thomas, G. Sanker, S. Bromley, R. Oldroyd, L. Gladden and M. D. Mantle, Chem. Commun. (1999) 1167.
12. P. Sutra, D. Brunel, Chem. Commun (1996) 2485.
13. D. Brunel, F. Fajula, J. B. Nagy, B. Deroide, M. J. Verhoef, L. Veum, J. A. Peters and H. van Bekkum, Appl. Catal. A: 213 (2001) 73.
14. C-J. Liu, S-G. Li, W-Q. Pang and C-M. Che, Chem. Commun (1997) 65.

15. C. M. Crudden, D. Allen, M. D. Mikoluk and J. Sun, Chem. Commun (2001) 1154.

16. T. Joseph and S.B.Halligudi, J. Mol. Catal. A: “In Press”.

CHAPTER 5

SUMMARY AND CONCLUSIONS

The synthesis, characterization and catalytic properties of cobalt, ruthenium and vanadium schiff base complexes encapsulated/immobilized in microporous and mesoporous materials have been investigated. The complexes were encapsulated in zeolite-Y by flexible ligand method. The complexes immobilization on mesoporous materials were mostly acheived by modifying the mesoporous materials with various modifying agents (functionalization) and the covalently anchoring the metal complex on to the functionalized mesoporous materials. Functionalization of mesoporous materials is achieved by silanation of the mesoporous surface by 3-amino or 3-halogeno-propyl alkoxysilane in an apolar solvent.

The formation and structural integrity of the complexes were investigated by using a variety of physicochemical techniques such as elemental analysis, XRD, TG-DTA, sorption studies, FT-IR, XPS, EPR and NMR spectroscopic techniques. EPR spectroscopy, especially of VO(IV)Saloph complex has provided clear evidence for the encapsulation/immobilization of the complex inside the cavities and channels of micro and mesoporous materials. The ESR spectra of the encapsulated/immobilized complexes were different from that of "neat" complexes. Sorption studies have also provided an indirect evidence for the encapsulation of the complexes. The encapsulated/immobilized complexes have lower surface area and pore size than the parent micro and mesoporous materials. The comparative spectroscopic studies on "neat" and encapsulated/immobilized metal complexes have revealed that the complexes are located inside the cavities and channels of microporous (zeolite-Y) and mesoporous (MCM-41 and SBA-15) materials respectively.

The catalytic activities of the complexes encapsulated in zeolite-Y were studied in different industrially important oxidation reactions viz., oxidation of *p*-

cresol, β-Isophorone, α-pinene and epoxidation of styrene and *t*-stilbene. The encapsulated complexes showed enhanced catalytic activities than the "neat" complexes. Substitution of the hydrogen atoms in the aromatic nuclei of the Saloph molecule by electron withdrawing (halogens and nitro groups) groups increases the reactivity of these catalysts. The depletion of electron density perhaps promotes the nucleophillic attack of the oxidant molecule at the metal center forming catalytically active metal-superoxo/metal-hydroperoxides. Further the electron withdrawing substituents also facilitates the cleavage of these metal-superoxo/metal-hydroperoxides species. The ease of formation and cleavage of these intermediate species in the complex with electron withdrawing substituents have been correlated to the increased catalytic activity of these complexes in oxidation reactions.

The catalytic activity of the vanadium and ruthenium complexes immobilized/anchored on mesoporous materials (MCM-41 and SBA-15) were studied for oxidation/epoxidation and hydrogenation reactions. Vanadium Schiff base complex was immobilized/anchored on MCM-41 and its catalytic activity for the epoxidation of styrene and *t*-stilbene using TBHP as oxidant and oxidation of adamatane using anhydrous urea hydrogen peroxide (UHP) as oxidizing agent. The conversion for adamantane was more on using UHP as the oxidant compared to H_2O_2. This is because of the slow release of hydrogen peroxide and hence oxygen from the urea hydrogen peroxide adduct. The result obtained with the immobilized catalyst is compared with those obtained with the corresponding homogeneous catalyst. The catalytic activity of immobilized octahedral hydrido chlorocarbonyl tris-(triphenylphosphine) ruthenium(II)complex $[RuHCl(CO)(PPh_3)_3]$ on inorganic-organic hybrid (APTES modified mesoporous) materials like NH_2-MCM-41/ NH_2-SBA- 15 for hydrogenation

of olefins was also studied. The complex gets attached to the amine modified Si-MCM-41 and Si-SBA-15 by displacement of a phosphine ligand. The trans bond weakening effect of the hydride ligand in [$RuHCl(CO)(PPh_3)_3$] accounts for the ready displacement of trans phosphine by strongly bonding amine.

The studies presented in this thesis have provided definite convincing evidence for the biomimitic nature of these heterogenized catalysts. Just as the protein environment in metalloenzymes dictates the geometry and redox properties of the active site in addition to providing sterio- and regio-selectivities, the zeolite mantle as revealed from the present investigations also modifies the molecular and electronic structural properties of the complexes and enhances the rate of the chemical transformations. Thus the modified solid catalysts can be called as inorganic mimic of enzymes. These catalysts systems are found to be advantageous and hold promise for application in chemical industry due to their high thermal stability, ease of operation in industry, prevention of catalyst deactivation due to dimer formation, higher activity compared to their homogenous analogues, ability to recycle, and in utilizing O_2 as well as singlet oxygen sources like H_2O_2, TBHP and UHP which leave no harmful dissociation products.

LISTS OF PUBLICATIONS

1. Oxidation of p-cresol catalyzed by neat and zeolite encapsulated cobalt salen complexes.

   T. Joseph, C. S. Sajanikumari, S. S. Deshpande and S. Gopinathan, Indian Journal of Chem 38 (A) (1999) 792.

2. Oxidation by molecular oxygen using zeolite encapsulated Co(II)Saloph complexes

   T. Joseph, S. B. Halligudi, C. Satyanarayan, D. P. Sawant and S. Gopinathan, J. Mol. Catal (A) Chemical 168 (2001) 87.

3. Zeolite encapsulated ruthenium and cobalt schiff base complexes catalyzed allylic oxidation of α-pinene

   T. Joseph, D. P. Sawant, C. S. Gopinath and S. B. Halligudi, J. Mol. Catal (A) Chemical 184 (2002) 289.

4. Spectroscopic and catalytic activity studies of VO(Saloph) complexes encapsulated in zeolite-Y and Al-MCM-41 molecular sieves

   T. Joseph, D. Srinivas, C. S. Gopinath, and S. B. Halligudi, Catal. Lett., 83, 3-4 (2002) 209.

5. Oxidation of Adamantane by Urea Hydroperoxide using vanadium complex anchored onto functionalized Si-MCM-41

   T. Joseph and S. B. Halligudi, J. Mol. Catal (A) Chemical "In Press".

6. Hydrogenation of olefins over hydrido chlorocarbonyl tris-(triphenylphosphine) ruthenium (II) complex immobilized on functionalized MCM-41 and SBA-15

   T. Joseph, S. S. Deshpande and S. B. Halligudi, J. Mol Catal (A) Chemical

"Communicated".

7. Allylic Oxidation Of α-Pinene To D-Verbenone Catalyzed By Zeolite Encapsulated Metal Schiff Base Complexes

T. Joseph, D. P. Sawant, S. B. Halligudi and S. Gopinathan, Bull. Catal. Soc. India, Aug, (2000) 8.

8. Catalysis by heteropolyacids: A convenient route for the preparation of methyl chloride and methyl bromide.

N. A. Alekar, C. S. Sajanikumari, **T. Joseph**, I. R. Unny, S. Gopinathan and C. Gopinathan

Indian Journal of Chemical Technology, 7 (2000) 79.

9. Au and Au-Pt Bimetallic Nanoparticles in MCM-41 materials: Applications in CO Preferential Oxidation

S. Chilukuri, **T. Joseph**, S. Malwadkar, C. Damle, S. B. Halligudi, B. S. Rao, M. Sastry and P. Ratnasamy, Stud. Surf. Sci. Catal.

LISTS OF PATENTS

1. An improved process for the preparation of supported copper catalysts

   Indian Patent Ref. No. NF-356/98.

2. An improved process for the production of aminodicarboxylic acid salts

   Indian Patent Ref. No. NF-357/98.

PAPERS AND POSTERS PRESENTED AT NATIONAL AND INTERNATIONAL SYMPOSIA

1. Allylic oxidation of α-pinene by zeolite encapsulated Ru(III) and Co(II) complexes.

   T. Joseph, D. P. Sawant, C. S. Gopinath and S. B. Halligudi

   Presented at the International Symposium on Catalysis at National Chemical Laboratory, Pune. January 1999.

2. Au and Au-Pt Bimetallic Nanoparticles in MCM-41 materials: Applications in CO Preferential Oxidation

   S. Chilukuri, **T. Joseph**, S. Malwadkar, C. Damle, S. B. Halligudi, B. S. Rao, M. Sastry and P. Ratnasamy.

   Presented at IMMS 2002: 3rd International Mesostructured Materials Symposium at Korea during 8-11 July 2002.

3. Vanadium Schiff Base complexes encapsulated in Micro and mesoporous Materials: Spectroscopic and Catalytic investigations.

   T. Joseph and S. B. Halligudi

   Fourth National Symposium In Chemistry, at National Chemical Laboratory,

Pune, February 1-3, 2002.

4. Oxidation by urea-hydrogen peroxide adduct (UHP) using MCM-41 anchored vanadium complex

T. Joseph and S. B. Halligudi

Poster presented at Catalysis: Concepts to Practice, at National Chemical Laboratory, Pune, 26-27 June, 2002.